Title
Illuminating degradation: The coordination and timing of substrate processing by the 26S proteasome

Author
Bard, Jared

Publication Date
2018

Peer reviewed|Thesis/dissertation

Illuminating degradation: The coordination and timing of substrate processing by the 26S proteasome

by

Jared A Bard

A dissertation submitted in partial satisfaction of the

requirements for the degree of

Doctor of Philosophy

in

Molecular and Cell Biology

in the

Graduate Division

of the

University of California, Berkeley

Committee in charge:

Professor Andreas Martin, Chair
Professor Jeremy Thorner
Professor James Hurley
Professor Matthew B. Francis

Summer 2018

Abstract

Illuminating degradation: The coordination and timing of substrate processing by the 26S proteasome

by

Jared A Bard

Doctor of Philosophy in Molecular and Cell Biology

University of California, Berkeley

Professor Andreas Martin, Chair

Selective protein degradation is a constant and critical process in cells. It is essential for maintaining tight control over protein abundance, which allows for finely tuned regulatory responses in a variety of cellular pathways. The degradation of certain proteins is also an important step in the regulation of many physiologically important cellular processes, such as cell cycle progression and stress responses. In addition, misfolded proteins accumulated both spontaneously and as a result of cellular stress must be degraded to prevent the formation of cytotoxic protein aggregates, which have been implicated as the cause of several neurodegenerative diseases. The 26S proteasome is the principal macromolecular machine responsible for protein degradation in eukaryotes. To reliably process all the proteins presented to it in the complex cellular environment, the proteasome must combine high promiscuity with exceptional substrate selectivity. Recent structural and biochemical studies have shed light on some of the steps involved in proteasomal substrate processing but have been mostly limited to static views of the process with little information about the dynamics of substrate processing. Hence, much remains to be learned about the detailed kinetics and coordination of the underlying substrate-processing steps of the proteasome, and how they correlate with observed conformational states.

The goal of my thesis work described here was to develop assays which would measure the kinetics of proteasomal degradation and reveal important details of the processing mechanism. I began by developing a method for the targeted incorporation and labeling of unnatural amino-acids at specific residues in recombinantly expressed sub-complexes of the 26S proteasome. I then designed a series of FRET and anisotropy-based assays to probe substrate-proteasome interactions, the individual steps of the processing pathway, and the conformational state of the proteasome itself. Using these assays, I developed a complete kinetic picture of proteasomal degradation, which reveals that the engagement steps prior to substrate commitment are fast relative to subsequent deubiquitination, translocation and unfolding. Furthermore, by modulating the architecture of the substrate and then investigating the kinetics of its processing, I found that non-ideal substrates are rapidly rejected by the proteasome, which thus employs a kinetic proofreading mechanism to ensure degradation fidelity and substrate prioritization.

Table of Contents

Acknowledgements

The work described here would not have been possible without the many people who prepared me for and supported me throughout graduate school. Special thanks to my dedicated and brilliant advisor Andreas Martin, whose curiosity inspired me everyday. I learned from you to critically observe and consider every aspect of my experiments and to embrace the daunting unknown with enthusiasm. Thank you for leading and cultivating a wonderful atmosphere of inquisitiveness, rigor, and support in lab.

I would also like to thank the many other mentors and teachers I have had throughout my education, including my thesis committee, Professors Jeremy Thorner, James Hurley and Matt Francis for their many hours of attention, their encouragement and their insight. Thank you to Professors Mark Hochstrasser, Xing-Wang Deng, Hong-Wei Wang, and Richard Dutton for guiding me as a young and not very useful undergraduate researcher as I explored the many wonderful facets of biology and thanks also to the many postdocs and graduate students who patiently trained me.

Thank you to the entire Martin lab, past and present, for being great labmates and friends and for their countless ideas, suggestions, criticisms, and encouragements. Thank you to the pioneers Mary and Robyn, who still inspire us, and to Kris, Evan and Eric (Estrin) for your creativity. Thanks to Charlene for first teaching me biochemistry and for providing much of the intellectual groundwork for my project. Brooke was a constant inspiration for how to pursue science as a career and to expand my scientific awareness out of a test tube. Ellen helped me struggle through many thorny technical problems throughout graduate school and I would likely still not be done without her advice. Mike and Stephanie provided much needed outside perspective and Eric (Greene) and Dom provided great insight and helped keep me from getting too stuck in my ways. Ken’s wisdom and knowledge were invaluable. Erik was a perfectly suited bay-mate and wonderful, patient collaborator. Good luck to Erika, Matt, Santi and Cameron and thank you for continuing to make science feel new and exciting.

The many friendships I made in Berkeley are much more enduring and valuable than this thesis. Thanks to my classmates and colleagues and to everyone who drank tea, ate pizza, baked and cooked, hiked, commiserated and celebrated with me.

Thank you to my wonderful family, especially my mom and dad who gave me all of their love, nurtured my curiosity and carefully prepared me for my life. Your support still carries me. Thank you also to my adopted family, the Scher-Altmans, who gave me a loving West-Coast home and retreat.

Finally, thank you to my incomparable life-partner and wife, Alison Altman. For many years past and to come you have been my companion in adventure, struggle, joy and rest. Your contributions to this thesis are tangible and include much editing, insight and a drive to excellence. Your love, support and wisdom are the foundation upon which I stand every day and your smile is what gets me up in the morning.

Chapter 1: Introduction

The following chapter was adapted from Bard JAM, Goodall EA*, Greene ER, Jonsson E, Dong KC, & Martin A (2018) Structure and Function of the 26S Proteasome.* Annu Rev Biochem *87:697-724. The article was written collaboratively by all authors.*

The 26S proteasome is the major protease in eukaryotic cells, responsible for protein degradation in both the cytosol and the nucleus. Ubiquitin modifications target condemned proteins to the proteasome. These modifications are covalently attached to lysine side chains by a large network of ubiquitin ligases and conjugating enzymes, and they are removed at the proteasome prior to substrate degradation (for more details, see (1). As a compartmental protease of the AAA+ (ATPases associated with various cellular activities) family, the proteasome uses ATP hydrolysis to disrupt higher-order structures of its substrates and translocate the unfolded polypeptides into an internal degradation chamber for proteolytic cleavage. This ability to unravel native structures allows the proteasome to function as a modulator of the eukaryotic proteome and degrade numerous regulatory proteins in addition to damaged or misfolded polypeptides. Therefore, the 26S proteasome not only is essential for general protein and amino acid homeostasis but also controls a myriad of essential cellular processes, including the cell cycle, DNA replication, transcription, signal transduction, and stress responses (2-5).

The high selectivity and tight control required for such promiscuous intracellular proteolysis are accomplished, on the one hand, by the specific ubiquitin labeling of appropriate substrates for degradation and, on the other hand, through the complex architecture of the 26S proteasome holoenzyme (Figure 1.1a) (6). The holoenzyme's proteolytic active sites reside within the chamber of the barrel-shaped 20S core particle and are accessible only through narrow axial pores, which exclude folded and even large unfolded polypeptides. Gating of these pores is controlled by the 19S regulatory particle (RP) (7-13), which caps one or both ends of the 20S core peptidase and mechanically translocates appropriate substrates into the degradation chamber. Many years of work have led to an extensive body of knowledge about the 20S core peptidase (4, 14). However, only recently has detailed information about the structure, function, and conformational dynamics of the 19S RP become available, and this review largely focuses on these findings.

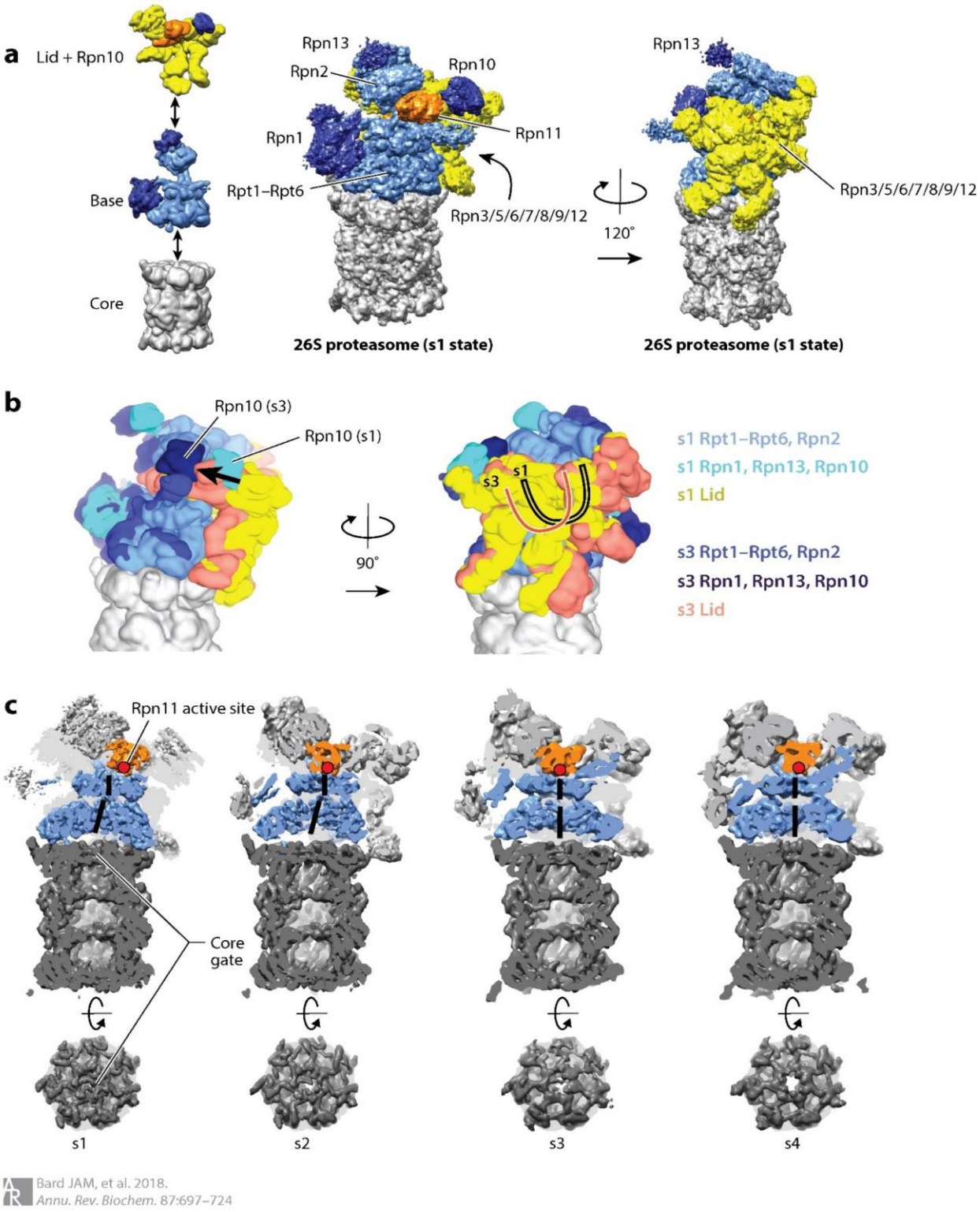

Figure 1.1. Architecture of the 26S Proteasome.

Structure and conformational changes of the proteasome. (a) The 26S proteasome is composed of three subcomplexes: the core (gray); the base (with Rpn2 and the motor subunits Rpt1–Rpt6 in light blue and the ubiquitin-binding subunits Rpn1 and Rpn13 in dark blue); and the lid (with Rpn3, Rpn5, Rpn6, Rpn7, Rpn8, Rpn9, Rpn12, and Sem1 in yellow, and the DUB Rpn11 in orange). The ubiquitin receptor Rpn10 is shown together with the lid (dark blue). (Left) The three subcomplexes are depicted individually; (center and right) the entire 26S proteasome structure is shown (EMDB: 3534) (40). The center orientation allows a view of the entrance to the central pore and the Rpn11 active site, and the right orientation, rotated by 120°, emphasizes the lid subcomplex with its hand-shaped structure of the PCI (proteasome-CSN-initiation factor 3) domain-containing subunits. (b) Conformational switching of the 19S regulatory particle between the s1 state (EMDB: 3534) and the s3 state (EMDB: 3536) (15), with the core particles aligned. Shown are the views from the right and back of the proteasome relative to the center orientation in panel a. In the s1 conformer, the Rpt ring and Rpn2 are depicted in light blue; Rpn1, Rpn10, and Rpn13 in cyan; and the lid in yellow. In the s3 conformer, the Rpt ring and Rpn2 are depicted in medium blue; Rpn1, Rpn10, and Rpn13 in dark blue; and the lid in salmon. For both conformers, the core is shown in gray. During the transition from s1 to s3, the lid and Rpn10 rotate by ∼30° relative to the Rpts. (c) Cutaway representations of the proteasome in the conformations s1–s4, emphasizing differences in the location of Rpn11; the width of the central processing channel; and the coaxial alignment of the N-ring, the AAA+ (ATPases associated with various cellular activities) ring, and the 20S core. The central channels through the N-ring and AAA+ ring are highlighted by a solid black line. The coaxial alignment is most pronounced in the s3 and s4 conformers, leading to the formation of a wide continuous channel for substrate translocation, with the Rpn11 active site (red dot) located directly above the entrance. Also shown are top-down views of the 20S core particle, emphasizing the changes in the 20S gate, which has the most density in the s1 state and the least in the s4 state.

The RP can be separated biochemically into the base and lid subcomplexes (Figure 1.1a) (16, 17). The base subcomplex includes three non-ATPase subunits, in *Saccharomyces cerevisiae* called Rpn1, Rpn2, and Rpn13, with Rpn1 and Rpn2 containing large alpha solenoids that provide multiple binding sites for ubiquitin and ubiquitin-like proteins (UBLs) (on Rpn1) and a binding site for the ubiquitin receptor Rpn13 (on Rpn2) (18-20). An additional ubiquitin-receptor subunit, Rpn10, is not considered part of the base or lid per se, but instead bridges both subcomplexes in the assembled RP (21, 22). At the center of the base are six distinct ATPase subunits (Rpt1–Rpt6 in yeast), whose AAA+ domains form the ring-shaped heterohexameric motor of the proteasome. Each Rpt also contains an N-terminal alpha helix and an OB (oligonucleotide/oligosaccharide binding)-fold domain that in the hexamer assembles into a distinct N-ring above the AAA+ domain ring. The Rpts use conserved loops projecting from their AAA+ domains into the central pore of the motor to engage protein substrates, apply mechanical pulling force for unfolding, and then translocate the unfolded polypeptide into the associated 20S core (23-27).

The lid subcomplex acts as a scaffold that braces one side of the base (28, 29) and includes six PCI (proteasome-CSN-initiation factor 3) domain–containing subunits (Rpn3, Rpn5, Rpn6, Rpn7, Rpn9, Rpn12) as well as two subunits (Rpn8 and Rpn11) with an MPN (Mpr1-Pad1 N-terminal) domain. Rpn11 is a Zn^{2+}-dependent deubiquitinase (DUB) of the JAMM/MPN family and responsible for the removal of substrate-attached ubiquitin chains before they enter the AAA+ ATPase (30-32). The proteasome also contains one or two additional stably associated DUBs, Ubp6 and Uch37. Ubp6 (Usp14 in mammals) is a ubiquitin-specific protease (USP) that

interacts with Rpn1 of the base and uses an active site cysteine to cleave supernumerary ubiquitin chains from substrates (33). The ubiquitin C-terminal hydrolase Uch37 (also called UCHL5) associates with the ubiquitin receptor Rpn13 and likely functions in cleaving or editing distal ubiquitin chains on proteasome substrates (34-37).

The past few years have bestowed a major leap in our structural and functional understanding of the RP, especially through cryo-electron microscopy (EM) studies that have identified several new conformations (15, 38-45). The combination of newly available structural information with a large body of biochemical studies has provided us with an intriguing molecular model for substrate processing by the 19S RP (Figure 1.2). Substrates are targeted to the proteasome through interactions between attached ubiquitin modifications and several ubiquitin receptors on the proteasome (see the section titled Ubiquitin Recognition at the Proteasome). An unstructured region of the substrate is then engaged by the AAA+ motor, which subsequently pulls on, translocates, and unfolds the substrate (see the sections titled Substrate Requirements for Proteasome Degradation, and The Proteasome AAA+ ATPase Motor) (46). Substrate engagement is accompanied by a major conformational change that switches the RP into a state ideally suited for processive substrate translocation and translocation-coupled deubiquitination (see the sections titled Proteasome Conformational Changes, and Proteasomal Deubiquitinases) (42). The proteasome's various conformational states thus appear to differentially facilitate and coordinate the individual steps of substrate processing (15, 38-45, 47). On the basis of these findings, it is now clear that proteasome function depends on complex conformational equilibria, which are influenced by a range of factors, including the nucleotide state of the Rpt subunits, the presence of protein substrate, and the occupancies of DUBs and ubiquitin receptors. In addition, major advances in localizing and characterizing the various ubiquitin receptors and DUBs have provided a first glimpse into how the proteasome may differentially use them to recruit certain substrates and fine-tune degradation activities. The following sections focus on the recent progress in our understanding of the 19S RP, its fascinating dynamics, and versatile functions in substrate selection and processing.

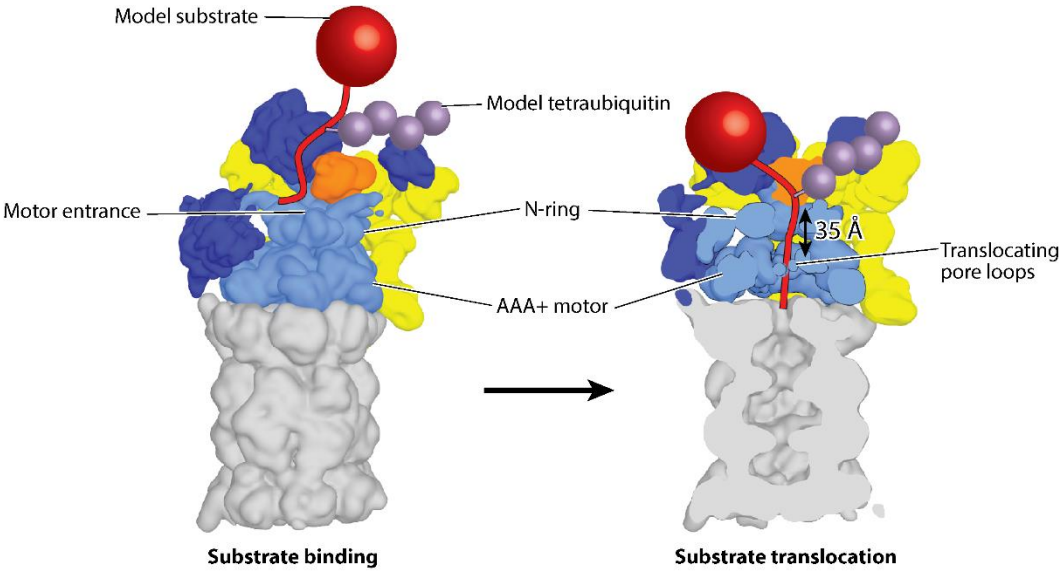

Figure 1.2. Model for substrate engagement by the proteasome.
(Left) Proteasome is shown in the s1 state (EMDB: 3534) with a model substrate (red) tethered through a tetraubiquitin chain (purple) near the presumed location of the Rpn10 ubiquitin-interacting motif. In this s1 state, Rpn11 (orange) is offset to the right, making the entrance to the central pore accessible for insertion of a substrate's unstructured initiation region. (Right) Substrate engagement shifts the proteasome to the s3 or s4 state (s4 is shown; EMDB: 3537) (15) in which the N-ring and AAA+ (ATPases associated with various cellular activities) ring are coaxially aligned to facilitate substrate translocation and the 20S gate is open for polypeptide transfer into the internal degradation chamber. Rpn11 is located directly above the entrance to the central pore, where it acts as a gatekeeper and removes ubiquitin chains from substrates during translocation. The initiation region of the substrate must be long enough to bridge the gap between the N-ring and the pore loops of the Rpts.

Conformational Changes of the Proteasome

Recent high-resolution cryo-EM work on the 26S proteasome has revealed that the 19S RP has a complex conformational landscape. Two conformations were initially identified and assigned to the substrate-free (s1) and the substrate-processing (s3) states. These two states predominate in in vitro structural studies of purified proteasomes from *S. cerevisiae* (27, 29, 38-41, 48) and *Homo sapiens* (44, 49-52), and they are also observed in situ by cryo-electron tomography of rat hippocampal neurons (53). Recent rapid technological advancement in EM has allowed for further subclassification of proteasome states, and now, up to seven different proteasome conformations have been identified (15, 43-45). It is likely that further structural and biochemical studies will continue to reveal additional conformational states. In the current nomenclature, the main states of the yeast proteasome are referred to as s1, s2, s3, and s4 (15, 40), whereas the closely related conformations of the human proteasome are termed S_A, S_B, S_C, and $S_{D(1,2,3)}$ (44, 45). For clarity, we use the yeast nomenclature in this review.

The order of the four main states is suggested by their structural comparison, as there is a progression of movement from the s1 state through the s2, s3, and s4 states, with s4 being least

similar to s1. Throughout all conformations, the general structure of the core particle remains virtually unchanged, whereas the orientation of the base and lid relative to each other and to the core particle varies dramatically (Figure 1.1*b*,*c*). Between the s1 and s4 conformations, the lid undergoes an ∼30° rotation relative to the base, pivoting around the contact points between its PCI domains and the AAA+ domains of the base. During the transition from s1 to s2, this lid rotation moves the essential DUB Rpn11 from an offset to a coaxially aligned position directly above the central processing pore of the base. Even though this position seems ideal for translocation-coupled deubiquitination, it likely restricts substrate access to the central pore, leading to the proposal that only the s1 state is capable of efficiently engaging an incoming polypeptide with its translocation machinery. The s1 state is therefore assumed to represent the primary substrate-binding conformation (Figure 1.2) (15, 38, 40, 41, 44). This conformation is also likely the resting state of the proteasome, as it is the major conformation observed for ATP-bound proteasomes in the absence of added substrate or other factors. The other conformations were induced by trapping the proteasome during substrate degradation or in the presence of ATP analogs (Figure 1.3), which leaves some uncertainty about their physiological role (15, 38, 40, 41, 43-45).

Whereas the transition from s1 to s2 involves mainly the lid subcomplex, the subsequent transition to s3 is accompanied by major rearrangements in Rpt1–Rpt6, the ATPase subunits of the base (40, 44). The N-ring of the Rpts shifts toward Rpn1, and the AAA+ domains move and tilt in the same direction, creating a wider, continuous central channel that is aligned with the axial pore of the core particle (Figure 1.1c) (15, 38, 40, 44). Concurrently, the interfaces between the AAA+ domains of neighboring Rpts become more uniform and adopt a conformation more similar to other AAA+ motors (15, 38).

Finally, during the transition from s3 to s4, the gates to the core particle appear to open up (Figure1.1c) (40, 44), completing a substrate passage that extends from the N-ring through the AAA+ motor domains into the core. Conformations with more open gates, such as s4, are therefore assumed to reflect the actively translocating states of the RP. The variable opening of the gates is likely induced by differential interactions between the C-terminal tails of Rpt subunits and the 20S core particle (8, 9, 12, 13, 44, 54). The C termini of Rpt2, Rpt3, and Rpt5 contain conserved hydrophobic-Tyr-X (HbYX) motifs, whose docking into hydrophobic pockets on the axial face of the core particle induces gate opening (8, 9, 12, 13, 55). In the s4 state, the C terminus of Rpt6 makes additional contacts with the 20S core, which may trigger the more complete gate opening observed for this state (15)).

Other important changes that are coupled with the conformational transitions involve the intrinsic ubiquitin receptors Rpn10 and Rpn1, one of the most flexible subunits of the proteasome complex. Between s1 and s3 or s4, Rpn1 changes its interactions with the N-terminal coiled coil of Rpt1 and Rpt2; thus, it rotates relative to the ATPase ring and the central pore (15, 38, 40, 43, 44). The rotation of Rpn1 brings its binding site for the UBL of Ubp6 closer to the base ATPases, allowing Ubp6 to make stable contacts with the base ATPase site that is responsible for stimulation of Ubp6 DUB activity in non-s1 states. This dependence on the rotation of Rpn1 explains the ability of Ubp6 to sense the conformational state of the proteasome

in its DUB activity (47, 56-58). During the same transitions, Rpn10 moves concomitant with Rpn11 and makes additional contacts with the N-terminal coiled coil of Rpt4 and Rpt5 (Figure 1.1b). Although the functional importance of these ubiquitin-receptor transitions has yet to be determined, the different positions may influence the proteasome's affinity for ubiquitin chains or direct substrates to the central pore.

The functional models derived from the EM structural data are supported by biochemical measurements of proteasomal peptide hydrolysis, ATP hydrolysis, and deubiquitination, which suggests an intimate relationship between these activities. Studies using freely diffusible fluorogenic peptides to read out gate opening have shown that the 19S RP finely controls the 20S gates and that this activity is stimulated by multiple factors, including the engagement of a protein substrate, the presence of Ubp6, and binding of nonhydrolyzable nucleotide analogs to the base ATPases (26, 58-62). Thus, there is consistency between structural and biochemical studies indicating these factors bias the proteasome toward the open-gate s3 and s4 states and influence gate-opening activity.

Another major difference between conformations is the arrangement of the AAA+ domains, and here too, biochemical and structural studies converge. Substrate engagement, for instance, induces the transition from s1 to s3 or s4 (38), where the contacts between neighboring AAA+ subdomains are more fully formed. Correspondingly, substrate engagement increases the ATPase activity of the Rpt motor (26, 47, 58, 63). Similarly, Ubp6 stimulates proteasomal ATPase activity, and it also shifts the conformational equilibrium of the RP away from the s1 state (47, 51, 56, 63). These data are consistent with a model where the s1 conformation is the ground state of the proteasome in which the base hydrolyzes ATP slowly. Factors that stimulate ATPase activity do so by biasing the proteasome toward different conformations that hydrolyze ATP more quickly. This assumption is further corroborated by the fact that nonhydrolyzable nucleotide analogs that likely stabilize uniform Rpt-subunit interfaces also bias the proteasome conformational landscape away from the s1 conformer (15, 39).

Although much effort has been dedicated to defining different proteasome conformations, the biochemical activities are only correlative at this point, and the relevance of any conformer to on-pathway proteasome degradation has not yet been assessed. Moreover, posttranslational modifications regulate proteasome function in vivo (64, 65), but their effects on the conformational landscape and biochemical activities have not yet been studied.

The AAA+ Motor of the Proteasome

Unfolding and translocation of protein substrates into the proteolytic core is driven by the Rpt1-Rpt6 heterohexameric motor, which functions as the engine of the proteasome, converting the chemical energy of ATP binding and hydrolysis into mechanical work. The architecture of the Rpt ring resembles a trimer of dimers, with the N-terminal helices forming coiled coils between pairs of neighboring subunits (Rpt1/Rpt2, Rpt6/Rpt3, and Rpt4/Rpt5) that contribute to proper arrangement of subunits during assembly (66, 67) (Figure 1.3a,b). Downstream of the coiled coils, the OB-fold domains of Rpt1–Rpt6 form the N-ring, which is essential for the structural

stability of the hexamer and acts as a bottleneck against which the AAA+ motor likely pulls the protein substrates during mechanical threading to induce their unfolding.

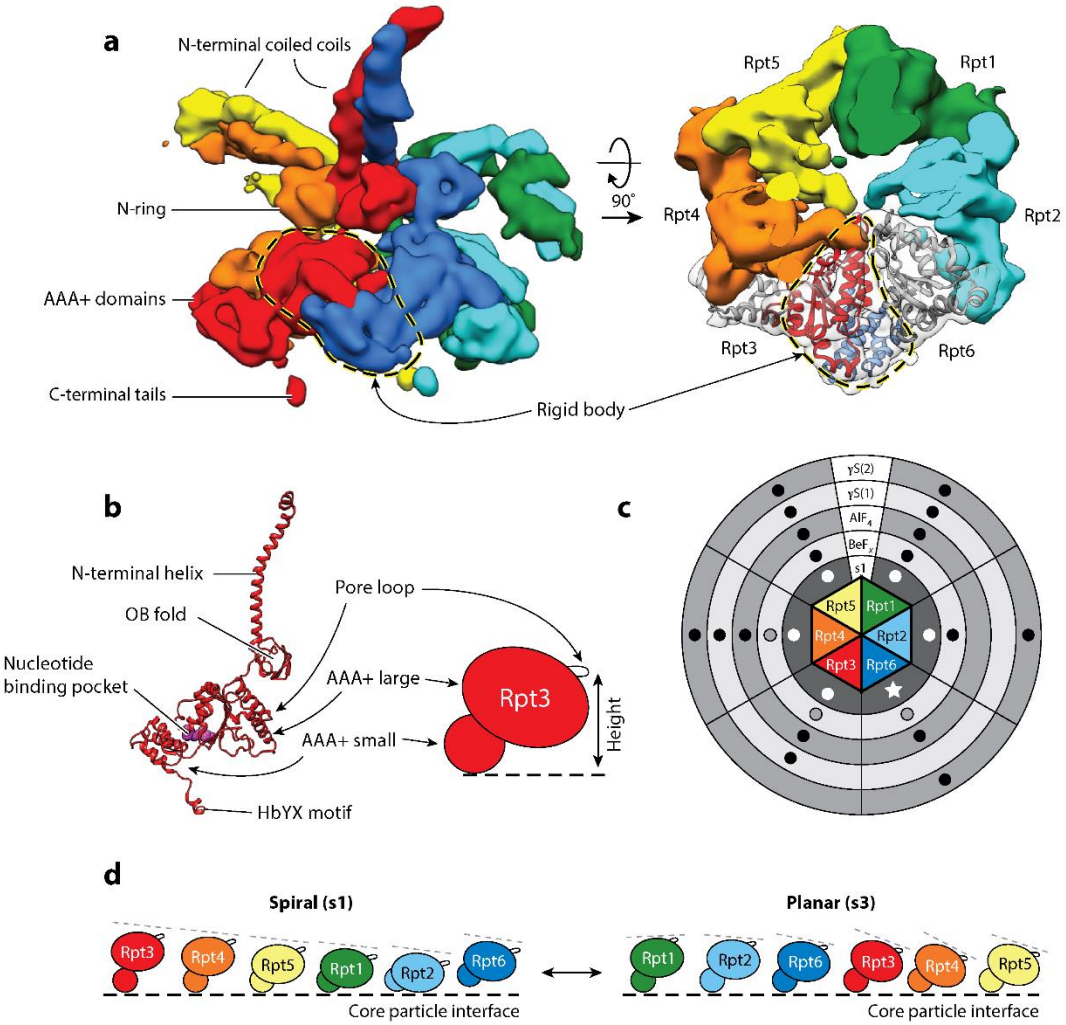

Figure 1.3. AAA+ motor architecture, nucleotide binding, and conformational changes. (a) Side (left) and top (right) views of the EM density for the Rpt1–Rpt6 hexamer in the s3 state (EMDB: 3536) (15). The small AAA+ subdomain of each Rpt forms a rigid body with the large AAA+ subdomain of the clockwise-next neighboring subunit. The rigid body formed between Rpt3 (red) and Rpt6 (dark blue) is shown with a dashed loop. In the top view (right), the EM densities for Rpt3 and Rpt6 are shown in transparent grey, and the molecular models for both Rpts are fitted into the density, with the large AAA+ subdomain of Rpt3 in red and the small AAA+ subdomain of Rpt6 in blue, to highlight the rigid-body interaction. (b, left) Molecular model of Rpt3 (PDB: 5mpb) (15); (right) representation of the relative positions of the large and small AAA+ subdomains as well as the pore loop responsible for mechanical substrate translocation. (c) Schematic of the Rpt1–Rpt6 hexamer, showing the reported nucleotide occupancy of each AAA+ binding pocket for EM reconstructions in the presence of ATP (s1 state) (innermost circle in dark gray) or different ATP analogs (ADP-BeFx, ADP-AlFx, and two distinct ATPγS structures): Black dots indicate the presence of nucleotide density, dots are absent from reported empty sites, and outlined gray dots denote sites with lower probability occupancy or lower affinity. For

the s1 state, all available data sets show nucleotide density in every pocket (white dots), although Rpt6 exhibits a smaller density and a lack of arginine-finger contacts, suggesting that the bound nucleotide is ADP (white star) (15, 43, 44, 50, 51). The two ATPγS data sets reflect the higher-certainty assignments from Zhu et al. (45), the results for ADP-AlF4-bound proteasomes were taken from Ding et al. (43), and the ADP-BeFx data set reflects the assignments of the s4 state described in Wehmer et al. (15). (d) Representations of the splayed-out Rpt subunits in the steep spiral arrangement of the s1 state and the more planar staircase conformation in s3. All subunits are oriented with the channel-facing pore loops pointing to the right. The dashed lines serve to highlight the apparent tilt of the AAA+ large domains. Abbreviations: AAA+, ATPases associated with various cellular activities; EM, electron microscopy; OB, oligonucleotide/oligosaccharide binding.

In the s3 and s4 conformations of the base, the small AAA+ subdomain of every Rpt subunit forms static contacts and thus a rigid body with the large AAA+ subdomain of the clockwise-next neighboring subunit (Figure 1.3a). Therefore, the AAA+ hexamer can be thought of as six rigid bodies that are connected by linkers between the large and small subdomains. They are expected to move in response to ATP hydrolysis and change their vertical arrangement in a topologically constrained fashion. The conserved pore loops that sterically interact with substrate in the central pore (Figure 1.3b) originate from the large AAA+ subdomains and are linked to movements of the rigid bodies, enabling the translation of nucleotide-dependent changes into mechanical pulling for substrate translocation. The AAA+ domain interfaces that form rigid-body contacts are similar to those seen for other polypeptide translocating AAA+ motors, including the archaeal proteasome homolog PAN (proteasome-activating nucleotidase) and the bacterial translocase ClpX (68-70). In addition, a number of structures have been recently solved of AAA+ motors actively translocating substrates, and they all exhibited rigid-body movements of their AAA+ domains as well (71-75).

An emergent feature common to these AAA+ motors is a spiral staircase (often termed lockwasher) arrangement of their rigid bodies, in which neighboring large AAA+ subdomains tilt progressively downward, with a break in the arrangement between the first and last units (Figure 1.3d) (76, 77). This staircase arrangement may be tied to the hydrolysis cycle of the motors, with each position in the staircase corresponding to a particular hydrolysis event. For the proteasome, cryo-EM studies have revealed that the Rpt ring is highly dynamic, with the most pronounced structural rearrangement occurring between the s1 and s3 states. In the s1 state, rigid-body interactions between neighboring Rpt subunits are largely absent; the large AAA+ domains are differentially lifted out of the plane of the ring; and their pore loops are arranged in an extended spiral, with Rpt3 in the highest position (Figure 1.3d). This arrangement is not typical of actively translocating AAA+ hexamers and may represent an “off” state for other motors (71). In the proteasome, this motor state may be stabilized in the s1 conformation by interactions between the base, lid, and core. During the transition from the s1 to the s3 and s4 states, the ring of ATPases flattens out and adopts a shallower staircase arrangement analogous to that of other active AAA+ translocases. In these conformations, a number of different Rpts have been observed at the top of the staircase, but these different states have not yet been assigned to particular steps in the hydrolysis or translocation cycle.

Mutational analyses of the base have shown that the Rpts are functionally nonredundant and may have differential roles according to their vertical position in the spiral arrangement of the hexamer. Active site mutations for each Rpt subunit in vivo showed that nucleotide binding by Rpt1 or Rpt5 is not required for viability, and the effects of pore loop mutations in vivo were similarly varied (27, 78). In a heterologous expression system that allows for detailed biochemical investigation of otherwise-lethal mutations in the proteasome ATPases, eliminating the ATP-hydrolysis activity in the Rpt subunits that adopt the top positions in the s1-state spiral (Rpt3 and 4) leads to the most severe defects in substrate processing, but not necessarily the strongest defect in ATP hydrolysis (26). These experiments suggest a particular role of those subunits closest to the pore entrance in facilitating substrate engagement and the transition out of the s1 state.

Another common feature of other related AAA+ motors is allosteric interactions that constrain subunits to bind at most four nucleotides per hexamer at any one time (75, 79-82). Similar allosteric networks have also been identified in the proteasome homolog PAN and in the 26S proteasome (60, 83-85). Recent higher-resolution EM studies have now begun to reveal the nucleotide occupancies of individual Rpt subunits in the proteasome, though in many cases the limited resolution of the nucleotide prevented distinguishing between ADP and ATP (Figure 1.3c). Another challenge is that averaging large numbers of particles for cryo-EM reconstructions may obscure the underlying heterogeneous arrangement of nucleotides. One intriguing study used extensive subclassifications to show that a planar s4 conformation of the Rpt ring has only four bound nucleotides, which is in agreement with scenarios observed for other motors (Figure 1.3c) (45). Thus, even though AAA+ hexamers can explore a large conformational landscape, they may share common mechanisms of translocation. In ClpX, for instance, ATP hydrolysis in one subunit can drive the motion of all other subunits owing to their rigid-body contacts and conformational coupling in the hexamer (84, 85). AAA+ motor subunits arranged in a spiral staircase may thus advance in a coordinated fashion by one register after each ATP hydrolysis event. The arrangements of Rpt pore loops in the s3, s4, and recently reported ADP-AlF_x-bound states of the proteasome also suggest a downward-directed paddling motion of individual subunits to propel substrate through the central pore (Figure 1.3d).

In addition, the substrate polypeptide seems to play a role in the allosteric control of AAA+ motor activity. For most AAA+ protein unfoldases, engagement and threading of a polypeptide stimulate ATPase activity, likely because subunits exert force on each other through substrate-mediated contacts between pore loops (84, 85). This bridging of pore loops by the substrate and the reciprocal application of force between ATPase subunits may also be responsible for the transition of the RP from the s1 to the s3 or s4 conformations upon substrate engagement. Moreover, an intriguing consequence of the proteasome's complexity and architecture is a novel mode of long-range allosteric communication that is mediated by the ubiquitin-conjugated substrate polypeptide. Through mechanical tension on the substrate, the proteasomal AAA+ motor appears to induce a conformational switch in the Rpn11 DUB located ~40 Å away, above the entrance to the central pore, thus stimulating cotranslocational deubiquitination (42).

Substrate Requirements for Proteasome Degradation

Even though the proteasome processes a large variety of proteins in the cell (4), all of its substrates must possess two essential parts: a targeting signal and an unstructured initiation region (86, 87) (Figure 1.2). Various recent studies using different model substrates have provided more clarity on the precise nature of both requirements. The predominant targeting signals in vivo are polyubiquitin chains, which are formed by first covalently attaching the C terminus of ubiquitin via an isopeptide bond to a substrate lysine and then repeatedly linking additional moieties to lysines in ubiquitin (1). Depending on the lysine-linkage type, these chains exhibit variable compactness and distinct conformations, which serve as a ubiquitin code to control substrate targeting. Proteins modified with one or several K11-, K48-, K29-, and, at least in vitro, also K63-linked chains are recruited to the proteasome by interacting with the intrinsic ubiquitin receptors Rpn1, Rpn10, and Rpn13, or the transiently bound ubiquitin receptors Rad23 and Dsk2 (19, 88-97). A single tetraubiquitin chain is a more effective targeting signal than a single monoubiquitin, but multiple short (mono- or di-) ubiquitin modifications can also lead to efficient degradation (98, 99). Some natural substrates have intrinsic affinity for the proteasome (100, 101), but proteins can also be targeted by artificial ubiquitin-independent tethering systems or fusions to proteasome components such as Rad23 and Rpn10 (47, 87, 102-105). These numerous delivery strategies imply sufficient flexibility provided by the ubiquitin chain, linkers in ubiquitin receptors such as Rpn10 and Rad23, or flexible segments in artificial recruitment systems to allow the substrate to properly orient itself for insertion of its initiation region into the pore (Figure 1.4).

The presence of an unstructured region, either at the terminus or as an internal flexible loop, is a strict prerequisite for degradation by the proteasome (106, 107). Intrinsic subunits of the proteasome complex or transiently bound factors lack flexible segments suitable for engagement and thus avoid degradation. As a proof of principle, the addition of a flexible initiation region at the terminus of Rad23 leads to efficient degradation, whereas an internal unstructured region inherent to Rad23 is not long enough to engage with the proteasomal motor (104). The minimum length requirement for a terminal initiation region is ~20–30 amino acids (the requirements for an internal initiation region are more strict), and its distance from the targeting signal, e.g., the substrate-attached ubiquitin chain, influences the rate of proteasomal processing (46, 98, 104). It remains unclear how the length requirement for the initiation region is affected by certain characteristics of the ubiquitin chain, for instance, linkage type or branching, that may determine which of the ubiquitin receptors on the proteasome is preferentially used for substrate delivery (see the section titled Ubiquitin Recognition at the Proteasome and Figure 1.4).

The requirements for a sufficiently long handle on the substrate are not surprising, given the structural features of the proteasome, with the static N-ring above the AAA+ domain hexamer forming the only entrance to the central processing channel (Figure 1.2). Thus, there is a 30–40-Å gap between this constriction point at the entrance and the pore loops of the motor that must engage the substrate polypeptide to drive translocation and unfolding. For proteasome substrates that do not contain an intrinsic, flexible initiation region, another hexameric AAA+ unfoldase, Cdc48 in yeast and p97 or VCP in higher eukaryotes, may completely or at least partially unfold

them to create a handle for proteasomal processing (108, 109). Cdc48 does not depend on extended flexible regions in its substrates, possibly because it lacks an N-ring above the AAA+ motor and the central channel with its translocating pore loops is more easily accessible even for well-folded proteins (110). However, the detailed mechanisms for substrate recognition and engagement by Cdc48 remain elusive.

An unstructured region not only is required for reaching the translocation machinery deep in the proteasome central pore but also plays an important role in committing substrates to proteasomal processing (111). This commitment step is critical for direct coupling between substrate degradation and deubiquitination at the proteasome (42). The sequence composition of this region has large effects on the rate at which a substrate is degraded both in vivo and in vitro (112-115). Compared with diverse regions, those with lower sequence complexity and small side chains (i.e., stretches of serines or glycines) lead to much less efficient degradation, and other parameters such as flexibility, hydrophobicity, and charge further modulate such effects (114). One explanation for sequence dependence could be that the AAA+ pore loops need a good grip on the substrate polypeptide chain both to prevent backsliding and escape and to apply a high enough unfolding force when the first folded domain of the substrate arrives at the entrance to the pore. For instance, introducing a low complexity sequence in front of a stably folded domain appears to compromise motor grip, thus encouraging slippage and subsequent release of partially processed substrate (106, 112, 113, 115). Such degradation stop signals allow for partial proteasomal degradation and consequent activation of transcription factors such as NFκB, Spt23, and Mga2, which are engaged at an unstructured but slippery internal loop (116). The biophysical basis for the sequence dependence of motor grip is still unclear, but it is conceivable that the lack of large side chains weakens the steric interaction between the substrate polypeptide and the pore loops of the AAA+ motor.

Although recent research has explored the minimum requirements for a substrate, a thorough mechanistic and structural understanding of how the proteasome recognizes a substrate is still lacking. The difficulty lies both in the complexity of substrate recognition by ubiquitin receptors (discussed in the following section) and in the significant challenges of producing large quantities of model substrates with defined ubiquitin modifications. Ideally, a structure with visibly bound substrate would help to fully elucidate the proteasome's interactions with ubiquitin and the substrate polypeptide.

Ubiquitin Recognition at the Proteasome

Before a flexible initiation region can engage with the AAA+ motor, the substrate needs to be recruited to the proteasome through interactions of its ubiquitin modification with intrinsic or extrinsic ubiquitin receptors. The proteasome contains at least three intrinsic receptors: the UIMs (ubiquitin-interacting motifs) of Rpn10/S5a, the Pru (plextrin-like receptor for ubiquitin) domain of Rpn13/ADRM1, and the T1 site of Rpn1/PSMD2 (Figure 1.4a) (19-22, 117).

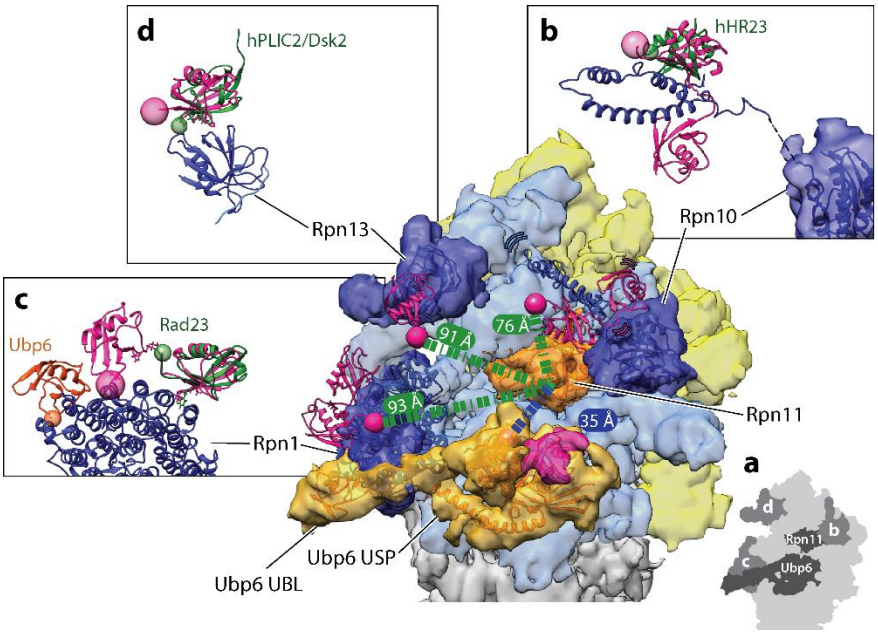

Figure 1.4. Ubiquitin receptors and DUBs (deubiquitinases) at the proteasome.
(a) Cryo-electron microscopy (EM) reconstruction of the 26S proteasome in complex with ubiquitin-bound Ubp6 (EM: 3034; PDB: 5a5b) (56), with EM density for the lid shown in yellow, the base in light blue, the core particle in gray, Rpn11 in orange, Ubp6 in lighter orange, and individual ubiquitin receptors in darker blue. A schematic version highlighting the DUBs and ubiquitin receptors labeled by figure panel is shown in the inset (lower right). The essential DUB Rpn11 (orange) sits just above the N-ring pore with its active site 35 Å away from the active site of Ubp6 (lighter orange, with bound ubiquitin density in pink). Bridging EM density links Ubp6's ATPase-contacting ubiquitin-specific protease (USP) domain to the UBL (ubiquitin-like) domain bound at the T2 site of Rpn1. The UBL domain of Mus musculus Ubp6 (PDB: 1wgg) (orange ribbon) is fit into the EM density seen at the T2 site of Rpn1, using Chimera's Fit in Map tool. The USP domain of Ubp6 (PDB: 5a5b) is also depicted as an orange ribbon within the EM density. Each ubiquitin receptor on the proteasome is shown with the ribbon diagram of the EM-based atomic model docked into the EM density. Proteasome-bound ubiquitin (pink ribbon) is modeled by docking existing ubiquitin-receptor costructures into the EM density for each ubiquitin receptor. K48-linked diubiquitin bound to the dual UIMs (ubiquitin-interacting motifs) of human S5a/PSMD4 (Rpn10) is shown in a possible location on the proteasome, placed by confining the most N-terminal residue of the UIM structure 17 Å from the most C-terminal residue of the EM docked Rpn10 VWA (von Willebrand factor type A) domain. This constraint is determined by the five amino acid linker unresolved between the UIM and VWA domains in the available structures of the Homo sapiens Rpn10 homolog (PDB: 2kde) (118). (b) The side view of the human S5a/PSMD4 (Rpn10) with bound diubiquitin highlights the gap (dashed line) between the VWA domain and the UIMs. In organisms containing more than a single UIM in Rpn10, UBLs such as hHR23 (dark green) can bind to the UIM2 site in a similar manner as ubiquitin, as illustrated by overlaying the hHR23 S5a structure with the ubiquitin dimer-bound structure of S5a (PDB: 1p9d) (119). Here, the C terminus of ubiquitin (pink sphere) is shown 76 Å from the active site of Rpn11, but this distance is only a single possibility owing to the flexibility in the linker between the UIMs and the VWA domain anchoring Rpn10 to the proteasome. (c) The T1 site of Rpn1 is shown bound to the K48-linked ubiquitin dimer, with the free ubiquitin C terminus (pink sphere) sitting 93 Å from the active site of Rpn11 (distance indicated as green dashed line) (PDB: 2n3v) (19). Side view compares the interaction of UBLs or ubiquitin with Rpn1. Rad23 (dark green) interacts with the portion of the T1 Rpn1 site that is bound by the distal ubiquitin (the ubiquitin without a free C terminus in the dimer) in the

ubiquitin dimer-bound structure (PDB: 2nbw) (120). The free C terminus of ubiquitin is highlighted with a pink sphere, whereas the most C-terminal residue of Rad23 is highlighted with a smaller green sphere. The *M. musculus* Ubp6 UBL is placed at the T2 site, which is distinct from the T1 ubiquitin binding site. The structure of the human Rpn13 homolog ADRM1 (dark blue) (PDB: 5v1z) (121) in complex with ubiquitin and the respective Rpn2 peptide is placed into the EM density, using the orientation defined by Wehmer et al. (15) (PDB: 5mpd). This orientation places the C terminus of ubiquitin 91 Å from the active site of Rpn11. (d) The UBL of Dsk2 binds to Rpn13 in a similar manner as ubiquitin, highlighted by the overlay of the ADRM1 bound to hPLIC2, a Dsk2 homolog (dark green) (PDB: 2nbv) (120), with the C-terminal residues indicated by same-colored spheres.

Each ubiquitin receptor is placed approximately the length of a tetraubiquitin from the entrance to the N-ring through which substrates are threaded into the motor (Figure 1.4a). Placement on the periphery of the proteasomal complex provides these receptors with some flexibility, which may allow the proteasome to accommodate substrates with diverse geometries of ubiquitin chains and folded domains, not only during initial recruitment, but also for engagement, unfolding, and deubiquitination. Accordingly, Rpn13 and Rpn1 consistently show the lowest resolution in EM reconstructions of the proteasome, and even the ubiquitin receptor–containing portion of Rpn10 has yet to be definitively localized. Rpn10 binds the proteasome via a VWA (von Willebrand factor type A) domain, and, depending on the organism, one to three UIMs are attached to this domain through flexible linkers (27, 122). This flexible attachment of UIMs allows them to explore a wide radius around the RP, which may also explain some of the previously observed unexpected crosslinking between ubiquitin and nonreceptor subunits (27), (122-124).

In addition to the intrinsic receptors Rpn1, Rpn10, and Rpn13, several extrinsic receptors can deliver substrates through dynamic interactions with both the proteasome and ubiquitin chains. These receptors act by combining ubiquitin-chain recognition through ubiquitin-associated (UBA) domains with proteasome binding via a flexibly tethered, N-terminal UBL domain (125-129). Whereas *S. cerevisiae* contains the shuttle receptors Rad23/hHR23 and Dsk2/hPLIC2/ubiquilins, higher eukaryotes contain many more paralogs, along with other UBL/UBA-containing proteins that have not been implicated in direct proteasome delivery. Despite their similar domain architectures, different shuttle-receptor paralogs appear to have distinct preferences for specific intrinsic ubiquitin receptors owing to differences in their individual UBL interfaces (120). The dynamic nature of these interactions has complicated a reliable determination of which intrinsic receptor is bound by individual shuttle receptors, and some UBLs can support proteasome delivery in vitro even if they are unlikely to act in that capacity in vivo (105, 130, 131). Differences in the number of UIMs present in Rpn10 also complicate the assignment of the preferential proteasomal binding site for UBLs. In organisms where Rpn10 contains multiple UIMs, the second UIM acts as a binding site for extrinsic receptors such as the Rad23 homolog hHR23 (Figure 1.4b) (118). However, recent structural studies on Rad23 and hPLIC2, a homolog of Dsk2, clearly define the molecular basis for their preferences to bind the Rpn1 T1 site and Rpn13/Adrm1, respectively, in a manner similar to ubiquitin binding to those sites (Figure 1.4c,d) (120).

Utilizing extrinsic receptors with their flexible domain architecture may allow the proteasome to accommodate an even wider variety of substrate geometries and ubiquitin modifications than with the stably bound intrinsic receptors alone. Extrinsic receptors can also provide proteasomal substrate selection upstream of ubiquitination by recognizing and binding disordered regions of substrates, and using their UBL domains to interact directly with E3 ubiquitin ligases, which allows them to shuttle condemned proteins from ubiquitination to proteasomal degradation (96, 132-135). As a result, misfolded or mistargeted proteins that would not be recognized by the proteasome's intrinsic ubiquitin receptors due to the lack of a permanently unstructured region or ubiquitin chains can still be directed to the proteasome (135).

The proteasomal ubiquitin receptors do not exhibit exclusive binding of certain ubiquitin-chain linkages, in agreement with in vivo and in vitro findings that all linkage types can be recognized as a signal for degradation at the proteasome (93, 136). However, each receptor provides unique contributions to linkage-type preferences, with intrinsic receptors preferring K48-linked chains over other linkage types, but the biological relevance of these overall preferences remains unclear (120, 123, 137, 138). In vivo, specific recruitment of substrates with K48-linked ubiquitin chains for proteasomal degradation may be largely determined by the linkage-type specificity of Cdc48-dependent processes upstream of the proteasome, rather than the linkage-type preferences of the proteasomal ubiquitin receptors (138)). Disruption of ubiquitin binding to single or several ubiquitin receptors is well tolerated in *S. cerevisiae* but leads to accumulation of polyubiquitinated species (139), speaking to the overlapping functions of ubiquitin receptors in substrate recruitment. Similarly, known proteasome substrates are stabilized in a variety of different receptor-knockout backgrounds, consistent with largely overlapping substrate pools for individual receptors (138, 140). In higher eukaryotes, deletion of single proteasomal receptors suggests incompletely overlapping roles in substrate recruitment. Deletion of Rpn10's UIMs, for instance, is embryonically lethal in *Mus musculus*, whereas deletion of Rpn13 produces viable mice with tissue-specific proteasome defects that can be magnified by codisruption of Rpn10 in those same tissues (141-143). So, even though receptor-specific essential substrates are apparently not present in *S. cerevisiae*, they seem to exist in higher eukaryotes.

Variations in the location and orientation of substrate when recruited through different binding sites may have consequences for the efficiency of engagement and degradation. For example, the geometries of substrate-attached ubiquitin chains relative to folded domains influences turnover by the proteasome (46). Multiple ubiquitin receptors might also work in tandem on the same substrate, not only to increase the substrate affinity through avidity, but also to funnel a substrate toward the central pore of the base in an ideal orientation for engagement of the unstructured initiation region. Because extrinsic receptors use the same sites on intrinsic receptors as ubiquitin, simultaneous disruption of all intrinsic receptors should prevent ubiquitin-dependent substrate delivery in general; however, current mutations are not lethal despite the essential nature of the proteasome (19). It is possible that these mutations incompletely disrupt the binding of ubiquitin and extrinsic receptors, but there may also be additional uncharacterized substrate-delivery mechanisms, as hinted by ubiquitin crosslinking to sites beyond the currently established receptors (124, 144).

Finally, as each ubiquitin receptor is placed in a distinct location on the proteasome, substrates recruited through them may have differential access to other proteasome-associated factors, such as the E3 ligases Hul5/UBE3C and parkin. Parkin interacts with the ubiquitin receptor Rpn13, whereas Hul5 binds to the proteasome through Rpn2 (145, 146), yet neither has been visualized in high-resolution EM reconstructions of the proteasome. Hul5 is thought to act mainly in extending substrate ubiquitin chains, and its location on Rpn2 may make Rpn13-bound chains, for example, more accessible to this ligase. Similarly, the peripherally associated proteasome DUBs Ubp6 and Uch37 are located adjacent to different ubiquitin receptors: Uch37 binds the proteasome through Rpn13, whereas the UBL of Ubp6 is tethered to Rpn1 at the T2 site that is distinct from the T1 ubiquitin binding site (19, 147). Their proximity to ubiquitin receptors may influence the extent to which ubiquitin chains bound to one receptor or another are susceptible to deubiquitination by these proteasome-associated DUBs.

Deubiquitinases of the Proteasome

Because ubiquitin receptors guide substrates decorated with ubiquitin and ubiquitin chains to the proteasome, it is not surprising that the proteasome contains DUBs capable of removing or editing the ubiquitin signal. In isolation, these DUBs have fairly poor isopeptidase activity, but their activities are increased upon interaction with the proteasome. This allosteric relationship between the DUBs and the proteasome works both ways: In turn, the various catalytic functions of the proteasome such as ATPase activity, gate opening, and substrate degradation are activated or repressed in the presence of DUBs. EM has identified these DUBs in key locations within the RP, either near ubiquitin receptors or, in the case of Rpn11, directly above the N-ring and the entrance to the central processing channel (Figure 1.4a). Recent studies have provided structural insights into DUB activation by the proteasome, how these enzymes affect the proteasome conformational states, and what potential role they play in substrate degradation.

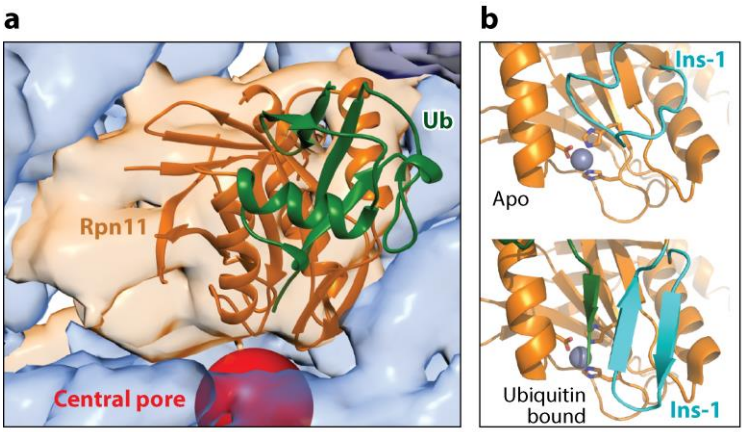

Figure 1.5. Crystal structures of proteasomal DUBs.
(a) Crystal structure of Saccharomyces cerevisiae Rpn11 (orange) bound to ubiquitin (green) (PDB: 5u4p) (42) and docked into the electron microscopy density with Ubp6 removed for clarity (EM: 3034; PDB: 5a5b) (56). The central pore is highlighted by a red sphere. (b) Arrangement of the Ins-1 loop of Rpn11 (cyan) in (top) the unbound apo state (PDB: 4o8x) (155) and in (bottom) the ubiquitin-bound state (PDB: 5u4p) (42), with the C-terminal tail of ubiquitin in green. The catalytic zinc ion (gray sphere) is shown

coordinated by the catalytic residues (stick representation). Abbreviations: DEUBAD, deubiquitinase adaptor; DUB, deubiquitinase; Ins-1, Insert-1; Ub, ubiquitin.

The most important proteasomal DUB is Rpn11, a JAMM metalloprotease closely related to the NEDD8 isopeptidase CSN5 of the COP9 signalosome (148). Rpn11 contains a catalytic zinc ion, coordinated by an $EX_nHXHX_{10}D$ metal-binding motif (31, 32), and is absolutely essential for proteasome function and cell viability (149-151). The catalytic-site mutations His109Ala and His111Ala (referred to as the AXA mutation) do not disrupt assembly of the proteasome or its conformational states, but they do inhibit degradation and are lethal in yeast (31). Rpn11 resides just above the N-ring of the AAA+ motor and adjacent to the ubiquitin receptor Rpn10, in a location that is ideally suited for its key role in deubiquitination after the substrate is engaged, but before the AAA+ ATPase would unfold ubiquitin (Figures 1.4 and 1.5a). Importantly, Rpn11's proximity to the N-ring sterically precludes cleavage between folded ubiquitin moieties and, thus, within ubiquitin chains (152). Instead, it removes ubiquitin modifications en bloc by hydrolyzing the isopeptide bond at the very base of the chain between the substrate lysine and the C terminus of the first ubiquitin moiety (32).

Rpn11 and the neighboring lid subunit Rpn8 form an obligate heterodimer that can be expressed and purified in isolation. Crystal structures of this Rpn11/Rpn8 dimer elucidated that Rpn11 does not interact with the substrate moiety on the proximal side (the site closest to the substrate) of the scissile isopeptide bond (152, 153), explaining its high promiscuity and ability to remove ubiquitin chains from the wide variety of proteasome substrates. Crystal structures also revealed that the Insert-1 (Ins-1) region of Rpn11 forms a loop that covers the catalytic groove, restricts access to the active site, and inhibits DUB activity. Within the isolated lid, Rpn5 further stabilizes this inhibited state of the Ins-1 loop, preventing Rpn11 from acting as an efficient DUB until it is incorporated into the proteasome (154). This is in contrast to related DUBs, such as Sst2 and AMSH-LP, that act in isolation and whose Ins-1 region adopts a beta-hairpin conformation with an accessible active site (155-157). As shown by a recent ubiquitin-bound structure of Rpn11/Rpn8, interaction with ubiquitin induces the conformational switch of Rpn11's Ins-1 loop from the closed state to the active beta-hairpin structure (Figure 1.5b). Biochemical studies also uncovered how this switch and a tight regulation of Rpn11's DUB activity are critical for efficient substrate degradation by the proteasome (42). Disrupting the inhibitory closed state of Ins-1 increases DUB activity but leads to surprising degradation defects and substrate escape from the proteasome owing to premature ubiquitin-chain removal prior to engagement. The inhibitory closed state of Rpn11's Ins-1 loop enables the essential coupling between degradation and deubiquitination in which substrate translocation by the AAA+ motor accelerates the conformational switch of Rpn11 and deubiquitination only for committed substrates.

Ubp6 (Usp14 in human) was first identified as a proteasomal DUB by using the inhibitor ubiquitin-vinylsulfone, which specifically targets the catalytic cysteine of this USP (158). Deleting Ubp6 from the proteasome accelerates the degradation of model substrates in vitro (57)

and is not lethal in *S. cerevisiae* (150). However, this deletion leads to a growth defect owing to increased degradation of proteasome substrates, aberrant ubiquitin turnover, and depletion of free ubiquitin (147). Mouse embryonic fibroblasts with a Usp14 knockout show increased presence of Rpn13 and Uch37 on the proteasome, suggesting overlapping roles for Usp14 and Uch37 (159).

Interaction with the proteasome activates Ubp6 ∼300-fold (147), and shifting the RP conformation toward s3 by trapping Rpts with the slowly hydrolyzed ATPγS leads to an additional twofold increase in cleaving the ubiquitin-AMC model substrate (47). An N-terminal UBL domain tethers Ubp6 to Rpn1, but contacts of its catalytic USP domain with the coaxially aligned N-ring and the AAA+ ring of the base are required to displace inhibitory loops, expose the active site, and stimulate DUB activity (19, 47, 147). Owing to this specific interaction with the base in the engaged states, Ubp6's DUB activity acts as a sensor of the proteasome conformation (47, 57). At the same time, ubiquitin-bound Ubp6 stimulates the ATPase activity and 20S gate opening and inhibits substrate engagement by destabilizing the s1 state or preventing proteasome conformational switching back to s1 (47, 58). The interaction with the base places the active sites of Ubp6 and Rpn11 just 35 Å apart, allowing Ubp6 to also interfere with ubiquitin binding to Rpn11 (Figure 1.4a). Taken together, these findings indicate that Ubp6 plays a key role in allosterically regulating the proteasome, in part depending on its own occupancy with ubiquitin.

Interestingly, when the USP domain is docked against the base and thus fully activated, the N-ring of the ATPase hexamer sterically overlaps with the proximal ubiquitin binding site of Ubp6, similar to the N-ring clash that prevents binding of a proximal ubiquitin moiety to Rpn11.Therefore, the biochemical behavior of Rpn11 and Ubp6 is similar: With poor cleavage of free ubiquitin chains and a preference for cleavage at the base of substrate-attached chains, they release ubiquitin modifications en bloc (33). However, Ubp6 cleaves long, unanchored K48-linked chains better than does Rpn11 (160), and it can cleave ubiquitin chains only when more than one chain is attached to a substrate (33). Furthermore, it cannot substitute for Rpn11 in complete deubiquitination of substrates. Ubp6 has thus been implicated in removing supernumerary ubiquitin chains (33), but the underlying mechanisms remain unknown.

Future Directions

The past few years have provided us with a wealth of exciting new insights into the structure, molecular mechanisms, and regulation of the 26S proteasome. Based on its architectural and functional complexity, the proteasome can certainly be seen as the destructive counterpart of the ribosome. Whereas the ribosome utilizes an intricate machinery to synthesize the entire multifarious pool of cellular proteins with high fidelity, the proteasome combines strict substrate selectivity with extreme promiscuity and nondiscriminative processing to degrade hundreds of different proteins with various structural, chemical, and biophysical characteristics. This balancing act is enabled by the complex architecture of the proteasome and a series of degradation steps that are well coordinated, in part through significant conformational changes of the RP.

Since the first subnanometer reconstruction of the proteasome in 2010 (161), cryo-EM and other structural techniques have yielded atomic-resolution models for most proteasomal subunits and revealed a whole series of conformational states that represent a critical structural framework for mechanistic studies of proteasome function and regulation. One of the important challenges lying ahead of us now is to correlate these proteasome conformations with individual steps of substrate processing and reconstruct the entire degradation pathway. Furthermore, we are just starting to understand how the ubiquitin code contained in the position, length, and linkage type of ubiquitin chains may affect substrate recognition and turnover. Recent progress in creating new model substrates with defined ubiquitin chains and biophysical characteristics, combined with advancing knowledge about proteasomal ubiquitin receptors and DUBs, will allow important investigations into the proteasome's selection of appropriate substrates and the fine-tuning of degradation activities. Such fine-tuning and preferential protein degradation may be prerequisites for the proteasome's ability to orchestrate many vital processes that depend on rapid turnover of regulatory proteins, while also fulfilling critical housekeeping functions in protein homeostasis.

Chapter 2: Recombinant expression, unnatural amino-acid incorporation, and site-specific labeling of 26S proteasomal subcomplexes

This chapter is a protocol for the incorporation and labeling of 4-azido-L-phenylalanine (AzF) into the recombinantly expressed base and lid sub-complexes. It was adapted from Bard JAM, Martin A. (2018) Recombinant expression, unnatural amino-acid incorporation, and site-specific labeling of 26S proteasomal subcomplexes. Methods in Molecular Biology. *In press.*

The method presented below was chosen after extensive testing of other methods for the site-specific labeling of the base which are not presented here. I relied on the help and expertise of a number of people during this process, including Corey Dambacher, Alison Altman and Matt Francis. The project started with the goal of introducing a fluorophore into the base which would FRET with an incoming substrate. The original attempt at labeling was to introduce a cysteine at Rpt1-I191, in the linker between the OB-fold and the AAA+ domain of Rpt1. Analysis of this labeled base by SDS-PAGE revealed extensive off-target labeling. This was unsurprising, as an inspection of molecular models of the proteasome revealed many surface-exposed cysteines. Rather than design a cysteine-lite version of the base, which would have required extensive mutation, I decided to pursue the incorporation and labeling of an unnatural amino-acid into the recombinantly expressed base. I originally received advice from Corey Dambacher, who recommended incorporating p-acetylphenylalanine (162). The Schultz group provided me with the appropriate plasmids for the expression of the tRNA synthetase. However, the labeling efficiency of the acetyl group was low and I thus turned towards the incorporation of either component of the "click" reaction between an azide and an alkyne. One option was to incorporate the pyrrolysine analog (S)-2-Amino-6-((prop-2-ynyloxy)carbonylamino)hexanoic acid, which contains a terminal alkyne group (163). The Chin group generously provided a plasmid containing the pyrrolysine synthetase and Alison Altman helped me with the synthesis of the pyrrolysine analog. However, I was unable to efficiently incorporate the unnatural amino acid.

I was aided by the timely work of Amiram et al., who developed a highly efficient synthetase for the incorporation of AzF (164). I successfully purified base with the incorporated AzF, but my original attempts at labeling using the copper-catalyzed click reaction were not successful. Recent high-resolution structures of the proteasome have revealed that the labeling location (Rpt1-I191) is slightly recessed. Thus, one reason for the failure of the copper-catalyzed reaction could be that the fluorophore and the required Cu(I) stabilizing catalyst (tris(benzyltriazolylmethyl)amine) were unable to colocate with the incorporated azide. My next attempt was to use dibenzocyclooctyne (DBCO)-linked fluorophores which do not require a catalyst. Initial trials of this reaction revealed it to be insufficiently specific, most likely as a result of off-target cysteine reactivity (165). Matt Francis suggested the use of a protecting agent, which led to the use of the reversible Ellman's reagent to protect cysteines. The final protocol has been used to label both the base and lid subcomplexes in a number of locations. The

efficiency of labeling is most likely limited by the reduction of the azide group in E. coli to an amine.

Introduction

The 26S proteasome is the major protease in eukaryotic cells, where it is not only responsible for protein quality control and homeostasis through the degradation of misfolded, damaged, and obsolete polypeptides, but also controls a myriad of vital cellular processes by the specific turnover of regulatory proteins (4, 5, 166). Due to this role as one of the most critical proteome regulators, elucidating the proteasome's structure, mechanisms of action, and regulation has been of prime interest in the ubiquitin-proteasome field. However, the high complexity of this 2.5 MDa molecular machine with more than 34 different subunits, its compositional heterogeneity, and the critical dependence of eukaryotic cell viability on fully functional proteasomes have previously limited *in vitro* studies and mutational analyses. To circumvent these limitations of working with endogenous proteasomes, we developed systems for the heterologous expression of two proteasomal subcomplexes, the lid and the base, from *Saccharomyces cerevisiae* in *Escherichia coli* and the incorporation of unnatural amino acids to allow specific fluorescence labeling and advanced spectroscopic studies of proteasome function.

At the center of the 26S proteasome is the 20S core peptidase that is capped on one or both ends by the 19S regulatory particle, which recognizes appropriate substrates by their covalently attached ubiquitin modifications, mechanically unfolds them, and translocates the unfolded polypeptides through a narrow axial pore into the 20S core for proteolytic cleavage (10, 12, 167). This regulatory particle can be further subdivided into the base and lid subcomplexes (16, 17), which also represent the intermediates of proteasome assembly *in vivo* (6) and thus can be used as stable building blocks together with the 20S core peptidase to reconstitute the 26S holoenzyme *in vitro*. The base contains six distinct AAA+ ATPases, Rpt1-Rpt6, that form a heterohexameric ring and constitute the molecular motor of the proteasome. It also includes three non-ATPases, in yeast called Rpn1, Rpn2, and Rpn13, with Rpn1 and Rpn13 functioning as ubiquitin receptors (19, 20). The assembly of the base proceeds through the initial formation of modules containing pairs of Rpt subunits (6), which then associate to form the ATPase hexamer in the order Rpt1-Rpt2-Rpt6-Rpt3-Rpt4-Rpt5 (66), with Rpn1 bound to Rpt1 and Rpt2, and Rpn2 plus Rpn13 associated with Rpt6 and Rpt3. Correct pairing of Rpt subunits in the three modules as well as their proper assembly into the base subcomplex is controlled by four assembly factors, Rpn14, Hsm3, Nas2 and Nas6 (168-170). While Nas2 is released during this process (66), Nas6, Rpn14, and Hsm3 remain bound to the C-terminal tails of Rpt subunits until they are displaced by the base docking with the 20S core peptidase (54).

The lid subcomplex includes six PCI (Proteasome-CSN-Initiation factor 3) domain-containing subunits, Rpn3, Rpn5, Rpn6, Rpn7, Rpn9, Rpn12, the small peptide Sem1, and two MPN (Mpr1-Pad1 N-terminal) domain containing subunits, Rpn8 and Rpn11, with the latter representing the essential Zn^{2+}-dependent deubiquitinase of the proteasome (31, 32, 171). A helical bundle

formed by the C-terminal helices of the eight globular lid subunits functions as a hub to control the ordered lid assembly (172), which is independent of any additional factors (6). Another ubiquitin-receptor subunit, Rpn10, is not stably associated with the isolated lid or base, but interacts with both subcomplexes in the assembled regulatory particle.

Given this knowledge about the *in vivo* formation of lid and base, we created recombinant expression systems in *E. coli* with three compatible plasmids coding for either the nine lid subunits or the nine subunits of the base plus the four essential assembly factors, as described below (3.1 and 3.2). While the lid subunits associate without additional chaperones, the base subunits assemble efficiently only in the presence of the assembly factors. Subcomplexes are isolated by tandem-affinity purification using tags on two subunits of the lid and the base followed by size-exclusion chromatography. The use of affinity tags on two separate subunits ensures that only fully assembled complexes are purified and thus corrects for differences in the expression levels or stability of individual subunits.

One of the advantages of these heterologous expression systems is that they can be easily combined with techniques for the incorporation of unnatural amino acids (UAAs) (173). By co-expressing a synthetase/tRNA pair that has been evolved to recognize one of the Amber/Ochre/Opal codons, an UAA can be placed anywhere within the expressed proteins. These UAAs allow for the incorporation of a variety of useful chemical properties into proteins, including reactive groups for cross-linking (173), photocaged amino acids such as lysine (174), and handles for orthogonal labeling (173). The protocol below (3.3) describes how to incorporate the UAA *p*-azido-L-phenylalanine (AzF) at a UAG codon that has been introduced at a specific position in the base or lid subcomplex. The azide group of the AzF can then be conjugated to an alkyne through a cycloaddition reaction, often referred to as “click” chemistry, allowing for the site-specific modification of the complex. Incorporation of AzF into the base will be used as an example below, though the protocol can be easily adapted to the lid or any other desired recombinant protein.

The vector used for UAA incorporation, pAM87, was constructed based on a synthetase variant (pAzFRS.2.t1) evolved by the Isaacs lab and a vector (pUltra) designed by the Schultz lab that also encodes the UAG-recognizing tRNA (164, 175). Proteins with the UAG codon inserted in the desired position are expressed in *E. coli* strains carrying pAM87 with AzF added to the growth media. Once the protein is purified, the azide group of the incorporated AzF can be modified with an alkyne-containing molecule using Cu-free click chemistry (176). In the protocol below, the base is modified with a fluorophore linked to dibenzocyclooctyne (DBCO), a strained cyclooctyne that allows for mild, copper-free conjugation (177). Though designed to be bio-orthogonal, it is known that DBCO reacts with exposed cysteines (165). To suppress this reaction, free thiols are protected with Ellman’s reagent before the labeling. Once the labeling reaction is complete, the cysteines are restored to their native state through reduction with dithiothreitol (DTT).

Materials

Reagents and equipment for base and lid expression and purification.

1. Electrocompetent *E. coli* BL21 Star (DE3) cells (178).
2. Electroporation apparatus.
3. Expression plasmids (see Table 2.1).
4. 1000X ampicillin: 300 mg/mL ampicillin sodium in 50% EtOH.
5. 1000X kanamycin: 50 mg/mL kanamycin monosulfate in water.
6. 1000X chloramphenicol: 25 mg/mL chloramphenicol in 100% EtOH.
7. LB-antibiotic plates: 1% (w/v) tryptone, 0.5% (w/v) yeast extract, 0.5% (w/v) NaCl, 1.5% (w/v) agar. Autoclave, cool to 60 °C or lower in a water bath before adding appropriate antibiotics to 1X from 1000X stocks.
8. dYT liquid media: 1.6% (w/v) tryptone, 1% (w/v) yeast extract, 0.5% (w/v) NaCl. Autoclave.
9. Terrific Broth (TB): 47 g of Novagen terrific broth (Millipore) in 1 L of water + 4 mL of glycerol. Autoclave.
10. 2.5 L Ultra Yield baffled shaking flask (Thomson).
11. 0.5 M IPTG: 0.5 M Isopropyl-beta-D-thiogalactoside in water.
12. 100X PMSF: 0.2613 g phenylmethylsulfonyl fluoride in 15 mL ethanol (safety note: protease inhibitors are hazardous and should only be handled after taking appropriate safety precautions).
13. 1000X aprotinin: 1 mg/mL aprotinin in 25% methanol/75% H_20 (safety note: protease inhibitors are hazardous and should only be handled after taking appropriate safety precautions).
14. 1000X pepstatin = 1 mg/mL pepstatin A in 90% methanol/10% acetic acid (safety note: protease inhibitors are hazardous and should only be handled after taking appropriate safety precautions).
15. 1000X leupeptin = 1 mg/mL leupeptin hemisulfate in H_20 (safety note: protease inhibitors are hazardous and should only be handled after taking appropriate safety precautions).
16. Benzonase nuclease.
17. NiA Buffer: 60 mM HEPES, pH 7.6, 100 mM NaCl, 100 mM KCl, 10 mM $MgCl_2$, 20 mM imidazole, 5% glycerol. Cool to 4 °C, adjust the pH, and then filter using a 0.22 µm filter.
18. NiB Buffer: NiA Buffer + 250 mM imidazole. Add dry imidazole to NiA buffer, then readjust pH to 7.6.
19. Ultrasonic homogenizer with horn attachment.
20. 125 mL metal beaker (Polar Ware).
21. 5 mL HisTrap FF crude (GE).
22. 5 M NaOH.
23. 0.5 M ATP: Dissolve 9.08 g ATP disodium trihydrate in 15 mL of water. Adjust pH to 7.0 with 5 M NaOH, then add water to a final volume of 30 mL. Aliquot and store at -20 °C.
24. Bradford reagent.
25. 2X SDS Loading Buffer: 100 mM Tris-HCL, pH 6.8, 4% (w/v) sodium dodecyl sulfate (SDS), 0.2% (w/v) bromophenol blue, 20% (w/v) glycerol. Add 10% (v/v) dithiothreitol (DTT) just before using.
26. Anti-FLAG M2 agarose (Sigma).
27. Gravity drip column.

28. TBS: 50 mM Tris-HCl, pH 7.6, 150 mM NaCl.
29. 3xFLAG peptide: Dissolve peptide in TBS. Adjust pH to 7.6 using 5 M NaOH. Then adjust final concentration of FLAG peptide to 20 mg/mL using TBS.
30. 100 kDa cutoff Ultra-15 and Ultra-0.5 centrifugal filter concentrator (Amicon).
31. Spin-X 0.22 µm 0.5 mL cellulose acetate centrifuge filter (Corning).
32. Superose 6 Increase 10/300 GL size-exclusion column (GE).
33. GF Buffer: 30 mM HEPES, pH 7.6, 50 mM NaCl, 50 mM KCl, 10 mM $MgCl_2$, 5% glycerol. Cool to 4 °C, adjust the pH, and then filter with a 0.22 µm filter.
34. 0.5 M TCEP: Add 5.73 g tris(2-carboxyethyl)phosphine-HCl to 30 mL of water. Adjust pH to 7.0 with 5 M NaOH, then adjust final volume to 40 mL with water. Aliquot and store at -20 °C.
35. 1 mg/mL BSA: Add 10 mg of bovine serum albumin (fatty acid free) to 10 mL of GF buffer. Adjust the concentration to 15 µM by measuring the A_{280} and using an extinction coefficient of 43,824 M^{-1} cm^{-1}.
36. Amylose resin (NEB).
37. 0.5 M Maltose: Add 18 g maltose monohydrate to water, adjust to 100 mL final volume, then filter sterilize with a 0.22 µm filter into a sterile bottle.
38. Human rhinovirus 3C protease (Thermofisher).
39. 8% NuPAGE SDS-PAGE gels (Thermofisher).
40. 10% NuPAGE SDS-PAGE gels (Thermofisher).
41. 20X NuPAGE MOPS running buffer (Thermofisher).
42. Coomassie blue stain: 0.25% Coomassie blue R-250, 45% methanol, 45% water, 10% glacial acetic acid. Filter before using.
43. Coomassie destain: 20% methanol, 10% glacial acetic acid.
44. UV-spectrophotometer.
45. Quartz cuvette, 20 µL sample volume (Hellma).

Reagents for expression and purification of multi-subunit complexes incorporating *p*-azido-L-phenylalanine.

1. 1000X Spectinomycin: 100 mg/mL spectinomycin dihydrochloride pentahydrate in water.
2. Unnatural amino acid incorporation plasmid (see Table 1).
3. 10X phosphate-buffer: 0.17 M KH_2PO_4, 0.72 M K_2HPO_4. Autoclave.
4. UAA Media: Add 24 g yeast extract, 20 g of tryptone and 10 mL of glycerol to 880 mL of water. Autoclave. Prepare 1 L of UAA media by adding 100 mL of 10X phosphate-buffer to 900 mL of media.
5. *p*-azido-L-phenylalanine (Amatek Chemical).
6. 5 mM DTNB: Add 5 mg of 5,5'-dithiobis-(2-nitrobenzoic acid) to 5 mL of GF buffer. Make fresh.
7. 1 M DTT: Add 1.54 g dithiothreitol to 10 mL of water. Aliquot and store at -20 °C.
8. 40 mM Fluorophore-DBCO: Dissolve fluorophore conjugated to dibenzocyclooctyne (DBCO) in DMSO to 40 mM (Click Chemistry Tools).

Methods

1 Expression and purification of the Base.

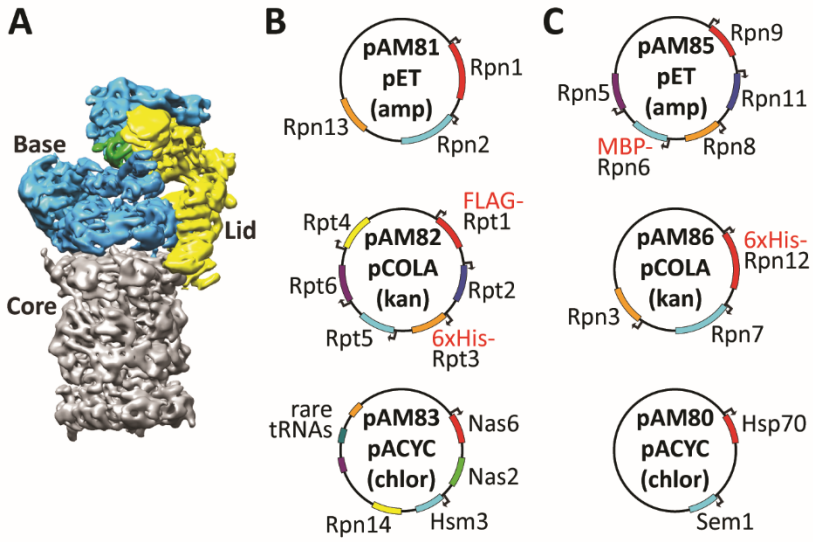

Figure 2.1. Reconstitution of the 26S proteasome.
(A) The 26S proteasome consists of three sub-complexes, the 20S core (grey), the base (blue, containing the AAA+ motor), and the lid (yellow, containing the deubiquitinating enzyme Rpn11 shown in green). (B,C) Maps of the plasmids used for expression of the base (B) and lid (C). Each plasmid was constructed by insertion of the respective proteasome-subunit genes from *Saccharomoyces cerevisiae* S288C into a duet vector (pETDuet, pCOLADuet, pACYCDuet). The majority of genes are expressed with their own T7 promoter (indicated by an arrow at the beginning of the ORF), but there is only one T7 terminator per plasmid.

Plasmid #	Description	Vector Backbone	Antibiotic marker
pAM81 (26)	Rpn1, Rpn2, Rpn13	pETDuet	ampicillin
pAM82 (26)	FLAG-Rpt1, Rpt2, 6xHis-Rpt3, Rpt5, Rpt6, Rpt4	pCOLADuet	kanamycin
pAM83 (26)	RIL rare tRNAs, Nas6, Nas2, Hsm3, Rpn14	pACYCDuet	chloramphenicol
pAM85 (modified from (28)	Rpn9, Rpn11, Rpn8, MBP-HRV-Rpn6, Rpn5	pETDuet	ampicillin
pAM86 (modified from (28)	6xHis-HRV-Rpn12, Rpn7, Rpn3	pCOLADuet	kanamycin
pAM80 (28)	Sem1, Hsp90	pACYCDuet	chloramphenicol
pAM87 (constructed from (164, 175)	pAzFRS.2.t1, UAG tRNA	pCDF	spectinomycin
pAM82* (modified from (26)	pAM82 with the UAG codon inserted at the desired location	pCOLADuet	kanamycin

Table 2.1. Expression plasmids used in this protocol.

1.1 *E. coli* Transformation and Expression of the Base.

1. Prepare electrocompetent *E. coli* BL21 Star (DE3) cells, then transform them with 50 ng each of pAM81, pAM82, and pAM83 (see Figure 1 and Table 1 for more information on the plasmids). Plate on LB + ampicillin/kanamycin/chloramphenicol. Grow at 37 °C overnight (see **Note** 1).
2. Select a single colony from the plate to inoculate 50 mL of dYT medium containing ampicillin (300 µg/mL), chloramphenicol (25 µg/mL), and kanamycin (50 µg/mL). Grow overnight at 30 °C, shaking at 180 rpm.
3. Pellet the overnight culture in a conical tube by centrifuging at 3000 rcf for 4 minutes, pour off the supernatant, and resuspend the pellet of cells in 50 mL of fresh dYT. Repeat this wash step once. Resuspend the pellet in 25 mL of dYT and divide evenly between three 2.5 L baffled flasks, each containing 1 L of TB + ampicillin (300 µg/mL), chloramphenicol (25 µg/mL), and kanamycin (50 µg/mL) (see **Notes** 2 and 3).
4. Grow cells at 37 °C in a shaker at 180 rpm for 3-5 hours, until OD_{600} reaches 0.7. Turn down the temperature to 30 °C, wait 30 minutes, then induce protein expression by adding 1 mL of 0.5 M IPTG (0.5 mM final concentration) to each flask.
5. Incubate cells for 5 hours at 30 °C, shaking at 180 rpm, and then change temperature to 16 °C and let induce overnight.
6. Spin down the culture in three 1 L centrifuge bottles for 15 minutes at 3500 rcf, pour off the supernatant and resuspend the cell pellets in cold NiA buffer + protease inhibitors and benzonase (1 µg/mL aprotinin, 1 µg/mL pepstatin, 1 µg/mL leupeptin, 174 µg/mL PMSF, 50 units of benzonase). The final volume of the combined, resuspended pellets should be 75 mL. The pellets can be transferred to 50 mL conical tubes and stored at -80 °C or carried on directly to the purification.

1.2 Purification of the base.

1. If using frozen pellets, thaw them in a water bath**. All remaining purification steps should be performed at 4 °C.** Combine the lysate into one 125 mL metal beaker, and use an ultrasonic homogenizer to sonicate the lysate on ice for 3 minutes at 75% amplitude, using a cycle of 15 s on and 60 s off (see **Note** 4).
2. Centrifuge the lysate for 30 minutes at 26,000 rcf in a pre-chilled rotor at 4 °C.
3. Prepare a 5 mL HisTrap charged with Ni^{2+} by washing the resin with 15 mL of NiA buffer (see **Note** 5).
4. Flow the lysate supernatant at 1 mL/min over the HisTrap. Take 1 µl of lysate supernatant and then take another 1 µl of HisTrap flowthrough for gel samples.
5. Wash the HisTrap with 50 mL of NiA + 1 mM ATP. **All following buffers should contain 1 mM ATP to ensure the stability of the complex** (see **Note** 6).
6. Elute the protein from the HisTrap with 20 mL of NiB buffer + 1 mM ATP. Take 2 µL of the eluate for a gel sample.
7. Prepare 5 mL of anti-FLAG M2 agarose in a gravity drip column by washing with NiA + 1 mM ATP (see **Notes** 7 and 8).

8. Flow the nickel eluate over the anti-FLAG resin 4-5 times, exposing the protein to the resin for at least 30 minutes. Take 2 µL of the flow-through for a gel sample to ensure good depletion of FLAG-Rpt1.
9. Wash the anti-FLAG column 2x with 25 mL of NiA + 1 mM ATP.
10. Elute with 12 mL of NiA + 1 mM ATP + 0.15 mg/mL 3xFLAG peptide. Take 5 µL of FLAG eluate for a gel sample (see **Note** 9).
11. Concentrate FLAG elution to 400 µL in a 15 mL 100kDa-cutoff spin concentrator by spinning at 2000 rcf at 4 °C (see **Note** 10).
12. Spin filter the concentrated protein using a 0.22 µm filter (see **Note** 11).
13. Load and run the protein on a pre-equilibrated Superose 6 Increase 10/300 GL size-exclusion column using GF buffer + 0.5 mM TCEP and 0.5 mM ATP (see Figure 2 for an example size-exclusion trace and a typical purification gel).
14. Collect the peak indicated in Figure 2, typically from 12 mL to 14 mL when run at a flow rate of 0.4 mL/min at 4 °C. Concentrate the protein by successive spins in a 0.5 mL 100kDa-cutoff spin concentrator to a final volume of 100 µL. Take 1 µL of concentrated protein for a gel sample.
15. As the presence of ATP masks the A_{280} signal for the protein, the Bradford assay is used to measure concentration of the complex with bovine serum albumin (BSA) as a standard. Typical concentrations are 5 - 15 µM base (see **Note** 12).
16. Mix gel samples with 2X SDS loading buffer and confirm the purity of the final complex by SDS-PAGE.
17. Aliquot the protein into 8 µL aliquots, flash freeze in liquid nitrogen and store at -80 °C.

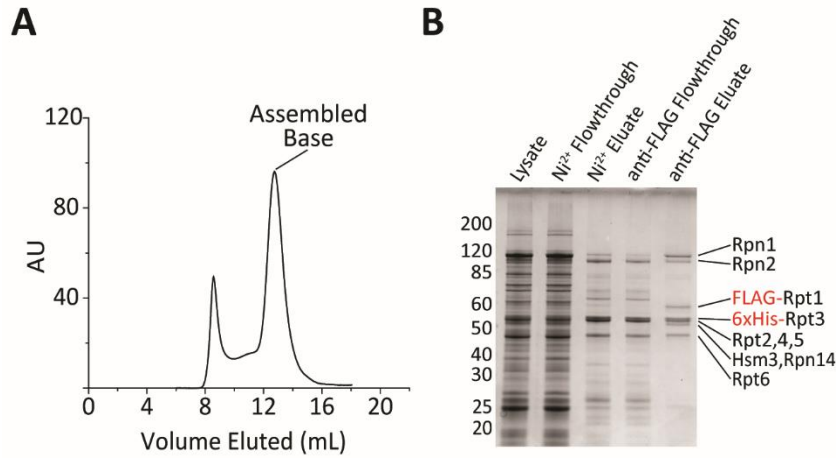

Figure 2.2. **Purification of Assembled Base.**
(A) The trace from a typical size-exclusion run of purified base is shown. The peak between the void and the assembled base contains misassembled base and on a gel looks similar to properly assembled base. (B) Gel samples from a typical base purification run on a 10% NuPAGE gel in MOPS buffer and stained using Coomassie blue.

2 Expression and Purification of the Lid.

2.1 *E. coli* Transformation and Expression of the Lid.

1. Prepare electrocompetent *E. coli* BL21 Star (DE3) cells, then transform with 50 ng of pAM85, pAM86, and pAM80 (see Figure 1 and Table 1 for more information on the plasmids). Plate on LB + ampicillin/kanamycin/chloramphenicol. Grow at 37 °C overnight (see **Note** 1).
2. Select a single colony from the plate to inoculate 50 mL of dYT medium containing ampicillin (300 µg/mL), chloramphenicol (25 µg/mL), and kanamycin (50 µg/mL). Grow overnight at 30 °C, shaking at 180 rpm.
3. Pellet the 50 mL of culture in a conical tube by centrifuging at 3000 rcf for 4 minutes, pour off the supernatant, and resuspend the pellet of cells in 50 mL of fresh dYT. Repeat this wash step once. Resuspend the pellet in 25 mL of dYT and divide evenly between three 2.5 L baffled flasks, each containing 1 L of TB + ampicillin (300 µg/mL), chloramphenicol (25 µg/mL), and kanamycin (50 µg/mL) (see **Notes** 2 and 3).
4. Grow cells at 37 °C in a shaker at 180 rpm for 3-5 hours, until OD_{600} reaches 0.7. Turn down the temperature to 18 °C, wait 30 minutes, then induce protein expression by adding 1 mL of 0.5 M IPTG (0.5 mM final) to each flask. Let the cells induce overnight.
5. Spin down the culture in three 1 L centrifuge bottles for 15 minutes at 3500 rcf, pour off the supernatant and resuspend the pellets in cold NiA buffer + protease inhibitors and benzonase (1 µg/mL aprotinin, 1 µg/mL pepstatin, 1 µg/mL leupeptin, 174 µg/mL PMSF, 50 units of benzonase). The final volume of the combined, resuspended pellets should be 75 mL. The pellets can be transferred to 50 mL conical tubes and stored at -80 °C or carried on directly to the purification.

2.2 Purification of the Lid.

1. If using frozen pellets, thaw them in a water bath**. All remaining purification steps should be performed at 4 °C.** Combine the lysate into one 125 mL metal beaker and use an ultrasonic homogenizer to sonicate the lysate on ice for 3 minutes at 75% amplitude, using a cycle of 15 s on and 60 s off (see **Note** 4).
2. Centrifuge the lysate for 30 minutes at 26,000 rcf in a pre-chilled rotor at 4 °C.
3. Prepare a 5 mL HisTrap charged with Ni^{2+} by washing the resin with 15 mL of NiA buffer (see **Note** 5).
4. Flow the lysate supernatant at 1 mL/min over the HisTrap. Take 1 µl of lysate supernatant and then take another 1 µL of HisTrap flowthrough for gel samples.
5. Wash the HisTrap with 100 mL of NiA.
6. Elute the protein from the HisTrap with 20 mL of NiB buffer. Take 2 µL of the eluate for a gel sample.
7. Prepare 7.5 mL of amylose resin in a gravity drip column by washing with 30 mL of NiA.
8. Flow the nickel eluate over the amylose resin 4-5 times, exposing the protein to the resin for at least 30 minutes. Take 2 µL of the flow-through for a gel sample to ensure good depletion of MBP-Rpn6.
9. Wash the amylose column twice with 25 mL of NiA.
10. Elute with 15 mL of NiA + 10 mM maltose. Take 5 µL of amylose eluate for a gel sample.

11. To cleave off the MBP fusion from Rpn6 and the 6xHis tag from Rpn12, add 20 µL of 2 units/µL human rhinovirus 3C protease to the eluate. Incubate overnight at 4 °C or for 2-3 hours at room temperature. After cleavage, take a 5 µL sample. Confirm complete cleavage through SDS-PAGE analysis.
12. Concentrate protein to 400 µL in a 15 mL 100kDa-cutoff spin concentrator by spinning at 2000 rcf (see **Note** 10).
13. Spin filter the concentrated protein using a 0.22 µm filter.
14. Load and run the protein on a pre-equilibrated Superose 6 Increase 10/300 GL size-exclusion column using GF buffer + 0.5 mM TCEP (see Figure 3 for an example size-exclusion trace and a typical purification gel).
15. Collect the peak indicated in Figure 3, typically from 13.5 mL to 15 mL when run at 0.4 mL/min at 4 °C. Concentrate the protein by successive spins in a 0.5 mL 100kDa-cutoff spin concentrator to a final volume of 100-200 µL. Take 1 µL of concentrated protein for a gel sample.
16. Quantify the concentration by measuring the A_{280}. The extinction coefficient calculated from the sequence is 349,000 M^{-1} cm^{-1} and the expected concentration is 10-50 µM (see **Note** 13).
17. Mix gel samples with 2x SDS loading buffer and confirm the purity of the final complex by SDS-PAGE.
18. Aliquot the protein into 8 µL aliquots, flash freeze in liquid nitrogen and store at -80 °C.

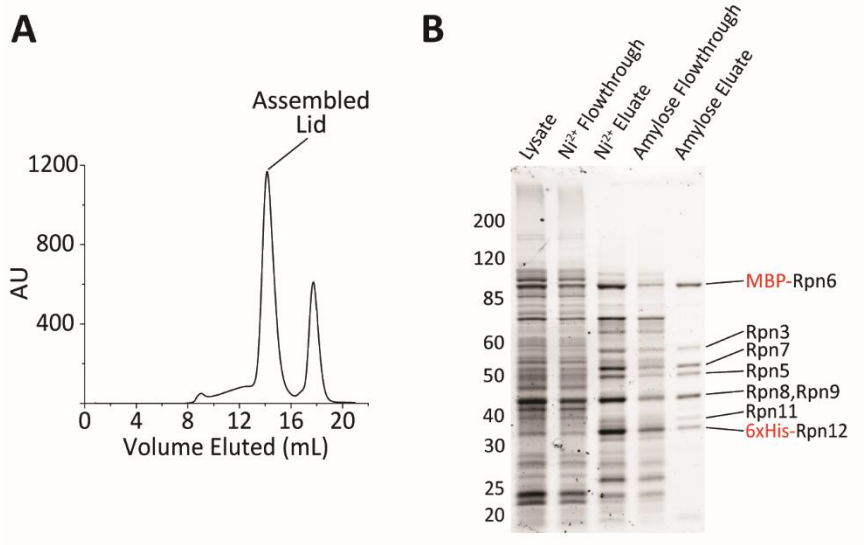

Figure 2.3. Purification of Assembled Lid.
(A) The trace from a typical size-exclusion run of purified lid is shown. The peak after the assembled lid contains mostly cleaved MBP. (B) Gel samples from a typical lid purification run on a 10% NuPAGE gel in MOPS buffer and stained using Coomassie blue.

3 Expression and purification of multi-subunit complexes incorporating unnatural amino acids.

This protocol will be presented as an abbreviated version of the base protocol presented above, focusing on the unnatural amino acid specific instructions. For more detail on the procedures see protocol 3.1. The modifications should be transferable to the purification of other complexes.

3.1 *E. coli* Transformation and Protein Expression.

1. Prepare electrocompetent *E. coli* BL21 Star (DE3) cells carrying pAM87, which contains the synthetase and tRNA for incorporation of AzF at the UAG amber codon. pAM87 confers resistance to spectinomycin. Please see **Note** 1 for a protocol.
2. Use standard molecular cloning techniques to insert the UAG amber codon at the desired location in the base subcomplex (see **Notes** 14, 15 and 16).
3. Transform pAM81, pAM82*, and pAM83 into the pAM87-containing electrocompetent *E. coli*.
4. Inoculate 2 x 50 mL cultures of dYT + ampicillin (300 µg/mL), chloramphenicol (25 µg/mL), kanamycin (50 µg/mL) and spectinomycin (100 µg/mL), grow at 37 °C overnight (see **Note** 17).
5. Wash the overnight cultures with fresh dYT twice, resuspend in 25 mL of dYT and then divide the cells evenly between 6 L of dYT + 0.5X antibiotic (ampicillin (150 µg/mL), chloramphenicol (12.5 µg/mL), kanamycin (12.5 µg/mL) and spectinomycin (50 µg/mL), in 2.5 L baffled flasks (see **Notes** 2 and 3)**.**
6. Grow the cultures at 37 °C until OD_{600} 0.7-1 is reached. Spin down the cultures in clean 1 L centrifuge bottles for 15 minutes at 3500 rcf at room temperature.
7. Gently (without vortexing), resuspend the cultures in 1 L total of UAA media, leading to a 6-fold concentration of cells. Divide into two 2.5 L baffled flasks to maximize aeration (see **Note** 18).
8. Add 0.24 g of AzF to each 500 mL culture (2 mM final), then shake for 30 minutes at 30 °C at 180 rpm (see **Note** 19).
9. Add 1 mL of 0.5 M IPTG (1 mM final) to each flask to induce expression of both the proteins of interest and the synthetase. Let induce at 30 °C for 5 hours and then 16 °C overnight.
10. Spin down the culture in two 1 L centrifuge bottles for 15 minutes at 3500 rcf at 4 °C, pour off the supernatant and resuspend the pellets in cold NiA buffer + protease inhibitors and benzonase (1 µg/mL aprotinin, 1 µg/mL pepstatin, 1 µg/mL leupeptin, 174 µg/mL PMSF, 50 units of benzonase). The final volume of the combined, resuspended pellets should be 75 mL. The pellets can be transferred to 50 mL conical tubes and stored at -80 °C or carried on directly to the purification.

3.2 Purification of the base.

1. Follow steps 1-11 of 1.2. In brief, the protein should be purified using Ni^{2+} affinity and anti-FLAG affinity columns, then concentrated to 400 µL (see **Note** 20).
2. To protect surface exposed cysteines, add DTNB to 150 µM final concentration from a freshly made 5 mM stock, incubate at 22 °C for 10 minutes (solution will turn yellow), and then cool the protein back down to 4 °C (see **Note** 21).
3. Add the DBCO-fluorophore to a final concentration of 300 µM and incubate at 4 °C overnight (see **Note** 22).
4. Add DTT to a final concentration of 5 mM from a 1 M stock to de-protect the cysteines and resolve any inter-protein disulfide bonds.
5. Follow steps 12-16 of protocol 1.2 to run the protein over the size-exclusion column. See Figure 4 for examples of labeling specificity. Typical yields are about half of the yield for unlabeled complexes.

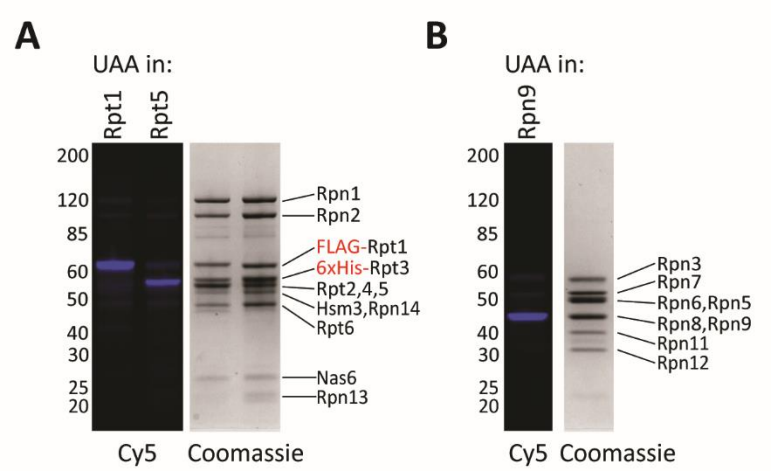

Figure 2.4. Purified and labeled sub-complexes.
(A) Base with AzF incorporated at either Rpt1 or Rpt5 was labeled with Cy5-DBCO. Shown here are the Cy5 fluorescence channel and Coomassie staining of those samples run on an 8% NuPAGE gel. (B) Lid with AzF incorporated into Rpn9 was labeled with Cy5-DBCO. As in A, the Cy5 fluorescence channel and Coomassie staining of those samples run on an 8% NuPAGE gel are shown.

Notes

1. It is important to use properly prepared electrocompetent cells. The protocol from Seidman et al. (2001) can be followed as a reference (178). Chemically competent cells are not efficient at taking up the large plasmids used here. It is possible to make electrocompetent cells from BL21 Star (DE3) *E. coli* already transformed with pAM83. This is advantageous because the efficiency of a double transformation is much higher than that of the triple transformation. For protocol 3.1 it is necessary to make electrocompetent cells containing pAM87 or another plasmid because quadruple transformations are not feasible.
2. The wash step is important to remove any secreted β-lactamase in the media, which would diminish selection for the ampicillin resistance containing plasmid pAM81.
3. The minimum recommended volume to prep is three liters, though the protocol can be scaled up.
4. The proper sonication conditions will vary depending on the instrument used, and should be optimized to maximize lysis without heating the sample. Other methods of cell lysis such as using a French Press will also work.
5. The purification can also be performed using Ni-NTA agarose. Modify the procedure by batch binding 5 mL of Ni-NTA beads with the cleared lysate for 45 minutes, then transferring to a gravity drip column for the wash and elution.
6. The purification can be monitored using Bradford reagent. Aliquot 40 µL of Bradford reagent into the wells of a 96-well plate. Then take 5 µL of column eluate and mix thoroughly with the Bradford reagent. The presence of protein will be indicated by a color change from brown to blue. After 50 mL of washing, the eluate from the HisTrap may still react with Bradford but you should nevertheless continue to the elution step. Excessive washing of the nickel column reduces yield of the final complex.

7. FLAG agarose must be regenerated before the first use by following the manufacturer's recommended protocol. The resin can then be reused by regenerating after each purification.
8. The amount of FLAG agarose used is often the limiting factor for the final yield of base. Fresh FLAG agarose has higher binding capacity than used and regenerated resin. It is recommended to confirm good depletion of FLAG-Rpt1. If FLAG-Rpt1 is still visible in the flow-through of the FLAG column, the FLAG binding, washing and eluting steps (3.1.2 7-10) can be repeated with freshly regenerated FLAG agarose.
9. Be sure to use 3xFLAG peptide (MDYKDHDGDYKDHDIDYKDDDDK), as 1xFLAG peptide does not effectively compete off the FLAG-Rpt1.
10. To prevent aggregation at the bottom of the concentrator, mix the sample by inverting the concentrator every 5-10 minutes.
11. Occasionally not all of the protein solution will go through the spin filter. If the filter has clogged, it may be necessary to switch to a fresh filter. Pool the filtered protein before running on the size-exclusion column.
12. Using BSA as a standard may result in concentrations inaccurate by as much as 2-fold due to the different reactivity of BSA with the Bradford reagent compared to the base proteins. For a more accurate concentration, the sample can be submitted for amino acid analysis. The molecular weight of the complex is 652,000 kDa, including Rpt1-6, Rpn1, Rpn2, Rpn13, Nas6, Hsm3, and Rpn14. Nas2 does not stay bound.
13. It is recommended not to use a nanodrop to measure the protein concentration as the high viscosity of the solutions interferes with accurate readings. Instead, measurements are typically taken in a 20 µL cuvette using a UV-Vis spectrophotometer.
14. The efficiency of incorporation seems to be dependent on the location of the Amber codon within the protein, but this effect is difficult to predict (179). Therefore, it is recommended to test out multiple locations within the protein to identify the ones that give the highest protein yields.
15. Another challenge is that some locations also yield truncated products, so it is also recommended to have a C-terminal tag or other means of selecting for full-length products. In the case of the base, truncated products do not incorporate well into the complex and are thus not purified with fully assembled base.
16. To ensure proper protein production, it is also necessary to replace any UAG codons that are being used as stop codons with either the Ochre or Opal stop codons.
17. The cells grow slowly under quadruple antibiotic selection, so it may be necessary to first inoculate a 5 mL culture, let that grow overnight, and then use it to inoculate the two 50 mL cultures at 1:500.
18. Concentrating the cells allows for a much higher cell density per liter of culture, allowing for more protein production for each gram of unnatural amino acid used.
19. This step gives the cells time to take up the AzF.
20. As AzF is sensitive to reducing agents, they should be avoided if possible until after the labeling step described in section 3.2 step 3. It has been reported that the azide group is somewhat compatible with βME if reducing agent is required (180).
21. Enough DTNB should be added to be in excess of the estimated number of exposed cysteines in solution, which varies between protein complexes.
22. The optimal concentration of fluorophores varies between proteins due to differences in the accessibility of the AzF. It is recommended to optimize the concentration of DBCO-

fluorophore. The efficiency of labeling can be calculated by the ratio of the concentration of fluorophore in the final protein solution (as measured by absorbance) to the concentration of protein. Specificity can be estimated by subjecting wild-type protein with no AzF incorporated to the same labeling conditions. The labeling was found to be significantly more specific at 4 °C than at room temperature.

Acknowledgements:

We thank the members of the Martin lab for helpful discussions, and the Prof. P. Schulz Lab at The Scripps Research Institute as well as the Prof. F. Isaacs Lab at Yale University for providing plasmid constructs for unnatural amino acid incorporation. J.A.M.B. acknowledges support from the NSF Graduate Research Fellowship. This research was funded in part by the US National Institutes of Health (R01-GM094497 to A.M.), the US National Science Foundation CAREER Program (NSF-MCB-1150288 to A.M.), and the Howard Hughes Medical Institute (A.M.).

Chapter 3: Deconvolution of substrate processing by the 26S proteasome reveals a selective kinetic gateway to degradation

The following chapter is adapted from Bard JAM, Bashore C, Dong KC, Martin A (2018) *Deconvolution of substrate processing by the 26S proteasome reveals a selective kinetic gateway to degradation*. Science. Submitted. *The FRET-based deubiquitination assay was originally designed and implemented by Charlene Bashore. Ken Dong prepared material including the ubiquitination machinery and 20S core particle. All authors contributed to the manuscript.*

The original impetus for this work was to investigate the timing of substrate engagement by the proteasome. The first hurdle was to site-specifically label the proteasome, which was accomplished using the protocol for unnatural amino acid labeling described above. The other major challenge was to design a suitable substrate for which both the kinetics of degradation and tail insertion could be measured. Many variants of a GFP-fusion substrate were tried, but the substrate did not behave consistently during expression and purification. The lysine-less titin and cyclin-based unstructured region were designed by Robyn Beckwith, Kris Nyquist and Charlene Bashore. The use of the titin-I27 domain alone as a substrate was facilitated by the development of an anisotropy assay to track degradation, which was designed together with Ellen Goodall and Evan Worden. One of the challenges was to dual-label the substrate, using both a cysteine for maleimide chemistry and an N-terminally linked fluorophore. The original attempt at N-terminal labeling used chemistry developed by Jim MacDonald in the group of Matt Francis (181). The 2-pyridinecarboxaldehyde conjugated fluorophore was synthesized by Kristin Wucherer, but the efficiency of labeling was insufficient. Kristin and the Francis group also generously provided access to their mass spectrometer, which was used to optimize the labeling conditions of the substrate. I was introduced to the sortase labeling method by Brooke Gardner and I received the appropriate plasmid and enough protein for initial tests from Michael Vahey in Dan Fletcher's group.

Introduction

Specific protein degradation is essential for quality control, homeostasis, and the regulation of diverse cellular processes, such as the cell cycle and stress response(182, 183). In eukaryotic cells, this degradation is primarily catalyzed by the 26S proteasome, which recognizes, unfolds, and degrades target proteins that have been modified with lysine-attached poly-ubiquitin chains(184). To accomplish its dual roles in quality control and signaling, the proteasome must be able to degrade certain proteins consistently and under tight kinetic constraints, while maintaining a high promiscuity necessary to process thousands of polypeptides with diverse characteristics, yet avoiding unregulated proteolysis of cellular proteins in general. This precise regulation is accomplished by the proteasome's complex molecular architecture and a bipartite degradation signal for substrate recognition that consists of a suitable poly-ubiquitin chain and an unstructured initiation region of sufficient length and appropriate sequence composition (46, 86, 87, 104, 111, 112).

The proteolytic active sites of the proteasome are sequestered inside a barrel shaped compartment termed the 20S core particle, which excludes folded proteins and even large

unfolded polypeptides (167). Substrate access to these active sites is controlled by the 19S regulatory particle that caps one or both ends of the 20S core, recruits ubiquitinated proteins, unfolds them, and translocates the unstructured polypeptides through a central pore into the 20S core for proteolytic cleavage. This regulatory particle can be further divided into two 9-subunit subcomplexes, the base and lid (16). The base contains multiple ubiquitin receptors and a ring-shaped AAA+ (ATPases Associated with diverse cellular Activities) motor formed by the six distinct ATPases Rpt1-Rpt6 (19-22, 96). Each ATPase subunit consists of an N-terminal helix, an OB-fold domain, and a C-terminal AAA+ motor domain. In the heterohexamer, the N-terminal helices of neighboring Rpt-subunit pairs engage in coiled-coil interactions, while the six OB-fold domains form a rigid N-ring that sits atop the ATPase ring. After ubiquitin binding, a substrate's flexible initiation region likely must reach through the N-ring before engaging with conserved pore loops of the ATPase domains for mechanical pulling that is driven by ATP binding and hydrolysis (26, 27). The lid subcomplex is bound to one side of the base and contains the deubiquitinating enzyme Rpn11. In the proteasome holoenzyme, Rpn11 is positioned near the entrance to the AAA+ motor, allowing it to remove ubiquitin chains *en bloc* from substrates during translocation (31, 32, 42, 152, 153).

Both *in vivo* and *in vitro* structural studies revealed that the 26S proteasome adopts multiple conformations, which can be divided into a substrate-free apo (s1) state and substrate-processing (s3-like) states (15, 28, 38, 39, 48, 185). In the s1 state, the primary conformation adopted by the ATP-bound proteasome in the absence of protein substrate, the ATPase domains form a steep spiral staircase, and Rpn11 is offset from the central pore of the motor, which itself is not aligned with the entrance to the 20S core. The s3-like state, which can be stabilized by stalling a substrate during translocation, appears more conducive to processive degradation, as the central channel of the motor aligns with the N-ring and the entrance to the 20S core, and it contains a more planar ATPase ring in which neighboring Rpt subunits form uniform interfaces (38). In addition, during the transition from the s1 to s3 states, the lid rotates relative to the base, placing Rpn11 in a position directly above the pore entrance, where it is able to remove ubiquitin from a substrate polypeptide as it translocates into the motor. Similar s3-like states have also been observed by incubating the proteasome with nucleotide analogs such as ATPγS (39).

Based on the available structural and biochemical information, we can infer the processing steps necessary for substrate degradation, which include the binding of ubiquitin to a proteasomal receptor, insertion of the unstructured initiation region into the pore of the ATPase motor, the removal of ubiquitin chains by Rpn11, and the unfolding and translocation of the polypeptide into the 20S core for proteolysis. However, very little is known about the relative timing and coordination of these events, and the rate-limiting step of proteasomal degradation is still unclear. It also remains elusive what induces the proteasome to switch from the s1 to the s3-like states and how these distinct conformations are coordinated with the processing pathway.

Here we reveal the complete kinetic picture of substrate processing by the 26S proteasome. We designed a series of fluorescence- and FRET-based assays to specifically measure the kinetics of individual degradation steps in a fully reconstituted and thus well-controlled system, without contamination by accessory proteins, like the non-essential deubiquitinase Ubp6 (186). These

novel tools allowed us to track the interactions between a substrate's initiation region and the AAA+ motor, the conformational changes of the proteasome, substrate deubiquitination by Rpn11, and cleavage into peptides. Our results reveal the rate-limiting step of degradation, identify the trigger for the conformational switch from the s1 to the s3 state of the proteasome, and elucidate the regulation of Rpn11's deubiquitination activity. Furthermore, we analyzed the degradation effects of varying substrate characteristics, including the stability of the folded domain, the number of ubiquitin chains, and the length and composition of the unstructured initiation region, offering new insights into how the proteasome selects and prioritizes its substrates in a complex cellular environment.

Unnatural amino-acid labeling of the proteasome

To deconvolute individual steps of substrate degradation and track the coupled conformational changes of the proteasome, we sought to develop Förster resonance energy transfer (FRET)-based assays sensitive to specific processing events. One requirement for these assays was the ability to site-specifically attach fluorophores to the 19S regulatory particle with minimal perturbation of its structure and function. Building on our previously established recombinant expression systems for base and lid sub-complexes of the *Saccharomyces cerevisiae* 26S proteasome and their purification from *Escherichia coli* (26, 28), we devised a method for the site-specific incorporation and labeling of 4-azido-L-phenylalanine (AzF) (173). We introduced a highly evolved AzF synthetase on an optimized plasmid into our base and lid expression systems, allowing for the purification of unnatural amino acid-containing sub-complexes and the covalent attachment of a fluorophore at specific sites within the 19S regulatory particle (Fig. 3.1A) (164, 175). To increase the labeling specificity, solvent-exposed cysteines of the lid and base were reversibly protected before reacting the incorporated AzF with a dibenzocyclooctyne-linked fluorophore (165). This procedure led to 50-80% labeling efficiency and minimal off-target reactions (Fig. 3.1A). Importantly, proteasomes reconstituted with these fluorescently labeled base and lid sub-complexes exhibited full activity in substrate degradation (Fig. 3.1B, Fig. 3.S1).

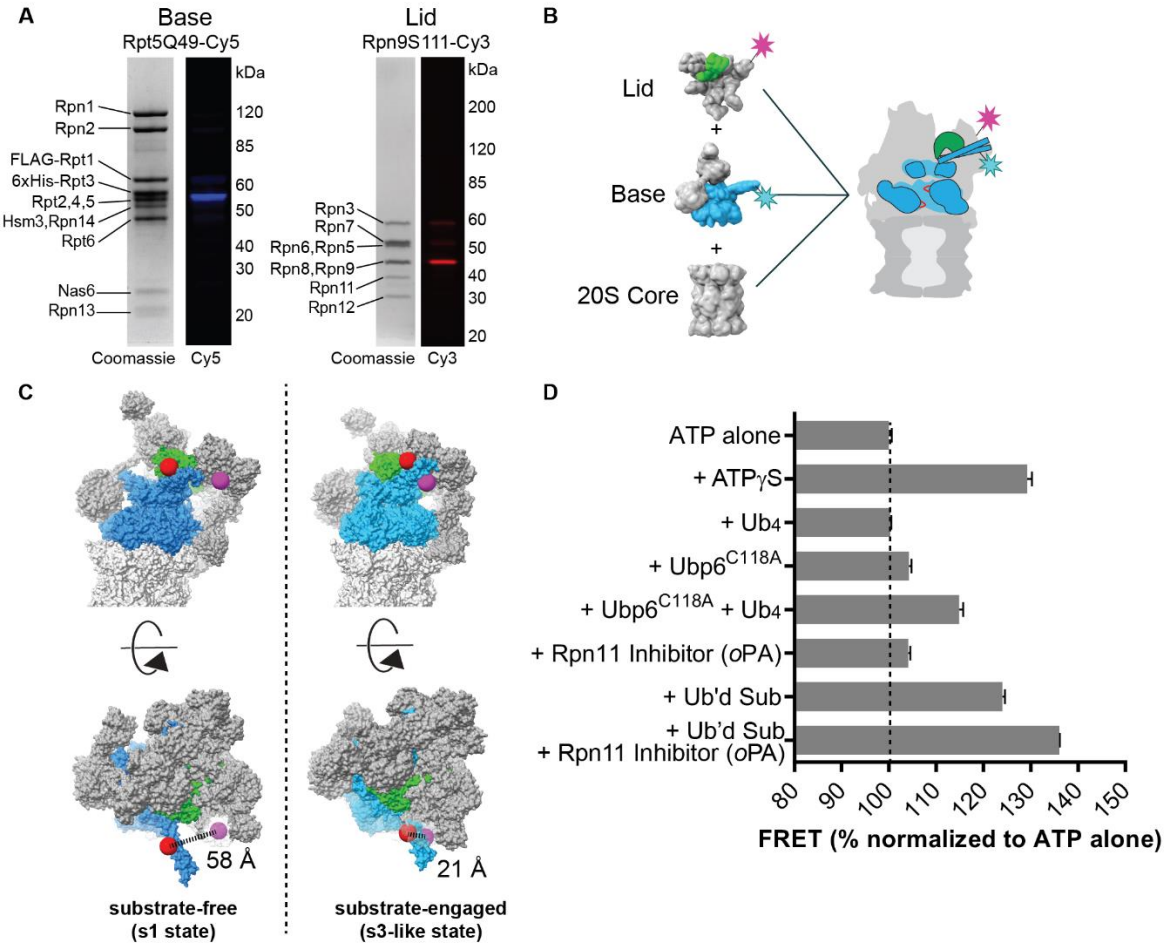

Figure 3.1. Site-specific labeling of the 26S proteasome and a steady-state assay for its conformations.

(**A**) SDS-PAGE analysis of base and lid subcomplexes with AzF incorporated into Rpn5 and Rpn9, and then labeled with Cy5 and Cy3, respectively. Images of both, the Coomassie-stained gels and fluorescence detection are shown. (**B**) Schematic for the *in vitro* reconstitution of the 26S proteasome from lid subcomplex with Cy3-labeled-Rpn9, base with Cy5-labeled-Rpt5, and 20S core. (**C**) A comparison of the substrate-free and substrate-engaged states, showing that the distance between Rpt5-Q49 and Rpn9-S111 changes by 37 Å during the conformational transition. The 26S proteasome is depicted with the AAA+ ATPases in blue, Rpn11 in green, and the rest of the regulatory particle as well as the 20S core in grey. Models were generated from surface representations of atomic models (PDB: 5mp9, 5mpd, 5mpb). The red and purple spheres indicate the positions of the labeled residues on Rpt5 and Rpn9, respectively. (**D**) Steady-state FRET signals between Cy3-labeled lid (RpnS111AzF-Cy3) and Cy5-labeled base (Rpt5Q49AzF-Cy5) under various conditions, normalized to the signal for proteasome with ATP alone. Ubp6^{C118A} is catalytically inactive, Ub_4 represents a linearly fused tetra-ubiquitin, and the ubiquitinated substrate is titin-I27^{V15P} with a 35-residue tail (titin-I27^{V15P}-35). Shown are the mean and s.d. for N=3.

Tracking the conformational state of the proteasome

Published cryo-EM structures of the 26S proteasome revealed major conformational changes between the substrate-free and substrate-processing states, yet it remains unclear how these

transitions are coupled to specific steps of substrate degradation. We identified the lid subunit Rpn9 and the N-terminal coiled-coil of the base subunits Rpt4 and Rpt5 as promising positions for the placement of a donor-acceptor pair to directly monitor the proteasome conformational dynamics through FRET (Fig. 3.1C). As the lid rotates relative to the base during the transition to a substrate-engaged state, the distance between Rpn9 and the N-terminal helix of Rpt5 decreases by almost 40 Å, and we predicted that the FRET efficiency for fluorophores at these positions would increase accordingly.

Proteasomes were thus reconstituted using lid with donor-labeled Rpn9-S111AzF and base with acceptor-labeled Rpt5-Q49AzF, and bulk FRET efficiencies were measured under steady-state conditions (Fig. 3.1D). Incubation with the non-hydrolyzable nucleotide analog ATPγS has previously been shown to induce the substrate engaged-like s3 state (39), and it correspondingly caused a significant increase in FRET compared to proteasome in ATP alone (Fig. 3.1D). Interaction with ubiquitin-bound Ubp6 has also been found to shift the conformational equilibrium towards the substrate-engaged state (47, 56), which was confirmed by our assay showing an increase in FRET efficiency when catalytically inactive Ubp6 was added together with tetra-ubiquitin. There was no change in FRET, however, when 100 μM unanchored ubiquitin chains were added, indicating that ubiquitin binding to proteasomal receptors does not induce a conformational change.

We then measured the FRET signal of actively degrading proteasomes and observed an increase in FRET similar to that of proteasomes trapped in the s3 state by ATPγS. The signal increased further upon addition of ubiquitinated substrate in the presence of 1,10-phenanthroline (*o*PA), an inhibitor of the deubiquitinating enzyme Rpn11 (31). Preventing Rpn11-mediated deubiquitination inhibits degradation by stalling substrate translocation through the central channel, most likely when the attached ubiquitin chain reaches the narrow entrance to the N-ring pore, thus trapping and synchronizing the proteasomes in a substrate engaged state (Fig. 3.S1) (42). We conclude that actively processing proteasomes spend most of the time in an s3-like conformation.

Rapid substrate engagement induces the proteasome conformational switch

While the steady-state FRET-based assay confirmed that actively degrading proteasomes switch away from the s1 state, it provided no information about when this switch occurs. To determine the relationship between the conformational change and specific processing steps, and to gain insight into the overall coordination of substrate degradation, we developed a series of fluorescence-based assays for measuring detailed kinetics (Fig. 3.2). The model substrate for these assays consisted of a titin-I27 domain that was destabilized by a V15P mutation and fused with a C-terminal unstructured initiation region (a 35 amino acid 'tail', see Table 3.S2) (47, 187). This titin-$I27^{V15P}$-35 substrate also contained a single lysine to enable the attachment of a poly-ubiquitin chain in a defined position.

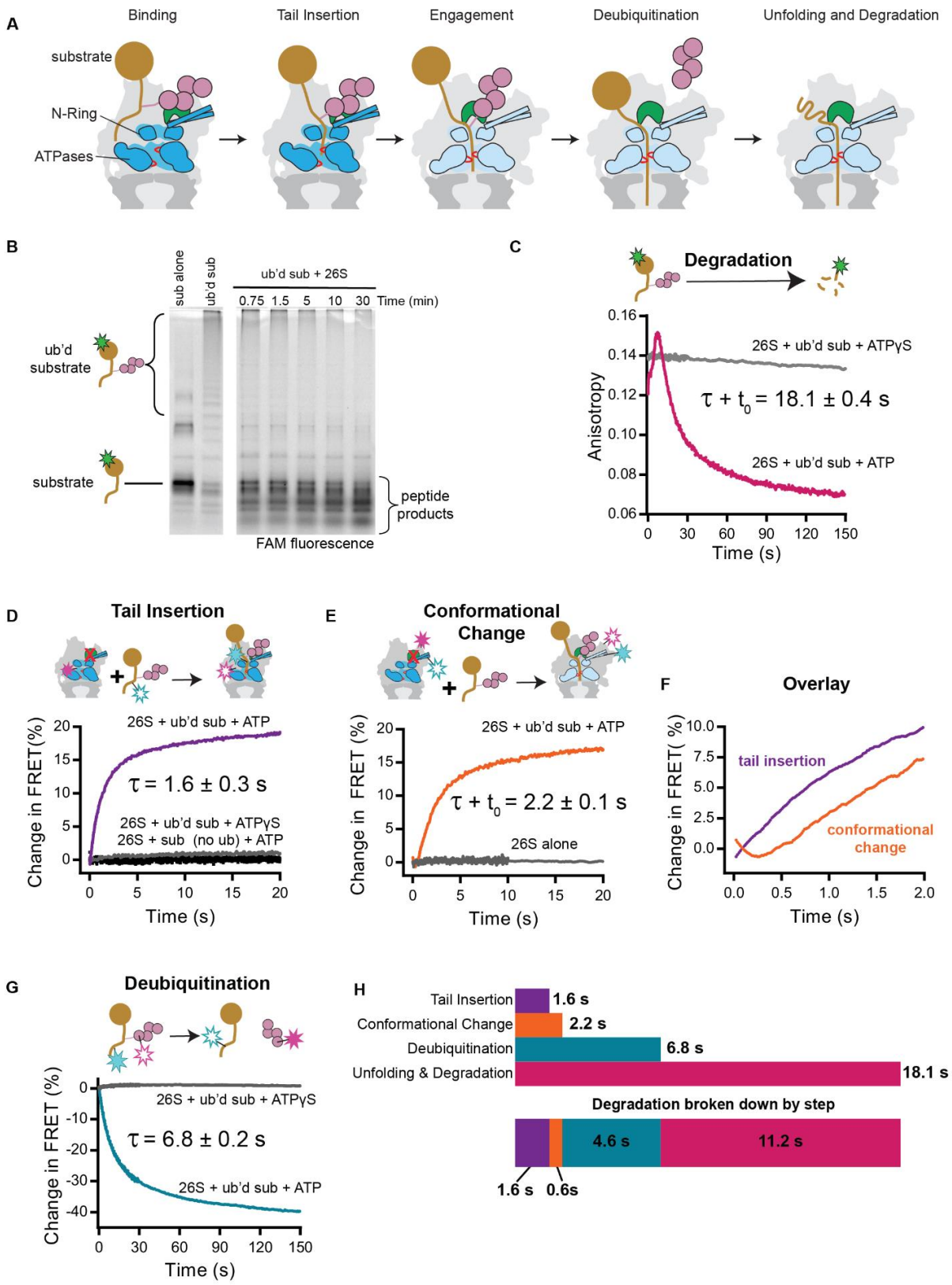

Figure 3.2. Substrate engagement triggers the conformational switch of the proteasome.

(**A**) Schematic model for the substrate processing pathway. Ubiquitin chains (pink) target a substrate (gold) to bind to the 26S proteasome, which resides in the substrate-free, s1 state. The unstructured tail of a substrate is inserted into the pore of the AAA+ motor (blue), where it interacts with pore loops (red) that drive translocation. After this substrate engagement, a major conformational change rearranges the AAA+ motor and shifts Rpn11 (green) to a central position above the entrance to the pore, allowing translocation-coupled deubiquitination. Ubiquitin-chain removal is followed by mechanical substrate unfolding and threading of the polypeptide into the 20S core for proteolytic cleavage. (**B**) Single-turnover degradation of ubiquitinated 5-FAM-titin-I27^{V15P}-35 by reconstituted 26S proteasome is tracked by SDS-PAGE and visualized by the fluorescence of the N-terminally attached 5-carboxyfluorescein (5-FAM, green star). (**C**) Single-turnover degradation of ubiquitinated 5-FAM-titin-I27^{V15P}-35 is tracked by fluorescence anisotropy in the presence of ATP or ATPγS. The total time for degradation is derived from the sum of the time constant τ for the exponential decay of anisotropy and the time t_0 for the initial anisotropy increase. (**D**) Substrate-tail insertion is tracked by FRET between the 26S proteasome reconstituted with Cy3-labeled base (Rpt1-I191AzF-Cy3) and ubiquitinated titin-I27^{V15P}-35 modified with Cy5 on its unstructured tail. At t=0, an excess of substrate was added to proteasomes with *o*PA-inhibited Rpn11 in the presence of either ATP or ATPγS. Shown is the Cy3 channel, normalized to initial fluorescence. (**E**) Conformational state of the proteasome over time, tracked by FRET between Cy5-labeled base (Rpt5Q49AzF-Cy5) and Cy3-labled lid (Rpn9S111AzF-Cy3). At t=0, an excess of ubiquitinated titin-I27^{V15P}-35 or buffer was added to double-labeled proteasomes with *o*PA-inhibited Rpn11. Shown is the Cy5 channel, normalized to initial fluorescence. The total time for the conformational change is derived from the sum of the time constant τ for the exponential increase of FRET and the time t_0 for the initial delay. (**F**) Overlay of fluorescence traces for tail insertion and conformational change from **D** and **E** reveal a delay of 400 ms. (**G**) Deubiquitination tracked by FRET between Cy3-labeled ubiquitin and a Cy5 label attached adjacent to the single ubiquitinated lysine in titin-I27^{V15P}-35. The substrate was ubiquitinated with Cy3-labeled ubiquitin, and at t=0 mixed with excess proteasome in the presence of ATP or ATPγS. Shown is the Cy5 channel, normalized to initial fluorescence. (**H**) Time constants of the substrate-processing steps as calculated from each assay individually or after accounting for the preceding steps. All curves in **C** – **G** are representative traces, and time constants are derived from averaging fits of independent experiments, shown with s.d. ($N \geq 3$).

The total time required for degradation of this substrate was determined by tracking the anisotropy of a fluorophore attached to the N-terminus of the titin folded domain (188). Gel-based assays confirmed the rapid degradation into peptides (Fig. 3.2B), and Michaelis-Menten analyses established the substrate affinity (K_M = 0.22 μM) and degradation rate (k_{cat} = 2.34 sub enz^{-1} min^{-1}) under multiple-turnover, steady-state conditions (Fig. 3.S2). In subsequent single-turnover degradation experiments with saturating concentrations of proteasome, we observed an initial fast increase in anisotropy, followed by a second increase, and an exponential signal decay (Fig. 3.2C, 3.S3, Table S3). When the substrate was mixed with proteasomes containing the catalytically dead Rpn11^{AXA} mutant, the signal also rapidly increased, but did neither show the second increase nor the exponential decay of anisotropy (Fig. 3.S3). Mixing of the substrate with ATPγS-bound wild-type proteasomes led to no change in signal (Fig. 3.2C). The initial anisotropy increase is thus likely a result of substrate engagement by the AAA+ motor, with a further increase seen after the deubiquitination event, as the folded domain is pulled towards the pore. The decay then reflects the mechanical unfolding, translocation, and cleavage of the substrate into small peptides. This decay (and all kinetic traces later measured for the individual substrate-processing steps) fit best to a double exponential curve, consisting of a dominant fast phase and a low-amplitude slow phase. Since the slow-phase likely originates from a small

population of partially aggregated or incompletely ubiquitinated substrate, we focused our analyses on the fast phase, as done in previous studies (26, 42). Combining the time constant for the exponential decay in anisotropy (τ = 11 s) and the delay associated with the initial increase (t_0 = 7 s) reveals that complete degradation of our titin model substrate occurs with a time constant of 18 s.

The first step of substrate processing after ubiquitin binding requires the insertion of the unstructured initiation region into the pore of the proteasomal motor (111). We specifically tracked the kinetics of this tail-insertion process using a FRET-based assay that relied on the energy transfer between a donor fluorophore placed near the central channel of the motor, in the linker between the N-domain and the ATPase domain of Rpt1 (Rtp1-I191AzF), and an acceptor fluorophore attached to the initiation tail of the substrate (Fig. 3.2D, Table 3.S4). To kinetically isolate tail-insertion from subsequent steps of substrate processing, we treated the proteasome with *o*PA, thereby preventing progression past the ubiquitin-modified lysine and trapping the proteasome with the inserted substrate in a high-FRET state. After stopped-flow mixing of acceptor-labeled substrate and donor-labeled, *o*PA-treated proteasome, we observed a rapid increase in FRET as measured by the quenching of donor fluorescence. This was accompanied by a reciprocal increase in acceptor fluorescence, confirming that the observed signal change was caused by an energy transfer between the donor and acceptor (Fig. 3.S4). Fitting of the FRET change revealed a time constant of 1.6 s (Fig. 3.2D). Since ubiquitin binding to the proteasome has previously been found to occur significantly faster (98), we can conclude that the 1.6 s time constant is largely determined by substrate-tail insertion after ubiquitin interaction with a proteasomal receptor. The tail insertion occurred on a time scale similar to the change in substrate anisotropy seen upon mixing with $Rpn11^{AXA}$-containing proteasome (Fig. 3.S4). No signal change was observed when mixing proteasome with substrate lacking a ubiquitin chain, and we also confirmed that the fluorophore on the unstructured initiation region had no major effects on the rate of substrate degradation (Table 3.S4).
Tail insertion could be prevented by the pre-incubation of the proteasome with ATPγS (Fig. 3.2D). In the ATPγS-induced s3 state of the proteasome, Rpn11 is relocated to directly above the central pore and therefore expected to sterically interfere with the insertion of a substrate's initiation region. The lack of a FRET signal when mixing substrate with ATPγS-bound proteasomes hence confirms that initial binding to a ubiquitin receptors does not lead to FRET and that substrate engagement by the AAA+ motor requires the s1 conformation of the proteasome.

We next measured the kinetics of conformational switching after substrate addition to Rpn11-inhibited proteasomes, using the above-mentioned FRET-based assay that tracks the relative distance between the base and lid sub-complexes (Fig. 3.2E, Table 3.S5). Because binding of unanchored ubiquitin chains alone had no effect on the conformational state of the proteasome, we hypothesized that engagement of the substrate's unstructured region with the pore loops of the AAA+ motor is required to trigger the switch. Indeed, upon mixing proteasome with substrate, the acceptor fluorescence increased with a time constant of 2.2 s, closely tracking with the tail insertion event. A reciprocal signal change was observed in the donor channel,

confirming the underlying FRET. Examination of early time points revealed that the FRET signal for substrate tail insertion increased immediately after mixing, whereas the signal for the conformational switch showed a 0.4 s delay (Fig. 3.2F). This delay indicates that pore-loop contacts with a substrate must occur first, and that this interaction then leads to a rapid switch of the proteasome from the s1 to a substrate-engaged, s3-like state. This model is also supported by our previous studies showing that the pore-loops of Rpt subunits at the top of the s1-state spiral staircase, which are thought to make first contact with a substrate polypeptide, are particularly important for degradation (26).

After engagement of a substrate, the proteasome must remove attached ubiquitin chains before proceeding to unfold and translocate the rest of the polypeptide. Therefore, a final FRET-based assay was designed to selectively monitor the deubiquitination event, this time by tracking the energy transfer between donor-labeled ubiquitin and an acceptor fluorophore attached to the substrate adjacent to the ubiquitinated lysine. Co-translocational ubiquitin removal from the substrate caused a loss in acceptor fluorescence, while pre-incubation of proteasomes with ATPγS abolished the signal change (Fig. 3.2G, Fig. 3.S4D). Stopped-flow measurements of the FRET signal upon mixing substrate with saturating amounts of wild-type proteasome in the presence of ATP revealed that deubiquitination occurs with a total time constant of 6.8 s (Table 3.S6), which reflects the sum of the time required for binding, tail insertion, and deubiquitination. Mixing of the substrate with $Rpn11^{AXA}$-containing proteasome also led to a signal change, but with more than 50% reduced amplitude. This deubiquitination-independent change in FRET is likely caused by a change in fluorophore environment when ubiquitin binds to the catalytically-dead Rpn11 (Fig. 3.S5).

By comparing the various time constants described above, we can derive the first complete kinetic model of proteasomal substrate processing and estimate the time required for each sub-step following substrate binding (Fig. 3.2H). Initial tail insertion proceeds with a time constant of 1.6 s, followed by a rapid conformational switch after 0.4 s. The removal of the ubiquitin chain then happens within ~ 5 s, and mechanical substrate unfolding, translocation, and cleavage take an additional 11 s.

The proteasome can quickly remove multiple ubiquitin chains, but is slowed down by stable domains

Our kinetic characterization of proteasomal degradation revealed that most of the substrate processing time is spent on deubiquitination and unfolding or translocation of the substrate. To further probe the relative contributions of these steps to overall degradation time, we modified our model substrate, either by changing the stability of the folded domain (Fig. 3.3A,B Fig. 3.S6) or by increasing the number of ubiquitin chains that need to be removed during degradation (Fig. 3.3C, Fig. 3.S7).

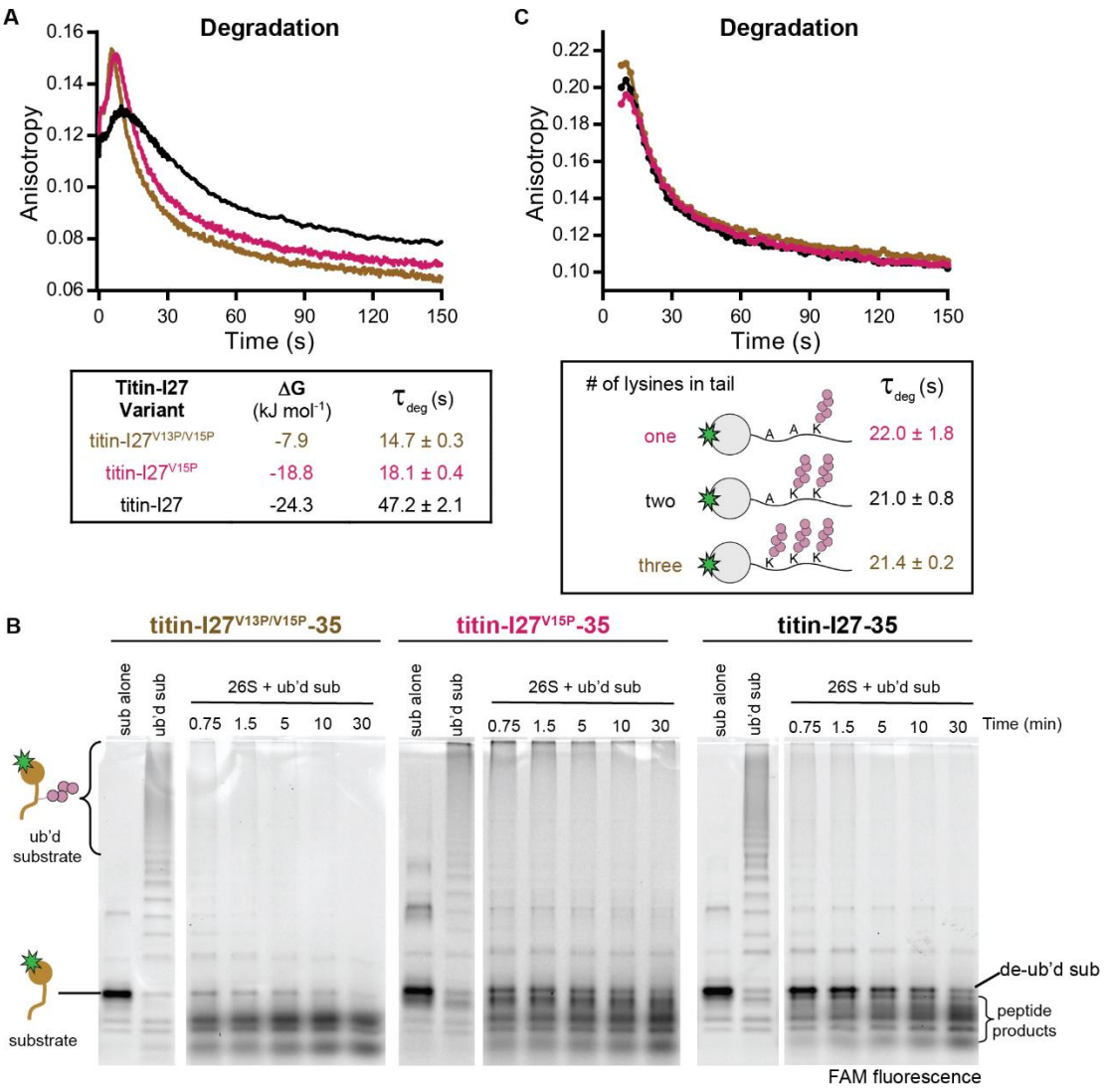

Figure 3.3. Increasing substrate stability slows degradation, but multiple ubiquitin chains can be rapidly removed.
(**A**) Single-turnover degradations of substrates with mutations in the titin-I27 folded domain tracked by anisotropy of N-terminally attached 5-FAM in a stopped-flow fluorimeter. The stabilities of titin-I27$^{V13P/V15P}$-35, titin-I27^{V15P}-35, and titin-I27-35 were determined by denaturant-induced equilibrium unfolding (see Fig. 3.S6). (**B**) Single-turnover degradations of the same substrates analyzed in **A**, but tracked by SDS-PAGE and visualized by 5-FAM fluorescence. (**C**) Single-turnover degradations of substrates with up to 3 lysine-attached ubiquitin chains in the unstructured tail tracked by anisotropy of 5-FAM. All curves are representative traces, and time constants are derived from averaging fits of independent experiments, shown with s.d. (N = 3).

A series of substrate variants was constructed based on previously reported mutations that change the thermodynamic stability of the titin-I27 domain (189). The experiments reported in Fig. 2 were performed with titin-I27^{V15P}-35, which has a thermodynamic stability of ΔG = -19 kJ

mol^{-1} (Fig. 3.S6). In addition, we measured the degradation rates for a further destabilized variant titin-$I27^{V13P/15P}$-35 (ΔG = -8 kJ mol^{-1}) and for the wild-type version, titin-I27-35 (ΔG = -24 kJ mol^{-1}). Increasing the stability of the folded titin domain significantly increased the overall time required for degradation, as seen for other substrates (62, 113, 190). Further analysis by SDS-PAGE showed that the most stable titin variant is rapidly deubiquitinated and then slowly unfolded and degraded (Fig. 3.3B), indicating that the substrate remains stably engaged after ubiquitin-chain removal, while the proteasome attempts to overcome the tough unfolding barrier. Thus, the unfolding event itself, as opposed to tail insertion, deubiquitination, or translocation, is the rate-limiting step of degradation for this substrate. The less stable titin variants exhibit no accumulation of the deubiquitinated species on the proteasome, indicating that unfolding and deubiquitination occur on similar time scales.

The least stable titin-$I27^{V13P/15P}$ variant was degraded with a total time constant of 15 s. Considering that all initial processing steps, including deubiquitination, take 6.8 seconds, and assuming rapid subsequent unfolding of the destabilized titin domain, we can estimate a minimum translocation rate of 15 residues s^{-1} for the 116 amino acids that remain to be threaded after unfolding.

To test the effects of additional ubiquitin chains on substrate degradation, we added a second or third lysine into the unstructured tail of our model substrate. The modification of all three lysine was confirmed by SDS-PAGE after ubiquitination with methyl-ubiquitin (Fig. 3.S7A,B) or by treating the poly-ubiquitinated substrate with the deubiquitinase AMSH (Fig. S7C), which trims K63-linked chains, but does not remove the substrate-attached ubiquitin moiety (191). Michaelis-Menten analyses showed that substrates with one, two, or three ubiquitin chains have similar binding affinities and degradation rates (Fig. 3.S2). Importantly, all three substrates also showed no difference in degradation rate under single-turnover conditions (Fig. 3.3C), suggesting that while the removal of the first ubiquitin chain takes 5 seconds, subsequent chains must be removed much more quickly. One model for this change in deubiquitination rate comes from our previous findings that the rate-limiting step of isopeptide cleavage by Rpn11 is a ubiquitin-induced conformational switch of its Insert-1 region (192). We propose that after Rpn11 removes the first ubiquitin chain, it does not immediately switch back to the inactive conformation, but instead is poised to bind and promote fast cleavage of nearby ubiquitin chains that rapidly approach Rpn11 as the substrate is translocated into the central pore. Many essential proteasome substrates, such as the cell-cycle regulators ubiquitinated by the anaphase-promoting complex (APC), are known to be modified with multiple ubiquitin chains (193, 194). Our data suggest that removal of ubiquitin chains is not rate-limiting for the degradation of these substrates.

Substrates with poor initiation regions fail to engage with the proteasome

It has been established that substrates with short (< 25 residues) or low-complexity initiation regions are not efficiently degraded *in vitro* and have extended *in vivo* half-lives (86, 104, 105, 112). To investigate the mechanisms behind this defect, we modified the initiation tail of our model substrate, either by varying the length of the terminal unstructured region following the

single ubiquitinated lysine or by replacing it with a low complexity, serine-rich sequence previously shown to severely impair degradation (104, 114).

Tracking of proteasomal processing by SDS-PAGE revealed that substrates with 35 or 25 AA tail were completely degraded into peptides, whereas the truncated tail variants with 11 or 1 AA were primarily deubiquitinated and released (Fig 3.4A, Fig. 3.S8, Fig. 3.S9). Deubiquitination and release of the short-tail substrates could be monitored by the decrease in anisotropy, though the magnitude of signal change was of course smaller than for complete proteolysis into peptides (Fig. 3.S10). Using this anisotropy readout in multiple turnover titrations revealed that the short tails cause significant K_M defects for the titin-I27^{V15P}-11 (K_M = 1.2 μM) and titin-I27^{V15P}-1 (K_M = 2.7 μM) substrates, compared to titin-I27^{V15P}-35 (K_M = 0.2 μM) (Fig. 3.S2, 3.S11).

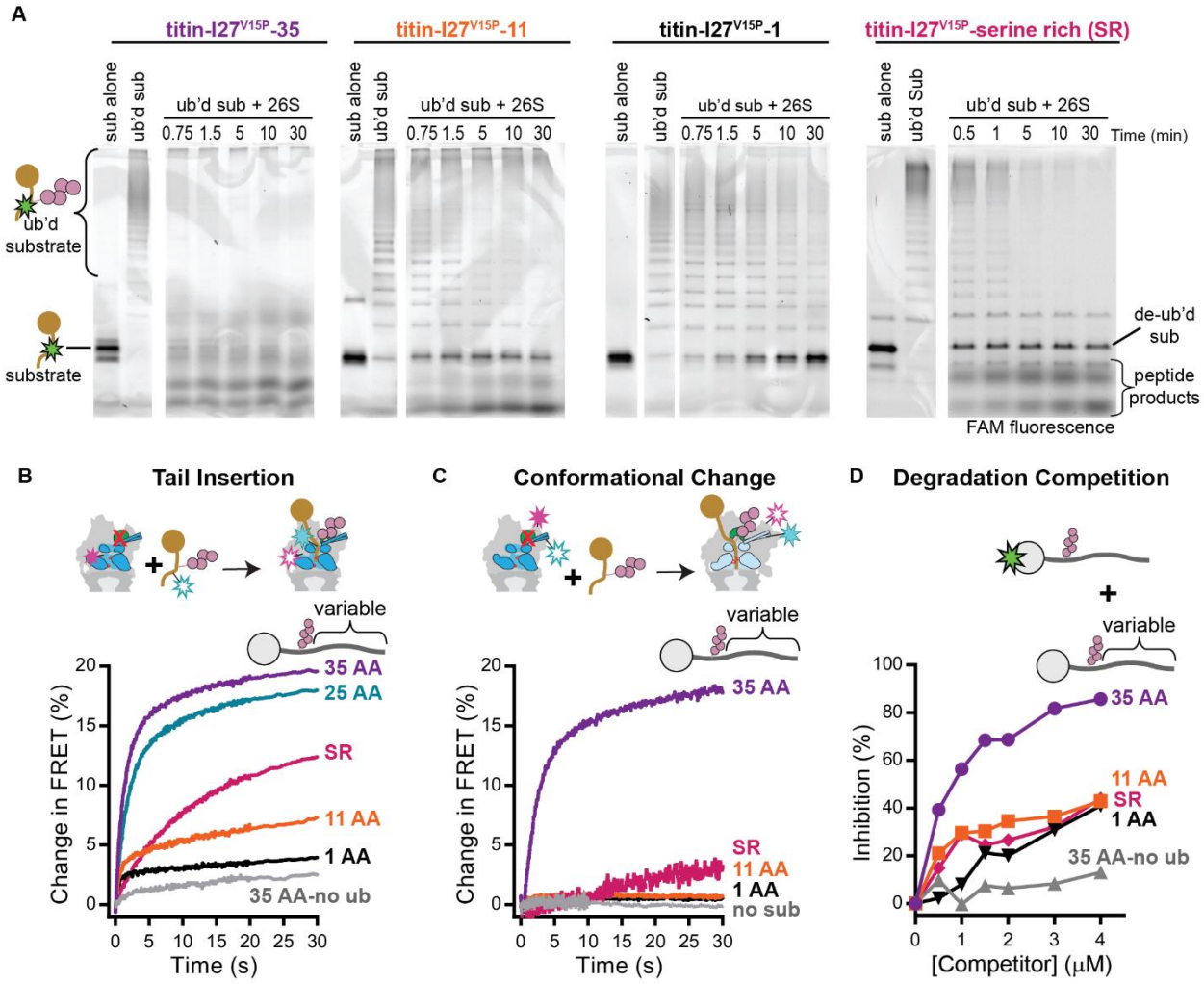

Figure 3.4. Substrates with poor initiation regions do not stably engage with the proteasome.
(**A**) Single-turnover degradations of substrates with varied unstructured initiation regions analyzed by SDS-PAGE and visualized by 5-FAM fluorescence. (**B**) Tail insertion kinetics of substrate variants tracked by FRET between the substrate and the proteasome as in Fig. 3.2D.

The corresponding time constants are listed in Table 1. (**C**) Conformational change of the proteasome after substrate addition, tracked by FRET between the base and the lid as in Fig. 3.2E. (**D**) Competitive inhibition of titin-I27^{V15P}-35 degradation by substrates with varied tails (same substrates as in **C**). The multiple-turnover degradation of 5-FAM-titin-I27^{V15P}-35 at 500 nM was measured by anisotropy in the presence of varying concentrations of unlabeled competitors. Shown is the percent inhibition as derived from the initial rates of degradation in the presence and absence of competitor. All curves are representative traces ($N \geq 3$).

We then analyzed the kinetics of tail insertion through the increase of FRET between donor labeled, Rpn11-inhibited proteasome and acceptor-labeled substrate, as in Fig. 3.2D (Fig. 3.4B, Table 1). We found that shorter tails appear to enter the central pore more rapidly, yet their FRET amplitude was severely reduced, with 11 and 1 AA tails showing only 25% and 16%, respectively, of the signal change detected for the 35-residue tail. These low amplitudes are most likely a consequence of the truncated tails being too short to reach from the narrow N-ring entrance to the pore loops, thus preventing a stable engagement with the AAA+ motor. After initial rapid insertion, these tails may therefore quickly escape again from the central channel, which is consistent with the observed increase in the apparent rate constants for short tail insertion, k_{app}, that reflects the sum of both, on and off rates (Table 3.1). The elevated off rates lead to an increase in K_M for the processing of short-tailed substrates under multiple-turnover conditions, even though their ubiquitin targeting signal is unchanged (Fig. 3.S11).

Substrate	τ_{app} (s)	k_{app} ($1/\tau_{app}$, s^{-1})	Amplitude (Normalized to 35)
titin-I27^{V15P}-35	1.61 ± 0.32	0.62 ± 0.12	1 ± 0.03
titin-I27^{V15P}-25 (serine rich)	7.15 ± 1.00	0.14 ± 0.02	0.51 ± 0.04
titin-I27^{V15P}-25	1.73 ± 0.02	0.58 ± 0.007	0.87 ± 0.05
titin-I27^{V15P}-11	0.7 ± 0.09	1.4 ± 0.18	0.24 ± 0.01
titin-I27^{V15P}-1	0.46 ± 0.03	2.2 ± 0.14	0.16 ± 0.001

Table 3.1. Fast phase kinetics and amplitudes of substrate tail insertion as seen in Fig. 3.4A. Shown are the mean and s.d. for $N \geq 3$.

Though short tails insert, at least briefly, into the pore of the motor, we found that substrates with those truncated initiation regions fail to trigger the conformational change of the proteasome (Fig. 3.4C). In contrast to the small amplitude and fast kinetics we observed for the tail-insertion traces, the conformational change traces for the truncated tails exhibited almost no amplitude. The inability of short-tailed substrates to induce a conformational change thus supports our model that interactions between the substrate polypeptide and the motor's pore loops drive the switch in proteasome conformation.

Despite their failure to engage and trigger proteasome conformational switching, short-tailed substrates are slowly deubiquitinated (Fig. 3.4A). The loss of anisotropy during the multiple-turnover processing of the 1 AA tail substrate (Fig. 3.S11) reveals a time constant of 45 s for this engagement-independent deubiquitination, which is significantly slower than the 6.8 s observed

for translocation-coupled deubiquitination of the long-tailed substrate (Fig. 3.2G). The almost 7-fold difference in deubiquitination rate agrees well with the previously revealed acceleration of Rpn11-mediated ubiquitin cleavage by mechanical substrate translocation into the AAA+ motor (42). Since short-tailed substrates fail to induce the conformational switch of the proteasome, their slow deubiquitination likely occurs while the proteasome is in the s1 state or during brief, spontaneous sampling of s3-like conformation. Despite not being coupled to translocation, this engagement-independent ubiquitin cleavage still results in the accumulation of only fully deubiquitinated substrate (Fig. 3.4A), as expected if steric hindrance by the subjacent N-ring of the AAA+ motor forces Rpn11 to cleave at the base of the ubiquitin chain, rather than between ubiquitin moieties.

Like the short tails, the low complexity serine-rich tail also led to a significant K_M defect in multiple-turnover processing and exhibited a decreased FRET amplitude for tail insertion (Fig. 3.S11, Fig. 3.4B). In contrast to the short tails, however, it also showed slower tail-insertion kinetics, with a k_{app} four times lower than that of a complex tail of the same length. Thus, in addition to having an elevated ratio of k_{off}/k_{on} (and therefore K_M), the on-rate of the serine-rich tail is decreased. The conformational change induced by this substrate was also slow and of a low magnitude, with the defects again being amplified compared to those measured in tail insertion. Both the tail-insertion and conformational change assays rely on a stalled state, with the substrate's initiation region stably engaged by the AAA+ motor. The small FRET-signal amplitudes for the serine-rich tail thus indicate a rapid substrate escape from the proteasome pore and a consequent low probability of commitment, explaining the observed slow degradation and frequent release (Fig. 3.4A). Low-complexity regions thus hinder substrate processing in several ways: by slowing the onset of tail insertion, inhibiting the conformational change, and likely by reducing the motor grip required for unfolding and translocation.

How are proteasomes *in vivo* able to rapidly turn over high priority substrates, such as cell-cycle regulators, while ubiquitinated proteins with poor initiation regions and therefore slow processing kinetics compete for proteasomal ubiquitin receptors? To test this scenario *in vitro*, we performed competition experiments, in which the degradation of a fluorescently labeled, ubiquitinated titin-I27^{V15P}-35 substrate was tracked in the presence of unlabeled ubiquitinated substrates with varying tail architectures (Fig. 3.4D). While the unlabeled substrate with a 35 residue tail effectively inhibited degradation of its labeled counterpart, substrates with short or serine-rich initiation regions were poor competitors, even at concentrations well above their measured K_M values. These results can be explained by the high off rates and poor engagement of these tails with the ATPase motor. Their inability to compete also suggests that the ubiquitin-chain interactions with receptors on the proteasome is short lived. The translocation-independent deubiquitination we observed for substrates with poor initiation regions (Fig. 3.4A) must happen during brief and presumably repetitive binding events. The proteasome thus has intrinsic mechanisms for removing poor substrates from the pool of ubiquitinated proteins, while still allowing the preferred and therefore rapid degradation of appropriate substrates. Accessory factors such as Ubp6 and Hul5, both proposed to be important for substrate triage, may act in concert with the proteasome's intrinsic mechanisms described here (145).

Conclusions

An intricate system of recognition and processing steps allows the 26S proteasome to select only appropriate substrates that contain both the correct ubiquitin-targeting signal and an unstructured initiation region, while maintaining the high promiscuity necessary to degrade hundreds of cellular proteins with diverse characteristics. Using FRET-based assays to measure the kinetics of individual substrate-processing events, we found that insertion and engagement of the unstructured initiation tail is fast, whereas most of the degradation time is spent on mechanical unfolding and translocation. We show that the proteasome rapidly transitions from the s1 state to a substrate-processing, s3-like state immediately after tail insertion, suggesting that substrate interactions with the pore loops of the AAA+ motor drive this global conformational switch. In the s1 state, the entrance to the central pore is well accessible for the substrate's flexible initiation region, and the ATPase domains of Rpt1-6 are arranged in a steep spiral staircase that likely helps substrate entry (26, 28, 48). The transition to the s3-like processing state, right after substrate engagement with the translocation machinery, is ideally timed to facilitate all subsequent processing steps, as it brings the ATPase ring into a more planar, translocation-competent conformation and moves Rpn11 to directly above the central pore to enable efficient coupling of translocation and deubiquitination (38, 42). Premature transition to this state, however, prevents tail insertion and engagement, which highlights the importance of this intricate coordination between substrate processing steps and conformational switching of the proteasome.

We identified mechanical unfolding as the rate-determining step for degradation of our model proteins and likely most proteasomal substrates in general. Consistent with previous studies, we found that increasing the thermodynamic stability of a substrate's structured domain extends the time required for degradation. In contrast, the presence of additional ubiquitin chains had no effect on the overall degradation rate. We propose that after the first ubiquitin-cleavage, which takes about 5 s, subsequent deubiquitination events can be significantly accelerated, because Rpn11 remains in its active state at least long enough to remove closely spaced ubiquitin chains from a translocating polypeptide. Multiple ubiquitin chains can thus confer additional affinity for the proteasome without reducing the degradation rate, and it is not surprising that high-priority substrates, such as those ubiquitinated by the APC, contain multiple, closely spaced ubiquitin modifications (193, 194). While the removal of ubiquitin chains may not be limiting, their orientation relative to a substrate's unstructured initiation region has been found to potentially affect the rate of degradation (46, 98). Future studies, utilizing the specific assays presented here, will have to address whether those differences in turnover rates are due to altered engagement kinetics or differential rates of deubiquitination depending on the spacing of ubiquitin chains relative to each other or a folded domain.

When investigating the requirements for substrate recognition and engagement, we found that ubiquitinated proteins with initiation regions of insufficient length or complexity were slowly deubiquitinated and released, rather than degraded, which explains previous findings of poor *in vitro* degradation or extended *in vivo* half-lives for those substrates (111, 112). Short or low-complexity initiation regions still rapidly enter the central channel of the proteasome, but cannot

stably engage with the AAA+ pore loops and quickly escape again, leading to a significant increase of the substrate's K_M. Remodeling factors such as Cdc48/p97 may thus play a critical role in preparing substrates for degradation by exposing unstructured initiation regions for efficient proteasomal engagement (109, 110).

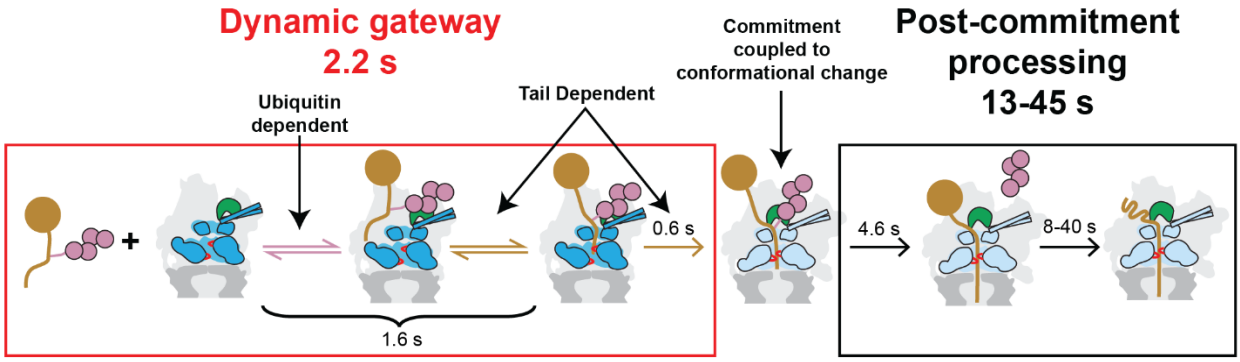

Figure 3.5. Model for kinetic proofreading by the proteasome.
Ubiquitin binding and tail insertion constitute a dynamic gateway to proteasomal substrate processing, with both fast on and off rates. If the substrate has the necessary requirements for degradation, engagement with the AAA+ motor reduces k_{off} for tail insertion and accelerates the conformational switch of the proteasome, thereby committing substrates to translocation-coupled deubiquitination, rate-limiting unfolding, and degradation.

We propose that the initial ubiquitin-binding and tail-insertion events represent a dynamic gateway that is characterized by both, fast on and off rates, and controls the selection of appropriate substrates for proteasomal degradation (Fig. 3.5). If a substrate has the necessary requirements for processing, then tail engagement with the AAA+ motor reduces the off rate and induces the proteasome conformational switch that commits the substrate to unfolding, translocation-coupled deubiquitination, and degradation. As a consequence of this rapid ubiquitin sampling by the proteasome, binding of poor substrates does not considerably inhibit the degradation of higher-priority substrates with proper initiation regions, as seen in our *in vitro* competition experiments with short and long tailed proteins. This mechanism is thus similar to the kinetic proofreading mechanism used by the ribosome to recognize cognate amino acyl-tRNAs, in which rapid initial binding interactions are followed by an irreversible committed step (195). In addition to this proofreading, the slow, translocation-independent deubiquitination of engagement-incompetent proteins at the proteasome removes them from the pool of potential substrates. Our studies thus provide exciting new insights into how the proteasome prioritizes its substrates in the cell and coordinates its processing steps and conformational changes to ensure efficient protein degradation.

Materials and Methods

All plasmids used for the purification of recombinant proteins are listed in Table 3.S1.

Purification of 20S core

S. cerevisiae 20S core was purified from the Pre1-3xFLAG yeast strain yAM14 (RJD1144, from Ray Deshaies, (196) as previously described (38). Briefly, yAM14 yeast were lysed and resuspended in lysis buffer (60 mM HEPES, pH 7.6, 500 mM NaCl, 1 mM EDTA, 0.2% NP-40). 20S core was immobilized on M2 anti-FLAG resin (Sigma), washed with buffer containing 1 M NaCl to remove bound regulatory particle, eluted from the resin using 3xFLAG peptide, and further purified by size-exclusion chromatography with a Superose 6 Increase 10/300 column (GE) equilibrated in GF buffer (30 mM HEPES, pH 7.6, 50 mM NaCl, 50 mM KCl, 10 mM $MgCl_2$, 5% glycerol) with 0.5 mM TCEP. Peak fractions were concentrated in a 100K MWCO Amicon Ultra concentrator (Millipore), aliquoted, flash frozen in liquid N_2, and stored at -80 °C. The concentration was determined by absorbance at 280 nm.

Purification of wild-type base

Recombinant yeast base was purified after heterologous expression in *E. coli* using a slight modification of previously published methods (26). *E. coli* BL21 Star(DE3) (Invitrogen) was co-transformed with the plasmids pAM81, pAM82, and pAM83 (derived from pETDuet, pCOLADuet, and pACYCDuet, respectively), coding for Rpt1 - Rpt6, Rpn1, Rpn2, Rpn13, the four base-assembly chaperones Rpn14, Hsm3, Nas2, and Nas6, and rare tRNAs. Bacteria were grown in 3 L of terrific broth (Novagen) to an OD_{600} = 1.0, then induced with 0.5 mM IPTG at 30 °C for 5 hours, followed by an overnight induction at 16 °C. The cells were pelleted and resuspended in NiA buffer (60 mM HEPES, pH 7.6, 100 mM NaCl, 100 mM KCl, 10 mM $MgCl_2$, 5% glycerol, and 20 mM imidazole) supplemented with 2 mg ml^{-1} lysozyme, benzonase (Novagen), and protease inhibitors (aprotinin, pepstatin, leupeptin and PMSF). Cells were lysed by sonication, the lysate was clarified by centrifugation, and the base subcomplex was purified by a three-step procedure, with 0.5 mM ATP present in all buffers. First, the His-Rpt3 containing complexes were purified using a 5 mL HisTrap FF crude (GE), then fully assembled complexes containing Flag-Rpt1 were selected for by using anti-Flag M2 affinity resin (Sigma), and finally, the complex was further purified using size-exclusion chromatography with a Superose 6 increase 10/300 column (GE) equilibrated in GF buffer with 0.5 mM ATP and 0.5 mM TCEP. The concentration of the base was determined by Bradford assay using bovine serum albumin (Sigma) as a standard.

Purification and labeling of unnatural amino acid-containing base

The base sub-complex containing 4-azido-L-phenylalanine (AzF) was expressed, purified, and labeled using a similar procedure with the following modifications: In addition to pAM81, pMA83, and an amber-codon containing variant of pAM82, a fourth plasmid (pAM87) containing the AzF tRNA synthetase/tRNA pair was used to co-transform Bl21 Star(DE3) *E. coli*. This plasmid was constructed by replacing the IPTG-inducible synthetase in the pULTRA-CNF construct designed by the Schultz lab with the AzFRS.2.t1 synthetase evolved by the Isaacs lab(164, 175). The pEvol-pAzFRS.2.t1 was a gift from Farren Isaacs (Addgene plasmid # 73546) and the pULTRA-CNF was a gift from Peter Schultz (Addgene plasmid # 48215). The cells were

grown in 3 L of dYT media to an OD_{600} = 0.6, then pelleted, and resuspended in 0.5 L of terrific broth (Novagen) with added 2mM AzF (Amatek Chemical). The cells were shaken for 30 minutes at 30 °C to allow for uptake of the AzF, followed by induction with 0.5 mM IPTG for 5 hours at 30 °C and then 16 °C overnight. Purification followed the same protocol as for AzF-free base, except that after elution from the anti-Flag resin, the base was incubated with 150 µM 5,5'-dithiobis-(2-nitrobenzoic acid) (DTNB) for 10 minutes at room temperature to temporarily block any exposed cysteines. The base was then cooled back down to 4 °C and labeled overnight with 300 µM dibenzocyclooctyne (DBCO) conjugated fluorophore (Click Chemistry Tools). The reaction was quenched using 1 mM free AzF, followed by 2 mM dithiothreitol (DTT), and labeled base was then purified using size-exclusion chromatography as described above. Labeling efficiencies were estimated by comparing the absorbance-based concentration of fluorophore with the base concentration calculated by the Bradford assay.

Purification of lid

Recombinant yeast lid was also purified using a three step procedure. The plasmids pAM80, pAM85, and pAM86, coding for Rpn3, Rpn5 – Rpn9, Rpn11, Rpn12, Sem1, and rare tRNAs, were modified from previously published plasmids to replace the affinity tags(28). Human rhinovirus (HRV) protease-cleavable maltose binding protein was inserted at the N-terminus of Rpn6, and the N-terminus of Rpn12 was modified with a HRV-cleavable 6xHis tag. *E. coli* BL21 star(DE3) was co-transformed with these plasmids and then grown, induced, and lysed as described above for the base. The fully assembled lid was purified using a HisTrap and amylose resin (NEB), cleaved with HRV-protease, and purified on a Superose 6 Increase size-exclusion column equilibrated in GF buffer with 0.5 mM TCEP. The concentration of the lid was determined by absorbance at 280 nm. Unnatural amino acid-containing lid was expressed and purified in a fashion similar to AzF-containing base, using the same DTNB blocking and DBCO-fluorophore labeling procedures after elution from the amylose resin.

Purification of substrates

All substrates were purified using the IMPACT system (NEB). The substrate was inserted into a T7-inducible plasmid derived from pET28a (Novagen) upstream of the intein and chitin binding domain (CBD) taken from pTXB1 (NEB). *E. coli* BL21 star(DE3) was transformed with this plasmid, grown in 3 L of dYT to an OD_{600} = 0.6, and induced with 0.5 mM IPTG for 3 hours at 30 °C. The cells were then resuspended in chitin buffer (60 mM HEPES, pH 7.6, 150 mM NaCl, 1 mM EDTA, 5% glycerol) with protease inhibitors (AEBSF, aprotinin, leupeptin, and pepstatin), and benzonase (Novagen). The cells were bound in batch to 10 mL of chitin resin (NEB) for 1 hour at 4 °C, which was then washed with 100 mL of chitin buffer supplemented with an additional 500 mM NaCl, 0.2% Triton X-100, and protease inhibitors. The substrate was cleaved from the column by overnight incubation at 4 °C in a buffer containing 60 mM HEPES, pH 8.5, 150 mM NaCl, 1 mM EDTA, 5% glycerol, and 50 mM DTT. The substrate was collected from the column, run over 3 mL of fresh chitin resin to remove any uncleaved substrate, and then purified on a S75 16/60 size-exclusion chromatography column (GE) in GF buffer with 0.5 mM TCEP. The concentration of substrate was determined by the absorbance at 280 nm.

Labeling of substrates

Fluorophores were covalently attached to a single engineered cysteine in the substrate by maleimide chemistry. While there are two additional cysteines in the titin-I27 domain used, they are not solvent exposed. Where noted, the N-terminus of the substrate was labeled by sortase A (SrtA)-mediated ligation of a peptide (197). For the sortase modification, peptide (HHHHHHLPETGG) was purchased with 5-FAM conjugated to its N-terminus (Biomatik), and then ligated to 100 µM substrate using 20 µM recombinant 6xHis-SrtA in GF buffer supplemented with 10 mM $CaCl_2$, and 0.5 mM peptide. The labeled substrate was selected for by binding to a 1 mL HisTrap HP (GE), followed by size-exclusion chromatography on a Superdex 75 10/300 column (GE) equilibrated with GF buffer. The concentration of substrate was determined by quantifying the absorbance of the attached fluorophore (5-FAM = 492 nm, Cy5 = 646 nm).

Purification and labeling of ubiquitin

In order to label ubiquitin, a variant was expressed with an N-terminal cysteine inserted before the first methionine (MC-ubiquitin). This variant was expressed and purified as described previously (42). Briefly, Rosetta II (DE3) pLysS *E. coli* cells were transformed with an IPTG-inducible expression plasmid (pET28a) containing MC-ubiquitin. The cells were grown in terrific broth (Novagen) at 37 °C until the OD_{600} = 1.5, and ubiquitin expression was induced with 0.5 mM IPTG overnight at 18 °C. After expression, the cells were resuspended in lysis buffer (50 mM Tris-HCl, pH 7.6) containing 2 mg mL^{-1} lysozyme, benzonase, and protease inhibitors (aprotinin, pepstatin, leupeptin and PMSF). The cells were lysed by sonication, and contaminating proteins were precipitated by the addition of 60% perchloric acid to a final concentration of 0.5%. The soluble fraction containing ubiquitin was dialyzed overnight into 50 mM Na-acetate, pH 4.5, and purified by cation exchange on a 5 mL HiTrap SP FF column (GE) using a gradient of 0 - 0.5 M NaCl in 50 mM Na-acetate, pH 4.5. Peak fractions were concentrated and further purified over a Superdex S75 16/60 column in storage buffer (20 mM Tris-HCl, pH 7.6, 150 mM NaCl, 1 mM DTT). Ubiquitin was labeled by dialyzing into labeling buffer (30 mM HEPES, pH 7.2, 150 mM NaCl, 1 mM EDTA) and reacted with an excess of maleimide-fluorophore. The labeled ubiquitin was purified on a Superose 75 16/60 size exclusion column equilibrated in GF buffer, and its concentration was measured by the Lowry assay using non-labeled ubiquitin as a standard.

A pET15b plasmid containing linearly fused tetra-ubiquitin with an N-terminal fusion to 6xHis-SUMO was generated by gene synthesis (Genscript). The protein was expressed in Rosetta II (DE3) pLysS *E. coli*, purified on a HisTrap, cleaved using SENP1 protease, then further purified by cation exchange on an SP FF column (as described above) and size-exclusion chromatography on a Superose 75 16/60 column equilibrated in GF buffer.

Purification of additional components

The plasmid used to express Usp2 was a gift from Cheryl Arrowsmith (Addgene plasmid # 36894). The plasmid used to express SENP2 protease was a gift from Guy Salvesen (Addgene plasmid # 16357) (198). Both proteins were expressed in *E. coli* BL21 star(DE3) and purified using a HisTrap, followed by size-exclusion chromatography on a Superose 75 16/60 column

equilibrated in GF buffer. The plasmid used to express mouse E1 (pet28-mE1) was a gift from Jorge Eduardo Azevedo (Addgene plasmid # 32534) (199). The plasmid used to express AMSH, pOPINB-AMSH*, was a gift from David Komander (Addgene plasmid # 66712) and was purified as described previously (191).

Additional recombinant proteins including Rpn10, ubiquitin, Rsp5, Ubc1, and E1 were purified as previously described (42). $Ubp6^{C188A}$ was purified as previously described (47).

Substrate ubiquitination

All substrates contained a PPPY motif in the unstructured region, which allows them to be ubiquitinated with long primarily K63-linked ubiquitin chains *in vitro* using the Rsp5 E3 ligase (38, 187). Purified substrates (10 µM) were incubated for 3 hours at 25 °C in GF buffer with E1 (2.5 µM), Ubc1 (2.5 µM), Rsp5 (2.5 µM), ubiquitin (400 µM), and 10 mM ATP. Substrates were ubiquitinated fresh for each day of experiments and evaluated by gel to ensure reproducible ubiquitination.

Enzymatic assays

All enzymatic assays were performed at 25 °C in GF buffer supplemented with 5 mM ATP, 0.5 mM TCEP, 0.5 mg mL^{-1} BSA, and an ATP regeneration system (0.03 mg mL^{-1} creatine kinase and 16 mM creatine phosphate) unless otherwise noted. Experiments were performed in at least three technical replicates.

Data processing and analysis

All curve fitting was done using Origin (Originlab, Northampton, MA). The fits were performed by least squares fitting, and evaluated by the distribution of the residuals to ensure there were no significant deviations from zero. The initial rates from substrate degradation or deubiquitination experiments were fit to the Michaelis-Menten equation to determine k_{cat} and $K_{M.}$ Exponential curves from single-turnover measurements were fit to either a double exponential increase/decay ($y=y_0 + A_1*e^{-t/\tau1} + A_2*e^{-t/\tau2}$) or a delayed double exponential increase/decay ($y=y_0 + A_1*e^{-(t-t0)/\tau1} + A_2*e^{-(t-t0)/\tau2}$), in which the delay was determined by visual inspection of the curves. In general, the channel with the largest signal change was used for fitting and representative traces. Some curves were smoothened by the Savitsky-Golay method for visualization, but all data analysis was done on the raw traces. The plotted curves were normalized to the initial fluorescence value for each trace.

The slow phase of the double exponential fit was not used in the analyses, because it is thought to arise from a small population of partially aggregated or incompletely ubiquitinated substrate. In support of this, the fast phase of the single-turnover degradation kinetics match well with the k_{cat} values measured in multiple turnover. The time constants for both phases and their relative distribution of amplitudes are reported in Tables S3-S6.

Anisotropy assays

Multiple-turnover degradations were monitored by tracking fluorescence anisotropy of fluorescein in a Synergy NEO2 multimode plate reader (Biotek). Reactions were initiated by mixing 6.5 µL of 2x reconstituted holoenzyme with 6.5 µL of 2x ubiquitinated substrate, then

transferring 10 µL of the reaction to a 384-well flat bottom, low volume microplate (Corning). Final concentrations were 25 or 50 nM core, 400 nM base, 600 nM lid, 750 nM Rpn10, and varying concentrations of substrate.

Initial rates of processing were calculated by using the measured anisotropy of ubiquitinated substrate alone and that of substrate fully cleaved by chymotrypsin to normalize the measured change in anisotropy during the reaction.

To determine the Michaelis-Menten constants for titin-I27^{V15P}-1-FAM, the initial rate was normalized using substrate that had been fully deubiquitinated by Usp2 rather than fully degraded substrate. Because titin-I27^{V15P}-11-FAM and titin-I27^{V15P}-serine rich-FAM exhibit both degradation and deubiquitination, the chymotrypsin degraded value was used to normalize the curves, but the k_{cat} is most likely underestimated.

Final concentrations for all single-turnover degradations were 1.25 µM core, 2.5 µM base, 2.5 µM lid, 3 µM Rpn10, and 300 nM substrate. Single-turnover degradation measurements that were performed in a plate reader used a similar procedure as described above, with a deadtime of 8-10 seconds between mixing and the first measurement. Degradation measurements were also performed in an Auto SF120 stopped-flow fluorimeter (Kintek) with two photomultipliers to measure fluorescein anisotropy. The stopped-flow was loaded with 140 µL of 2x reconstituted holoenzyme and 140 µL of 2x substrate, with the same final concentrations as those used in the plate reader. After loading, four blank shots were fired, followed by three measurements. The deadtime of mixing on the instrument is sub-millisecond.

The curves for degradations measured in the stopped-flow and those measured in the plate reader were fit to a delayed exponential.

Single-turnover degradation measurements that were analyzed by gel were performed by mixing 2x reconstituted holoenzyme and 2x substrate, taking 2 µL aliquots at the indicated time, quenching them in 2% SDS-containing buffer, and separating the reaction by SDS-PAGE on 12% NuPAGE gels (Invitrogen). The fluorescence was then measured on a Typhoon FLA 9500 variable mode scanner (GE) using a pixel density of 50 µm per pixel.

Tail insertion assays

Tail insertion was measured by tracking Förster resonance energy transfer (FRET) between Cy5-labeled base and Cy3-labeled substrate, while enforcing single-turnover conditions using 1,10-phenanthroline (*o*PA), an inhibitor of Rpn11 that stalls the proteasome at the site of ubiquitin linkage (42). Base containing Rpt1-I191AzF was labeled with Sulfo-Cy5-DBCO (Click Chemistry Tools) as described above. A 30 mM *o*PA stock was made in GF buffer. Reactions were performed in the Auto SF120 using 2x reconstituted holoenzyme and 2x Sulfo-Cy3 labeled substrate. Final concentrations were 100 nM Cy5-Rpt1 base, 400 nM core, 600 nM lid, 750 nM Rpn10, 3 mM oPA, and 3 µM substrate. An excitation wavelength of 550 nm was used, and the Cy3 and Cy5 emission channels were monitored simultaneously.

The kinetics of tail insertion were determined by fitting the quenching of the Cy3 signal. The amplitudes listed in Table 1 were calculated by normalizing the amplitudes of the fast-phases to

the initial fluorescence, and then comparing those to the normalized amplitude of titin-I27^{V15P}-35-Cy5. All measurements used in this calculation were from traces collected on the same day.

Conformational change assays

The conformational state of the proteasome was monitored using FRET between Cy3-labeled lid and Cy5-labeled base. Lid containing Rpn9S111AzF was labeled with Sulfo-Cy3-DBCO, and base containing Rpt5Q49AzF was labeled with Sulfo-Cy5-DBCO as described above. Steady-state measurements were performed by mixing 2x reconstituted holoenzyme (150 nM Cy5-Rpt5 base, 400 nM core, 500 nM Cy3-Rpn9 lid, and 750 nM Rpn10) with 2x substrate or other additive as indicated. Final concentrations of the reconstituted holoenzyme were 150 nM Cy5-Rpt5 base, 400 nM core, 500 nM Cy3-Rpn9 lid, and 750 nM Rpn10. Final substrate concentration was 3 μM. Final *o*PA concentration was 3 mM. Catalytically dead Ubp6(C188A) was added at 250 nM, and linear tetra-ubiquitin was added at 100 μM. ATPγS was added at 5 mM in place of the ATP regeneration system. The reactions were then transferred to a 384-well flat bottom, low volume microplate (Corning), and the fluorescence intensities were measured in a Synergy NEO2 plate reader (Biotek). Single turnover measurements were performed in the AutoSF 120 stopped-flow fluorimeter (Kintek) using 2x reconstituted holoenzyme with *o*PA (3 mM final) and 2x substrate, exciting at 550 nm and measuring Cy3 and Cy5 emission channels simultaneously.

The steady-state levels of FRET were calculated by the following equation: $I_{acceptor}/(I_{donor}+I_{acceptor})$. This value was calculated for each replicate and then averaged to determine the FRET signal for the respective condition. The FRET levels were then all normalized to that of the proteasome in ATP with no other additives. The kinetics of the conformational change were determined by fitting the gain of FRET observed in the Cy5 channel.

Deubiquitination assays

Deubiquitination was tracked using FRET between Cy3-labeled ubiquitin and a Cy5-labeled substrate. Sulfo-Cy3 labeled ubiquitin was used to ubiquitinate Sulfo-Cy5 labeled substrates in the same ubiquitination conditions as described above. Single-turnover degradation reactions were then performed as described above, but instead of tracking anisotropy, Cy3 was excited, and Cy3 and Cy5 emission were monitored. The kinetics of deubiquitination were determined by fitting the loss of FRET observed in the Cy5 channel.

Competition assays

The degradation competition experiments were performed similarly to the multiple-turnover degradation assays described above. The 2x reconstituted holoenzyme was mixed with a 2x solution containing both the labeled substrate and unlabeled competitor. The final concentrations used were 50 nM core, 400 nM base, 600 nM lid, 750 nM Rpn10, 500 nM FAM-titin-I27^{V15P}-35, and varying competitor concentration. The extent of inhibition was then calculated by comparison of the initial rates with and without the competitor.

Stability measurement

The equilibrium stability of titin mutants was measured by monitoring the tryptophan fluorescence of the substrate after equilibration at 25 °C with different concentrations of

urea(189). The fluorescence (excitation = 280 nm, emission = 325 nm) was monitored in a plate reader at 25 °C. The curves were fit to the following system of equations:

$y=(A+B*k)/(1+k)$
$A=A_0+m_A*[urea]$
$B=B_0+m_B*[urea]$
$k=e^{(-\Delta G/(RT)}$
$\Delta G= m*(c_m-[urea])$
All variables were fit globally across the three substrates, except for the c_m values. The ΔG_0 was then calculated using the equation $\Delta G_0= m*c_m$.

ATPase assays
The rate of ATP hydrolysis was measured using an NADH-coupled assay. Reconstituted proteasome (150 nM base, 400 nM core, 600 nM lid, 750 nM Rpn10, 1 mM ATP) was combined with ATPase mix (3 U ml^{-1} pyruvate kinase, 3 U ml^{-1} lactase dehydrogenase, 1 mM NADH, and 7.5 mM phosphoenolpyruvate), and the change of absorbance at 340 nm was monitored over time in a plate reader.

Supplementary Information

Table 3.S1. Plasmids used for protein purification generated for this study.

Plasmid Name	Plasmid Description	Amino acid sequence after titin-I27*
pAM81	Rpn1, Rpn1, Rpn13	
pAM82	3xFLAG-Rpt1, Rpt2, 6xHis-Rpt3, Rpt4, Rpt5, Rpt6	
pAM83	Nas2, Nas6, Hsm3, Rpn14, rare tRNAs	
pAM87	AzFRS.2.t1, UAG-tRNA	
pAM88	3xFLAG-Rpt1I191TAG, Rpt2, 6xHis-Rpt3, Rpt4, Rpt5, Rpt6	
pAM89	3xFLAG-Rpt1, Rpt2, 6xHis-Rpt3, Rpt4, Rpt5Q49TAG, Rpt6	
pAM80	Sem1, Hsp90	
pAM85	Rpn5, MBP-HRV-Rpn6, Rpn8, Rpn9, Rpn11	
pAM86	Rpn3, Rpn7, 6xHis-HRV-Rpn12	
pAM90	Rpn5, MBP-HRV-Rpn6, Rpn8, Rpn9S111TAG, Rpn11	
pAM91	GGG- titin-I27^{V15P}-23-K-9-C-25-intein-CBD	GGAGPPPYSAANDENYALAAHGGKHTFNNENVS**C**RLGGAASIAVQAPAQHTFNNENVSY
pAM92	GGG- titin-I27^{V15P}-21-C-2-K-35-intein-CBD	GGAGPPPYSAANDENYALAAH**C**GGKHTFNNENVSARLGGAASIAVQAPAQHTFNNENVSY
pAM93	GGG-titin-I27-23-K-9-C-25-intein-CBD	GGAGPPPYSAANDENYALAAHGGKHTFNNENVS**C**RLGGAASIAVQAPAQHTFNNENVSY
pAM94	GGG- titin-I27$^{V13P/V15P}$-23-K-9-C-25-intein-CBD	GGAGPPPYSAANDENYALAAHGGKHTFNNENVS**C**RLGGAASIAVQAPAQHTFNNENVSY
pAM95	GGG- titin-I27^{V15P}-43-K-8-C-25-intein-CBD	GGAGPPPYSAANDENYALAAHGGAHTFNNENVSAHTFNNENVSKHTFNNENV**C**RLGGAASIAVQAPAQHTFNNENVSY
pAM96	GGG- titin-I27^{V15P}-33-K-9-K-8-C-25	GGAGPPPYSAANDENYALAAHGGAHTFNNENVSKHTFNNENVSKHTFNNENV**C**RLGGAASIAVQAPAQHTFNNENVSY
pAM97	GGG- titin-I27^{V15P}-23-K-9-K-9-K-8-C-25	GGAGPPPYSAANDENYALAAHGGKHTFNNENVSKHTFNNENVSKHTFNNENV**C**RLGGAASIAVQAPAQHTFNNENVSY
pAM98	titin-I27^{V15P}-23-K-9-C-15	GGAGPPPYSAANDENYALAAHGGKHTFNNENVS**C**RLGGAASIAVQAPAY

pAM99	titin-I27^{V15P}-23-K-9-C-1	GGAGPPPYSAANDENYALAAHGGKHTFNNENVS**C**Y
pAM100	titin-I27^{V15P}-21-C-2-K-1	GGAGPPPYSAANDENYALAAH**C**GGKY
pAM101	titin-I27^{V15P}-23-K-9-C-15 serine rich	GGAGPPPYSAANDENYALAAHGGKSSSSSSASS**C**SSGSSSSSSASSSSY
pAM102	6xHis-Sumo-Ub-Ub-Ub-Ub	
pAM103	MC-Ubiquitin	

*The amino acid sequence of the lysine-less version of titin-I27 used is as follows:
LIEVERPLYGVEVFVGETAHFEIELSEPDVHGQWRLRGQPLAASPDCEIIEDGRRHILILH
NCQLGMTGEVSFQAANTRSAANLRVREL

Table 3.S2. Substrates used for each assay.

Plasmid Origin	Description	N-terminal modification	Tail modification	Figure
pAM91	titin-I27^{V15P}-35	-	-	1D, 2E-F, 4C-D, S4B, S6, Table S5, Table S7
pAM91	titin-I27^{V15P}-35	5-FAM	-	2B-C, 3A-B, 4D, S1-3, S4D, S7C, S10, Table S3
pAM91	titin-I27^{V15P}-35	-	5-FAM	4A, S9
pAM91	titin-I27^{V15P}-35	5-FAM	Cy5	Table S3
pAM91	titin-I27^{V15P}-35	-	Cy5	2D, 4B, S4A, Table S4
pAM92	titin-I27^{V15P}-35 (DUB)	5-FAM	Cy5	2G, S4C, S5, Table S6
pAM93	titin-I27-35	-	-	S6, Table S7
pAM93	titin-I27-35	5-FAM	-	3A, 3B, Table S3
pAM93	titin-I27-35	5-FAM	Cy5	Table S3
pAM94	titin-I27$^{V13P/V15P}$-35	-	-	S6, Table S7
pAM94	titin-I27$^{V13P/V15P}$-35	5-FAM	-	3A, 3B, Table S3
pAM95	titin-I27^{V15P}-1K	5-FAM	-	3C, S2, S7, Table S3
pAM96	titin-I27^{V15P}-2K	5-FAM	-	3C, S2, S7, Table S3
pAM97	titin-I27^{V15P}-3K	5-FAM	-	3C, S2, S7, Table S3
pAM98	titin-I27^{V15P}-25	-	Cy5	4B, Table S4
pAM98	titin-I27^{V15P}-25	-	5-FAM	Table S3, S8
pAM99	titin-I27^{V15P}-11	-	Cy5	4B, Table S4
pAM99	titin-I27^{V15P}-11	-	-	4C, 4D
pAM99	titin-I27^{V15P}-11	-	5-FAM	4A, S9, S11
pAM100	titin-I27^{V15P} -1	-	Cy5	4B, Table S4
pAM100	titin-I27^{V15P} -1	-	-	4C, 4D
pAM100	titin-I27^{V15P}-1	-	5-FAM	4A, S2, S9, S11
pAM101	titin-I27^{V15P}-serine rich	-	Cy5	4B, Table S4
pAM101	titin-I27^{V15P}-serine rich	-	-	4C, 4D
pAM101	titin-I27^{V15P}-serine rich	-	5-FAM	4A, S8-9, S11

Table 3.S3. Degradation fits.

Substrate Description	A_1/A_2	τ_1+t_0 (s)	τ_2+t_0 (s)	t_0 (s)
FAM- titin-I27-35	2.3 ± 0.3	47.2 ± 2.1	499 ± 98	11.0
FAM-titin-I27-35-Cy5	4.2 ± 0.3	45.0 ± 1.8	223 ± 18	11.5
FAM-titin-I27^{V15P}-35	2.1 ± 0.2	18.1 ± 0.4	89 ± 10	7.4
FAM-titin-I27^{V15P}-35-Cy5	3.0 ± 0.6	20.0 ± 0.7	139 ± 44	7.5
FAM-titin-I27$^{V13P/V15P}$-35	1.7 ± 0.1	14.7 ± 0.3	77 ± 5	6.0
titin-I27^{V15P}-25-FAM	5.4 ± 0.5	21.1 ± 0.5	157 ± 30	7.5
FAM-titin-I27^{V15P}-1k	2.6 ± 0.5	22.0 ± 1.8	111 ± 22	10.0
FAM-titin-I27^{V15P}-2k	3.1 ± 0.7	21.0 ± 0.8	108 ± 14	10.0
FAM-titin-I27^{V15P}-3k	3.2 ± 0.8	21.4 ± 0.2	126 ± 12	10.0

Table 3.S4. Tail insertion fits.

Substrate Description	A_1/A_2	τ_1 (s)	τ_2 (s)	A_1 (normalized to 35)
titin-I27^{V15P}-35-Cy5	2.0 ± 0.3	1.61 ± 0.32	17.3 ± 3.0	1.00 ± 0.03
titin-I27^{V15P}-srr-Cy5	1.1 ± 0.1	7.15 ± 1.00	31.5 ± 4.3	0.51 ± 0.04
titin-I27^{V15P}-25-Cy5	1.7 ± 0.1	1.73 ± 0.02	17.4 ± 0.9	0.87 ± 0.05
titin-I27^{V15P}-11-Cy5	0.6 ± 0.2	0.70 ± 0.09	61.9 ± 27.3	0.24 ± 0.01
titin-I27^{V15P}-1-Cy5	0.9 ± 0.1	0.46 ± 0.03	60.0 ± 12.6	0.16 ± 0.001

Table 3.S5. Conformational change fit.

Substrate Description	A_1/A_2	τ_1+t_0 (s)	τ_2+t_0 (s)	t_0 (s)
titin-I27^{V15P}-35	2.3 ± 0.2	2.22 ± 0.10	24.9 ± 1.8	0.4

Table 3.S6. Deubiquitination fit.

Substrate Description	A_1/A_2	τ_1 (s)	τ_2 (s)
FAM-titin-$I27^{V15P}$-35(DUB)-Cy5	0.9 ± 0.1	6.83 ± 0.17	35.6 ± 2.6

Table 3.S7. ATPase rates.

Sample	ATPase rate (ATP s^{-1} $enzyme^{-1}$)
26S alone	0.73 ± 0.02
26S + ub'd titin-$I27^{V13P/V15P}$-35	1.12 ± 0.11
26S + ub'd titin-$I27^{V15P}$-35	1.35 ± 0.12
26S + ub'd titin-I27-35	1.47 ± 0.11

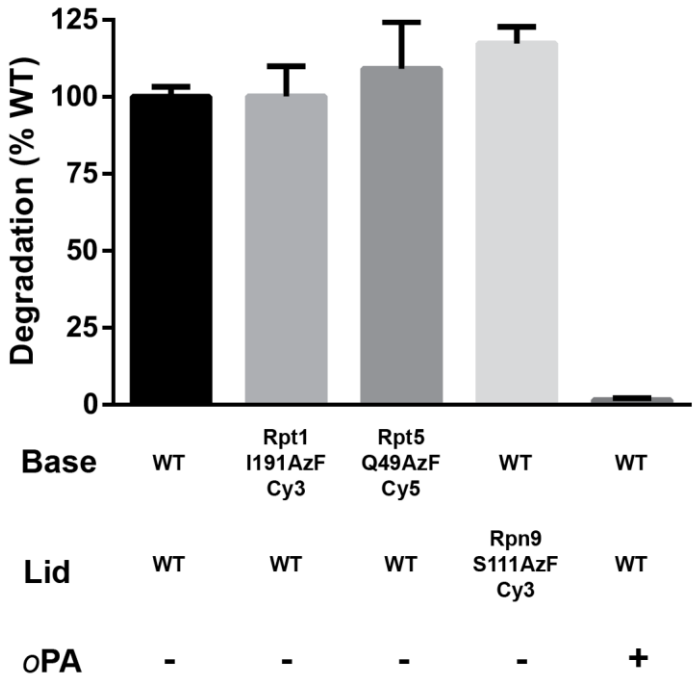

Figure 3.S1. Multiple-turnover degradations with labeled components.

Initial rates for multiple-turnover degradations of FAM-titin-I27^{V15P}-35 by 26S proteasome, tracked by anisotropy of 5-FAM covalently attached to the N-terminus of the substrate. Proteasomes were reconstituted using the indicated lid and base components, limiting 20S core, and Rpn10. Degradation rates are normalized to that of proteasomes reconstituted with all wild-type components. 1,10-phenanthroline (*o*PA) inhibits Rpn11 ubiquitin cleavage and thus prevents degradation. Data shown are means and s.d. (*N*=3).

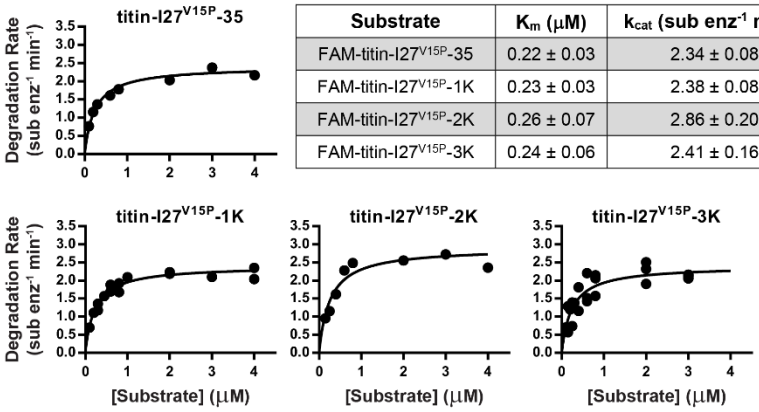

Substrate	K_m (μM)	k_{cat} (sub enz^{-1} min^{-1})
FAM-titin-I27^{V15P}-35	0.22 ± 0.03	2.34 ± 0.08
FAM-titin-I27^{V15P}-1K	0.23 ± 0.03	2.38 ± 0.08
FAM-titin-I27^{V15P}-2K	0.26 ± 0.07	2.86 ± 0.20
FAM-titin-I27^{V15P}-3K	0.24 ± 0.06	2.41 ± 0.16

Figure 3.S2. Michaelis Menten analysis of substrate variants.

The initial rates for multiple-turnover degradation of the indicated substrates at varying concentrations were determined by tracking anisotropy of 5-FAM attached to the N-terminus of the titin-I27 domain. The curves were fit to the Michaelis-Menten equation, and K_M and k_{cat} are reported with the standard error of the fits.

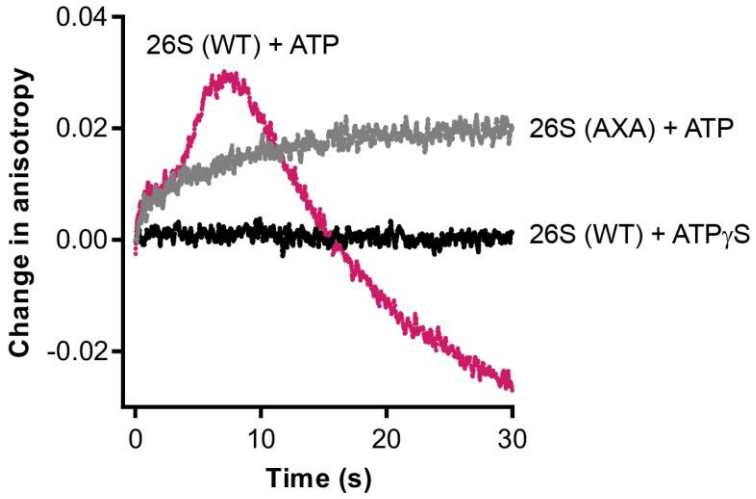

Figure 3.S3 Comparison of AXA vs. WT 26S.

The anisotropy change of FAM-titin-I27^{V15P}-35 after the addition of reconstituted 26S proteasome in the presence of either ATP or ATPγS. The 26S proteasome was reconstituted with either wild-type (WT) or catalytically-dead Rpn11^{AXA} (AXA) lid.

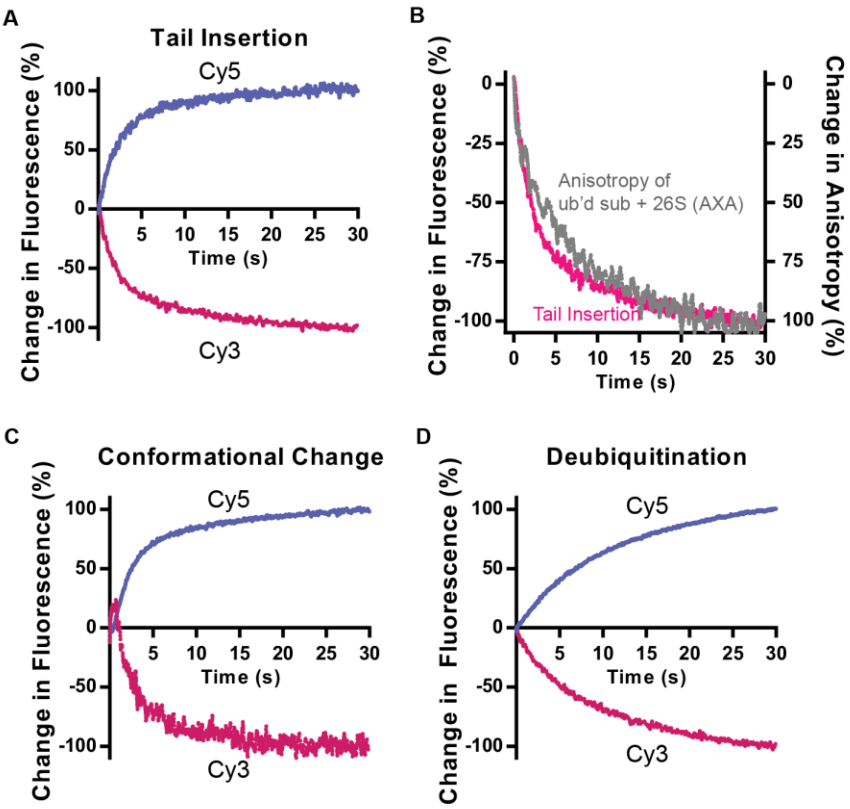

Figure 3.S4. Reciprocal relationship of Cy3 and Cy5 fluorescence during FRET experiments.

Representative traces of each fluorescence channel from the FRET experiments in Fig. 2. Each trace was normalized to both the initial fluorescence (0%) and the fluorescence after 30 s (100%). (**A**) Ubiquitinated titin-I27^{V15P}-35-Cy5 was mixed with *o*PA-treated, Rpt1-I191AzF-Cy3-containing proteasome in the presence of ATP, as in Fig. 2D. (**B**) Overlay of the Cy3 channel from **A** and the anisotropy of FAM-titin-I27^{V15P}-35 after mixing with 26S proteasome containing catalytically dead Rpn11^{AXA} (AXA), as in Fig. S3. Like the fluorescence channel, the anisotropy trace was normalized to both the anisotropy at t=0 (0%) and the anisotropy after 30 s (100%). (**C**) *o*PA-treated proteasome containing Rpn9S111AzF-Cy3 and Rpt5Q49AzF-Cy5, as in Fig. 2E, were mixed with ubiquitinated titin-I27^{V15P}-35 and ATP. (**D**) Titin-I27^{V15P}-35-Cy5 ubiquitinated with Cy3-ubiquitin as in Fig. 2G, was mixed with proteasome and ATP.

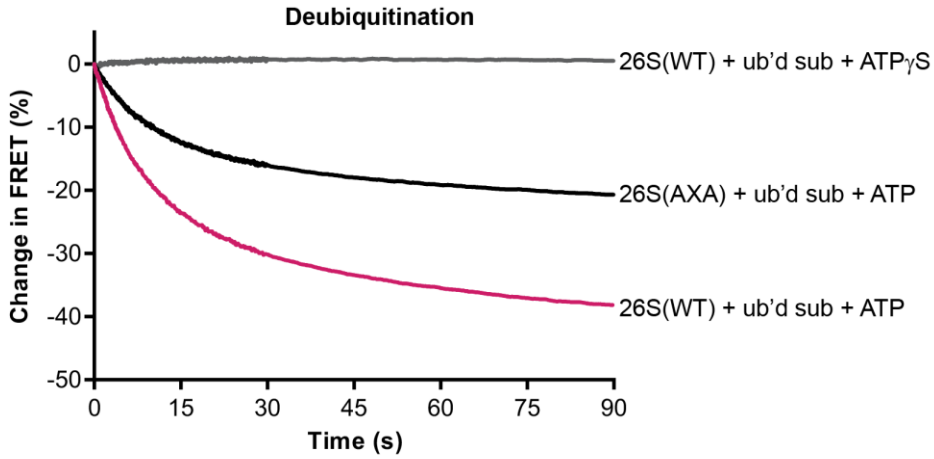

Figure 3.S5. FRET between ubiquitin and substrate.

Titin-I27^{V15P}-35-Cy5 substrate modified with Cy3-labeled ubiquitin was mixed with wild-type 26S proteasome in the presence of ATP or ATPγS, or with proteasome reconstituted with Rpn11^{AXA} lid, and monitored by Cy5 fluorescence.

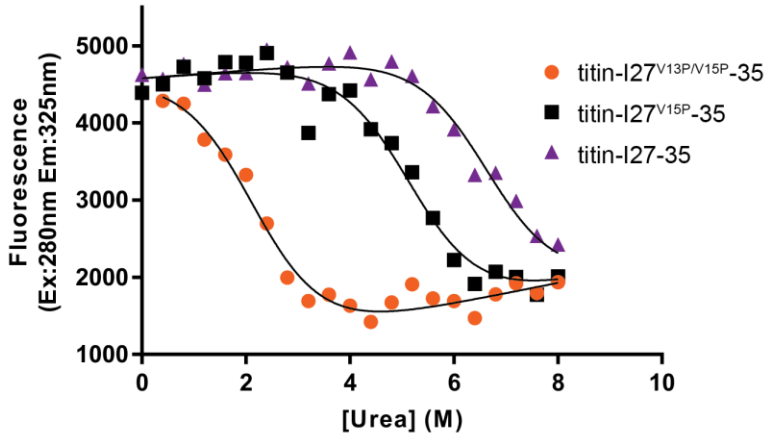

	A_0	m_A	B_0	m_B	m	c_m	ΔG_0 (kJ mol^{-1})
titin-I27$^{V13P/V15P}$-35	4579 ± 64	52 ± 28	840 ± 243	136 ± 36	-3626 ± 270	2.2 ± 0.1	-7.9 ± 1.4
titin-I27^{V15P}-35	”	”	”	”	”	5.2 ± 0.1	-18.8 ± 0.7
titin-I27-35	”	”	”	”	”	6.7 ± 0.1	-24.3 ± 1.8

Figure 3.S6. Determining the thermodynamic stability of titin variants.

Denaturant-induced equilibrium unfolding of substrates with different titin stabilities. The folded state of titin-I27 was monitored by tracking intrinsic tryptophan fluorescence. The curves were fit to the following system of equations: $y=(A+B*k)/(1+k)$, $A=A_0+m_A*[urea]$, $B=B_0+m_B*[urea]$, $k=e^{(-\Delta G/(RT)}$, $\Delta G= m*(c_m-[urea])$. All variables were fit globally across the three substrates, except for the c_m values. The ΔG_0 was then calculated using the equation $\Delta G_0= m*c_m$.

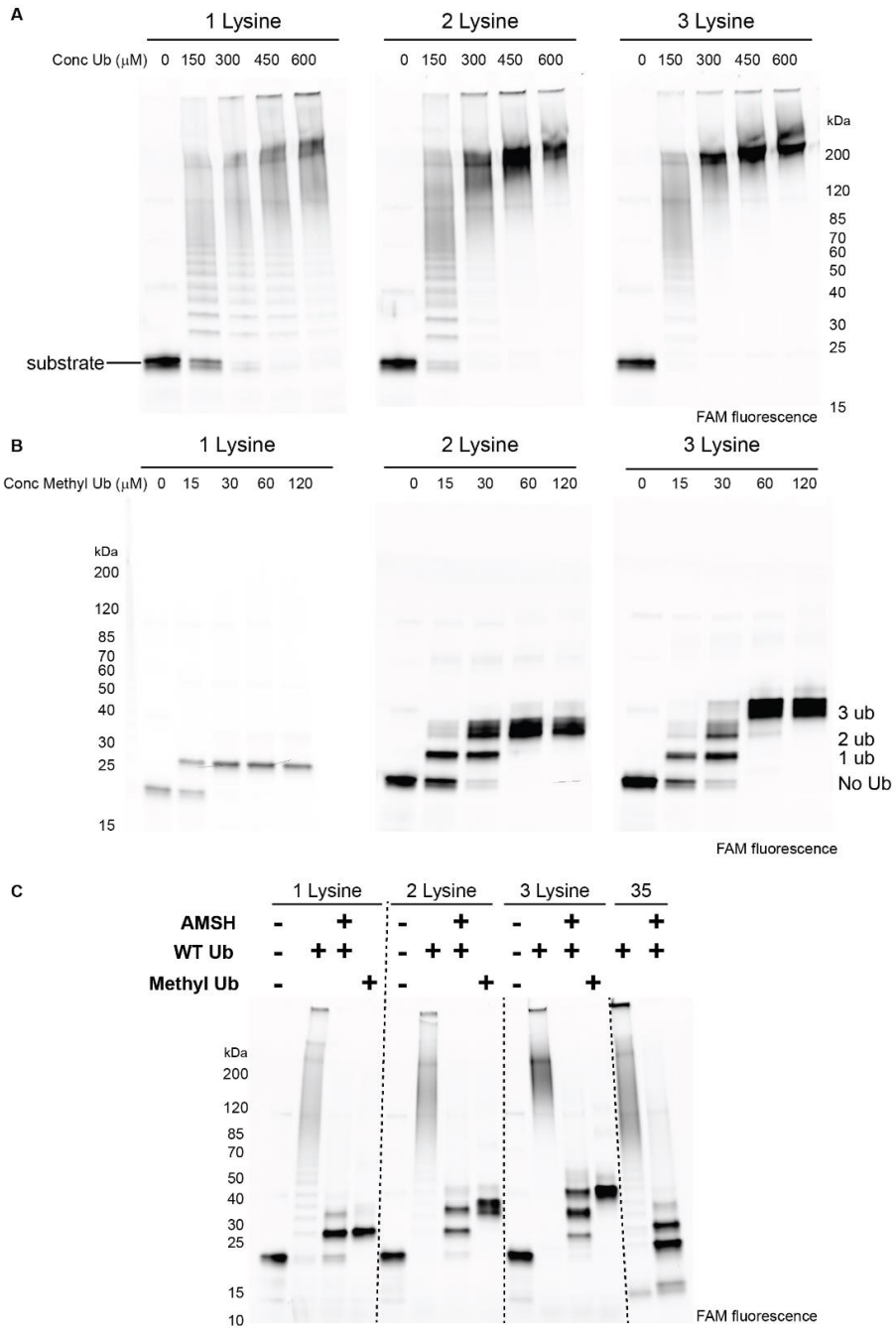

Figure 3.S7. Ubiquitination state of multiple lysine substrates.

Substrates with 1 , 2, or 3 lysines were ubiquitinated with varying concentrations of ubiquitin, analyzed by SDS-PAGE and visualized by 5-FAM fluorescence. Wild-type ubiquitin is used in (**A**), methyl ubiquitin, which is unable to form chains, is used in (**B**). In (**C**), the substrates were modified with either 400 μM wild-type ubiquitin or 120 μM methyl ubiquitin. The sample with wild-type ubiquitin was treated with the K63-specific deubiquitinase AMSH. Also in (**C**), the FAM-titin-I27^{V15P}-35 was ubiquitinated with 400 μM wild-type ubiquitin and treated with AMSH.

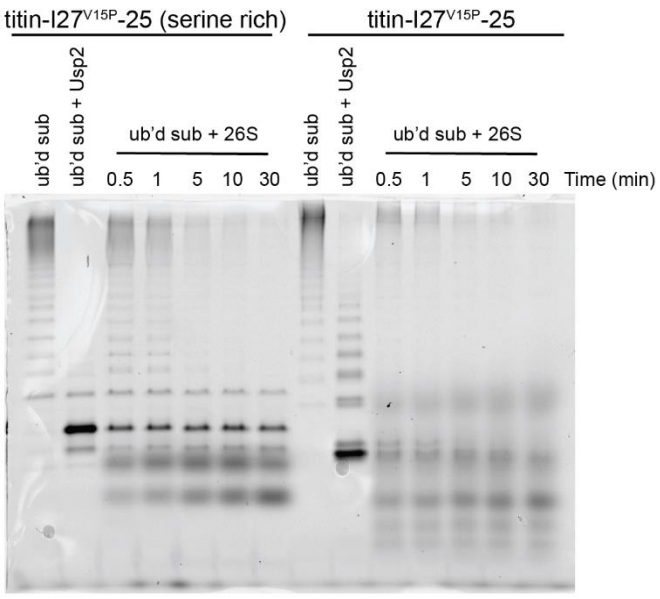

Figure 3.S8. Comparison of substrates with 25 amino acid tails.

Single-turnover degradations of substrates with 25 amino acid tails, labeled with 5-FAM on the C-terminal tail, analyzed by SDS-PAGE, and visualized by 5-FAM fluorescence. Also shown is a control with the ubiquitinated substrate after addition of the non-specific deubiquitinase Usp2.

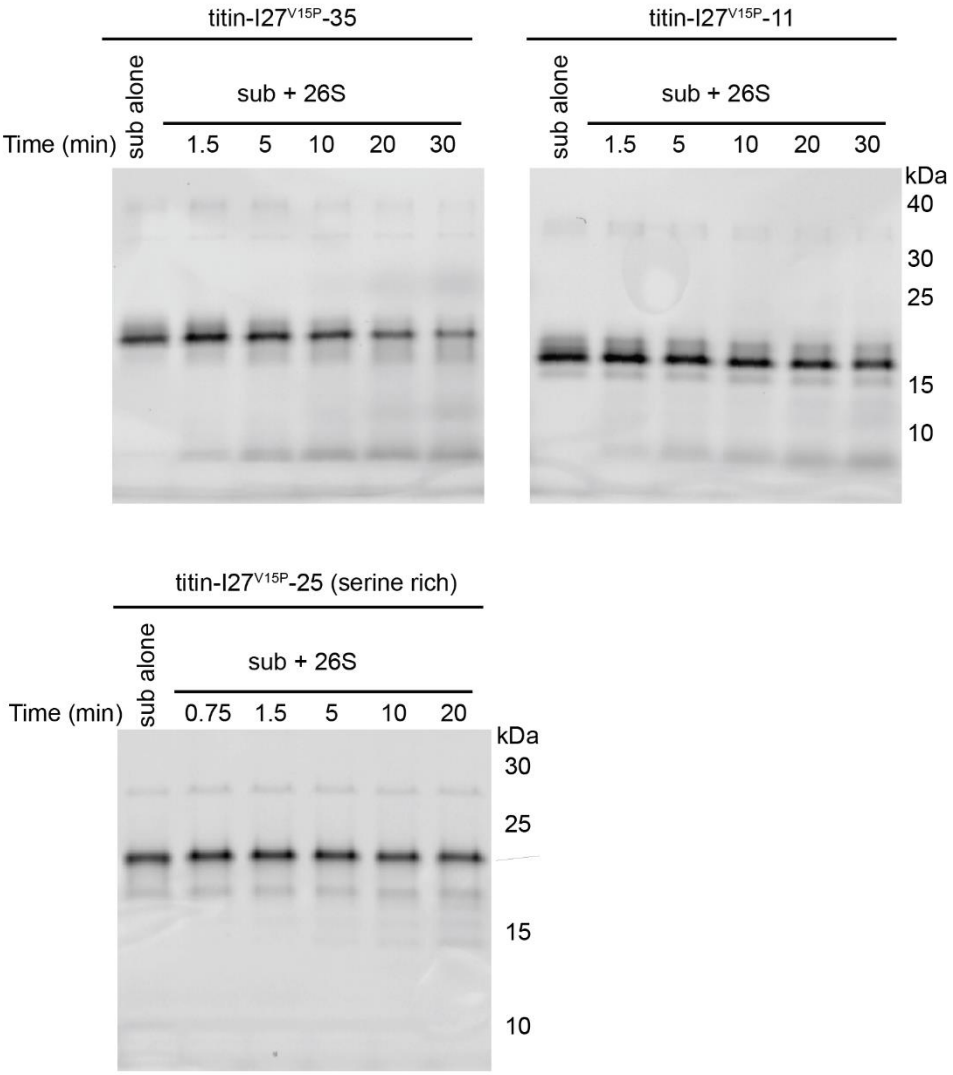

Figure 3.S9. Non-ubiquitinated substrate degradation.

Single-turnover degradations of non-ubiquitinated substrates, labeled with 5-FAM on the C-terminal tail, using the same reconstituted proteasome conditions as those used in Fig. 4D. The degradation observed may be a result of unbound 20S core particle directly proteolyzing substrates and could account for the small accumulation of peptide products observed for titin-I27^{V15}-11 in Fig. 4A.

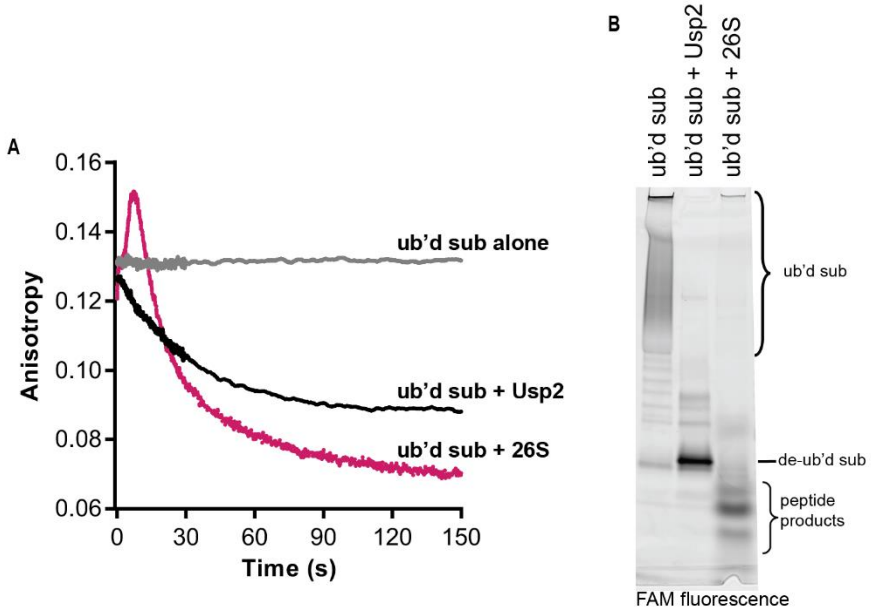

Figure 3.S10. Anisotropy can be used to track deubiquitination.

(**A**) Anisotropy change of FAM-titin-I27^{V15P}-35 after addition of reconstituted 26S proteasome with ATP or addition of the non-specific deubiquitinase Usp2. The anisotropy change is greater after addition of proteasome due to proteolytic cleavage of the substrate into small peptides. (**B**) SDS-PAGE analysis of ubiquitinated FAM-titin-I27^{V15P}-35 alone, after addition of Usp2 or 26S proteasome.

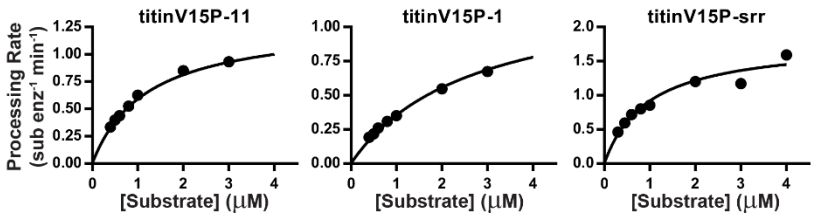

Substrate	K_m (μM)	k_{cat} (sub enz^{-1} min^{-1})
titin-I27^{V15P}-11-FAM	1.20 ± 0.06	1.34 ± 0.03
titin-I27^{V15P}-1-FAM	2.67 ± 0.31	1.32 ± 0.09
titin-I27^{V15P}-serine rich-FAM	0.96 ± 0.21	1.78 ± 0.15

Figure 3.S11. Michaelis-Menten analyses of substrate variants.

The initial rates of multiple-turnover processing of the indicated substrates at varying concentrations were determined by tracking the anisotropy of 5-FAM attached to the C-terminal unstructured region. The curves were fit to the Michaelis-Menten equation, and K_M and k_{cat} are reported with the standard error of the fits.

Chapter 4: Conclusions

Summary

This work arose out of a simple question: what is the rate-limiting step of degradation by the 26S proteasome? In order to answer this question, it was necessary to develop assays that would time individual steps of the processing pathway. These assays in turn required tools to site-specifically label the proteasome and a series of substrates whose degradation could be tracked. Just before undertaking this work, cryo-EM studies revealed the structure of the 26S proteasome, allowing for the precise design of fluorescent sensors (28, 48). In addition, the development of unnatural amino acid technology and biorthogonal click chemistry were well timed to enable the extension of these techniques to the complex reconstitution of the proteasome developed by previous members of the Martin lab (26, 28).

The synthesis of these various techniques led to the protocol described in Chapter 2 (200). This protocol allowed for the incorporation of 4-azido-L-phenylalanine at specific amino acid positions in the base and lid sub-complex, and the subsequent covalent attachment of fluorophores using bio-orthogonal chemistry targeting the azide group. This technique then allowed for the development of a series of fluorescence-based assays for investigating substrate processing, which are described in Chapter 3 (201). The kinetics of tail insertion, deubiquitination, unfolding and degradation were measured and compared with the kinetics of the conformational change of the proteasome using a model substrate. For this substrate, unfolding was the rate-limiting step, and it was also shown that the fast substrate tail insertion is the trigger for the proteasome to change into a substrate-processing conformation. Additional experiments using substrate variants confirmed that unfolding is rate-limiting, and also revealed that the proteasome uses a kinetic proofreading mechanism to ensure degradation fidelity.

Future Directions

The experiments discussed in Chapter 3 revealed many details of the mechanisms by which substrates are processed by the 26S proteasome, but also laid the groundwork for many important follow-up experiments. These include investigating the kinetics of processing for a wider variety of substrates, examining the effects of mutating components of the proteasome and extending the studies into cells.

While some variants of the base titin substrate were examined, many more remain which may be interesting. For instance, it has been proposed that varying the placement, type and number of ubiquitin chains on the substrate may affect processing kinetics (46, 98). This could be easily tested using the assays described above. In addition, the titin domain could be replaced with a variety of native substrates to determine if all proteasome substrates are processed with similar kinetics or if the rate of engagement varies. In addition, a number of polypeptide sequences are known to inhibit degradation (112). The mechanisms of this inhibition could also be investigated and may reveal important principles of how the proteasome triages substrates in the cell.

Mutations to a number of components of the 26S proteasome have been reported to have deleterious effects, but it is unclear what aspect of processing they effect (26, 27, 78). It is been proposed, for instance, that ATP hydrolysis by subunits near the top of the AAA+ spiral staircase is particularly important for substrate engagement (26). This hypothesis could be easily tested using the assays described above and would help further define the molecular mechanisms of substrate processing. There are also a number of phosphorylation events proposed to affect substrate processing, and it would be fascinating to determine which steps of processing are most altered (64, 65). Finally, accessory proteins such as Ubp6 are also known to modulate proteasome activity, but once again the mechanisms of their action need further investigation (47).

Most of the FRET-based assays described here are mostly suitable for *in vitro* reconstituted experiments, but the assay that tracks the conformational state of the proteasome is potentially transferable to *in vivo* experiments (Figure 3.1). Technologies such as the SNAP, CLIP or Halo tag allow for the covalent attachment of fluorophores in cells to specific locations (202, 203). Using these tags to attach a donor and acceptor to Rpn9 and Rpt5 may thus allow for a FRET-based readout of the conformational state of the proteasome in cells. This could potentially give a dynamic readout of proteasome activity and localization, and allow for direct visualization of the proteasomal response to a changing cellular environment.

Many experiments thus remain to uncover the details of how this fascinating molecular machine works.

References

1. Komander D & Rape M (2012) The ubiquitin code. *Annual review of biochemistry* 81:203-29.
2. Bhattacharyya S, Yu H, Mim C, & Matouschek A (2014) Regulated protein turnover: snapshots of the proteasome in action. *Nature Reviews Molecular Cell Biology* 15(2):122-33.
3. Collins GA & Goldberg AL (2017) The Logic of the 26S Proteasome.
4. Finley D (2009) Recognition and Processing of Ubiquitin-Protein Conjugates by the Proteasome. *Annual Review of Biochemistry* 78(1):477-513.
5. Goldberg AL (2007) Functions of the proteasome: from protein degradation and immune surveillance to cancer therapy. *Biochem Soc Trans* 35(Pt 1):12-7.
6. Budenholzer L, Cheng CL, Li Y, & Hochstrasser M (2017) Proteasome Structure and Assembly. *J Mol Biol* 429(22):3500-24.
7. Sadre-Bazzaz K, Whitby FG, Robinson H, Formosa T, & Hill CP (2010) Structure of a Blm10 complex reveals common mechanisms for proteasome binding and gate opening. *Mol Cell* 37(5):728-35.
8. Tian G, Park S, Lee MJ, Huck B, McAllister F, Hill CP, Gygi SP, & Finley D (2011) An asymmetric interface between the regulatory and core particles of the proteasome. *Nature structural & molecular biology* 18(11):1259-67.
9. Gillette TG, Kumar B, Thompson D, Slaughter CA, & DeMartino GN (2008) Differential roles of the COOH termini of AAA subunits of PA700 (19 S regulator) in asymmetric assembly and activation of the 26 S proteasome. *J Biol Chem* 283(46):31813-22.
10. Glickman MH & Rubin DM (1998) The regulatory particle of the Saccharomyces cerevisiae proteasome. *Molecular and Cellular …* 18(6).
11. Groll M, Bajorek M, Kohler A, Moroder L, Rubin DM, Huber R, Glickman MH, & Finley D (2000) A gated channel into the proteasome core particle. *Nat Struct Biol* 7(11):1062-7.
12. Rabl J, Smith DM, Yu Y, Chang SC, Goldberg AL, & Cheng Y (2008) Mechanism of gate opening in the 20S proteasome by the proteasomal ATPases. *Mol Cell* 30(3):360-8.
13. Smith DM, Chang S-C, Park S, Finley D, Cheng Y, & Goldberg AL (2007) Docking of the proteasomal ATPases' carboxyl termini in the 20S proteasome's alpha ring opens the gate for substrate entry. *Molecular cell* 27(5):731-44.
14. Finley D, Chen X, & Walters KJ (2016) Gates, Channels, and Switches: Elements of the Proteasome Machine. *Trends in Biochemical Sciences* 41(1):77-93.
15. Wehmer M, Rudack T, Beck F, Aufderheide A, Pfeifer G, Plitzko JM, Forster F, Schulten K, Baumeister W, & Sakata E (2017) Structural insights into the functional cycle of the ATPase module of the 26S proteasome. *Proc Natl Acad Sci U S A* 114(6):1305-10.
16. Glickman MH, Rubin DM, Coux O, Wefes I, Pfeifer G, Cjeka Z, Baumeister W, Fried Va, & Finley D (1998) A subcomplex of the proteasome regulatory particle required for ubiquitin-conjugate degradation and related to the COP9-signalosome and eIF3. *Cell* 94(5):615-23.
17. Saeki Y & Tanaka K (2012) Assembly and function of the proteasome. *Methods Mol Biol* 832:315-37.

18. He J, Kulkarni K, da Fonseca PC, Krutauz D, Glickman MH, Barford D, & Morris EP (2012) The structure of the 26S proteasome subunit Rpn2 reveals its PC repeat domain as a closed toroid of two concentric alpha-helical rings. *Structure* 20(3):513-21.
19. Shi Y, Chen X, Elsasser S, Stocks BB, Tian G, Lee BH, Shi Y, Zhang N, de Poot SA, Tuebing F, Sun S, Vannoy J, Tarasov SG, Engen JR, Finley D, & Walters KJ (2016) Rpn1 provides adjacent receptor sites for substrate binding and deubiquitination by the proteasome. *Science* 351(6275).
20. Husnjak K, Elsasser S, Zhang N, Chen X, Randles L, Shi Y, Hofmann K, Walters KJ, Finley D, & Dikic I (2008) Proteasome subunit Rpn13 is a novel ubiquitin receptor. *Nature* 453(7194):481-8.
21. van Nocker S, Sadis S, Rubin DM, Glickman M, Fu H, Coux O, Wefes I, Finley D, & Vierstra RD (1996) The multiubiquitin-chain-binding protein Mcb1 is a component of the 26S proteasome in Saccharomyces cerevisiae and plays a nonessential, substrate-specific role in protein turnover. *Mol Cell Biol* 16(11):6020-8.
22. Deveraux Q, Ustrell V, Pickart C, & Rechsteiner M (1994) A 26 S protease subunit that binds ubiquitin conjugates. *The Journal of biological chemistry* 269(10):7059-61.
23. Martin A, Baker Ta, & Sauer RT (2008) Pore loops of the AAA+ ClpX machine grip substrates to drive translocation and unfolding. *Nature structural & molecular biology* 15(11):1147-51.
24. Maillard RA, Chistol G, Sen M, Righini M, Tan J, Kaiser CM, Hodges C, Martin A, & Bustamante C (2011) ClpX(P) generates mechanical force to unfold and translocate its protein substrates. *Cell* 145(3):459-69.
25. Aubin-Tam ME, Olivares AO, Sauer RT, Baker TA, & Lang MJ (2011) Single-molecule protein unfolding and translocation by an ATP-fueled proteolytic machine. *Cell* 145(2):257-67.
26. Beckwith R, Estrin E, Worden EJ, & Martin A (2013) Reconstitution of the 26S proteasome reveals functional asymmetries in its AAA+ unfoldase. *Nature structural & molecular biology* 20(10):1164-72.
27. Erales J, Hoyt MA, Troll F, & Coffino P (2012) Functional Asymmetries of Proteasome Translocase Pore.
28. Lander GC, Estrin E, Matyskiela ME, Bashore C, Nogales E, & Martin A (2012) Complete subunit architecture of the proteasome regulatory particle. *Nature* 482(7384):186-91.
29. Lasker K, Förster F, Bohn S, Walzthoeni T, Villa E, Unverdorben P, Beck F, Aebersold R, Sali A, & Baumeister W (2012) Molecular architecture of the 26S proteasome holocomplex determined by an integrative approach. *Proceedings of the National Academy of Sciences of the United States of America* 109(5):1380-7.
30. de Poot SAH, Tian G, & Finley D (2017) Meddling with Fate: The Proteasomal Deubiquitinating Enzymes. *J Mol Biol* 429(22):3525-45.
31. Verma R, Aravind L, Oania R, McDonald WHH, Yates JR, Koonin EV, & Deshaies RJ (2002) Role of Rpn11 metalloprotease in deubiquitination and degradation by the 26S proteasome. *Science* 298(5593):611-5.
32. Yao T & Cohen RE (2002) A cryptic protease couples deubiquitination and degradation by the proteasome. *Nature* 419(6905):403-7.

33. Lee B-H, Lu Y, Prado MA, Shi Y, Tian G, Sun S, Elsasser S, Gygi SP, King RW, & Finley D (2016) USP14 deubiquitinates proteasome-bound substrates that are ubiquitinated at multiple sites. *Nature* 532(7599):398-401.
34. Lam YA, Xu W, DeMartino GN, & Cohen RE (1997) Editing of ubiquitin conjugates by an isopeptidase in the 26S proteasome. *Nature* 385:737-40.
35. Yao T, Song L, Xu W, DeMartino GN, Florens L, Swanson SK, Washburn MP, Conaway RC, Conaway JW, & Cohen RE (2006) Proteasome recruitment and activation of the Uch37 deubiquitinating enzyme by Adrm1. *Nat Cell Biol* 8(9):994-1002.
36. Hamazaki J, Iemura S, Natsume T, Yashiroda H, Tanaka K, & Murata S (2006) A novel proteasome interacting protein recruits the deubiquitinating enzyme UCH37 to 26S proteasomes. *EMBO J* 25(19):4524-36.
37. Qiu XB, Ouyang SY, Li CJ, Miao S, Wang L, & Goldberg AL (2006) hRpn13/ADRM1/GP110 is a novel proteasome subunit that binds the deubiquitinating enzyme, UCH37. *EMBO J* 25(24):5742-53.
38. Matyskiela ME, Lander GC, & Martin A (2013) Conformational switching of the 26S proteasome enables substrate degradation. *Nature structural & molecular biology* 20(7):781-8.
39. Śledź P, Unverdorben P, Beck F, Pfeifer G, Schweitzer A, Förster F, & Baumeister W (2013) Structure of the 26S proteasome with ATP-γS bound provides insights into the mechanism of nucleotide-dependent substrate translocation. *Proceedings of the National Academy of Sciences of the United States of America* 110(18):7264-9.
40. Unverdorben P, Beck F, Śledź P, Schweitzer A, Pfeifer G, Plitzko JM, Baumeister W, & Förster F (2014) Deep classification of a large cryo-EM dataset defines the conformational landscape of the 26S proteasome. *Proceedings of the National Academy of Sciences of the United States of America* 111(15):5544-9.
41. Luan B, Huang X, Wu J, Mei Z, Wang Y, Xue X, Yan C, Wang J, Finley DJ, Shi Y, & Wang F (2016) Structure of an endogenous yeast 26S proteasome reveals two major conformational states. *Proceedings of the National Academy of Sciences of the United States of America* 113(10):2642-7.
42. Worden EJ, Dong KC, & Martin A (2017) An AAA Motor-Driven Mechanical Switch in Rpn11 Controls Deubiquitination at the 26S Proteasome. *Mol Cell* 67(5):799-811 e8.
43. Ding Z, Fu Z, Xu C, Wang Y, Wang Y, Li J, Kong L, Chen J, Li N, Zhang R, & Cong Y (2017) High-resolution cryo-EM structure of the proteasome in complex with ADP-AlFx. *Cell Research* 27(3):373-85.
44. Chen S, Wu J, Lu Y, Ma YB, Lee BH, Yu Z, Ouyang Q, Finley DJ, Kirschner MW, & Mao Y (2016) Structural basis for dynamic regulation of the human 26S proteasome. *Proc Natl Acad Sci U S A* 113(46):12991-6.
45. Zhu Y, Wang WL, Yu D, Ouyang Q, Lu Y, & Mao Y (2018) Structural mechanism for nucleotide-driven remodeling of the AAA-ATPase unfoldase in the activated human 26S proteasome. *Nat Commun* 9(1):1360.
46. Inobe T, Fishbain S, Prakash S, & Matouschek A (2011) Defining the geometry of the two-component proteasome degron. *Nature Chemical Biology* 7(3):161-7.
47. Bashore C, Dambacher CM, Goodall EA, Matyskiela ME, Lander GC, & Martin A (2015) Ubp6 deubiquitinase controls conformational dynamics and substrate degradation of the 26S proteasome. *Nature structural & molecular biology* 22(9):712-9.

48. Beck F, Unverdorben P, Bohn S, Schweitzer A, Pfeifer G, Sakata E, Nickell S, Plitzko JM, Villa E, Baumeister W, & Förster F (2012) Near-atomic resolution structural model of the yeast 26S proteasome. *Proceedings of the National Academy of Sciences of the United States of America* 109(37):14870-5.
49. Haselbach D, Schrader J, Lambrecht F, Henneberg F, Chari A, & Stark H (2017) Long-range allosteric regulation of the human 26S proteasome by 20S proteasome-targeting cancer drugs. *Nature Communications* 8:15578-.
50. Schweitzer A, Aufderheide A, Rudack T, Beck F, Pfeifer G, Plitzko JM, Sakata E, Schulten K, Förster F, & Baumeister W (2016) Structure of the human 26S proteasome at a resolution of 3.9 Å. *Proceedings of the National Academy of Sciences of the United States of America* 113(28):7816-21.
51. Huang X, Luan B, Wu J, & Shi Y (2016) An atomic structure of the human 26S proteasome. *Nature Structural & Molecular Biology* 23(9):778-85.
52. da Fonseca PCa, He J, & Morris EP (2012) Molecular model of the human 26S proteasome. *Molecular cell* 46(1):54-66.
53. Asano S, Fukuda Y, Beck F, Aufderheide A, Forster F, Danev R, & Baumeister W (2015) Proteasomes. A molecular census of 26S proteasomes in intact neurons. *Science* 347(6220):439-42.
54. Park S, Li X, Kim HM, Singh CR, Tian G, Hoyt MA, Lovell S, Battaile KP, Zolkiewski M, Coffino P, Roelofs J, Cheng Y, & Finley D (2013) Reconfiguration of the proteasome during chaperone-mediated assembly. *Nature* 497(7450):512-6.
55. Yu Y, Smith DM, Kim HM, Rodriguez V, Goldberg AL, & Cheng Y (2010) Interactions of PAN's C-termini with archaeal 20S proteasome and implications for the eukaryotic proteasome-ATPase interactions. *The EMBO journal* 29(3):692-702.
56. Aufderheide A, Beck F, Stengel F, Hartwig M, Schweitzer A, Pfeifer G, Goldberg AL, Sakata E, Baumeister W, & Förster F (2015) Structural characterization of the interaction of Ubp6 with the 26S proteasome. *Proceedings of the National Academy of Sciences of the United States of America* 112(28):8626-31.
57. Hanna J, Hathaway Na, Tone Y, Crosas B, Elsasser S, Kirkpatrick DS, Leggett DS, Gygi SP, King RW, & Finley D (2006) Deubiquitinating enzyme Ubp6 functions noncatalytically to delay proteasomal degradation. *Cell* 127(1):99-111.
58. Peth A, Besche HC, & Goldberg AL (2009) Ubiquitinated proteins activate the proteasome by binding to Usp14/Ubp6, which causes 20S gate opening. *Mol Cell* 36(5):794-804.
59. Li X & Demartino GN (2009) Variably modulated gating of the 26S proteasome by ATP and polyubiquitin. *Biochem J* 421(3):397-404.
60. Smith DM, Fraga H, Reis C, Kafri G, & Goldberg AL (2011) ATP binds to proteasomal ATPases in pairs with distinct functional effects, implying an ordered reaction cycle. *Cell* 144(4):526-38.
61. Liu CW, Li X, Thompson D, Wooding K, Chang TL, Tang Z, Yu H, Thomas PJ, & DeMartino GN (2006) ATP binding and ATP hydrolysis play distinct roles in the function of 26S proteasome. *Mol Cell* 24(1):39-50.
62. Peth A, Nathan Ja, & Goldberg AL (2013) The ATP costs and time required to degrade ubiquitinated proteins by the 26 S proteasome. *The Journal of biological chemistry* 288(40):29215-22.

63. Peth A, Kukushkin N, Bossé M, & Goldberg AL (2013) Ubiquitinated proteins activate the proteasomal ATPases by binding to Usp14 or Uch37 homologs. *The Journal of biological chemistry* 288(11):7781-90.
64. Guo X, Wang X, Wang Z, Banerjee S, Yang J, Huang L, & Dixon JE (2016) Site-specific proteasome phosphorylation controls cell proliferation and tumorigenesis. *Nat Cell Biol* 18(2):202-12.
65. VerPlank JJS & Goldberg AL (2017) Regulating protein breakdown through proteasome phosphorylation. *Biochem J* 474(19):3355-71.
66. Tomko RJ, Funakoshi M, Schneider K, Wang J, & Hochstrasser M (2010) Heterohexameric ring arrangement of the eukaryotic proteasomal ATPases: implications for proteasome structure and assembly. *Molecular cell* 38(3):393-403.
67. Inobe T & Genmei R (2015) N-Terminal Coiled-Coil Structure of ATPase Subunits of 26S Proteasome Is Crucial for Proteasome Function. *PLoS One* 10(7):e0134056.
68. Zhang F, Hu M, Tian G, Zhang P, Finley D, Jeffrey PD, & Shi Y (2009) Structural insights into the regulatory particle of the proteasome from Methanocaldococcus jannaschii. *Molecular cell* 34(4):473-84.
69. Glynn SE, Martin A, Nager AR, Baker Ta, & Sauer RT (2009) Structures of asymmetric ClpX hexamers reveal nucleotide-dependent motions in a AAA+ protein-unfolding machine. *Cell* 139(4):744-56.
70. Glynn SE, Nager AR, Baker Ta, & Sauer RT (2012) Dynamic and static components power unfolding in topologically closed rings of a AAA+ proteolytic machine. *Nature structural & molecular biology* 19(6):616-22.
71. Gates SN, Yokom AL, Lin J, Jackrel ME, Rizo AN, Kendsersky NM, Buell CE, Sweeny EA, Mack KL, Chuang E, Torrente MP, Su M, Shorter J, & Southworth DR (2017) Ratchet-like polypeptide translocation mechanism of the AAA+ disaggregase Hsp104. *Science* 357(6348):273-9.
72. Ripstein ZA, Huang R, Augustyniak R, Kay LE, & Rubinstein JL (2017) Structure of a AAA+ unfoldase in the process of unfolding substrate. *Elife* 6.
73. Monroe N, Han H, Shen PS, Sundquist WI, & Hill CP (2017) Structural basis of protein translocation by the Vps4-Vta1 AAA ATPase. *eLife* 6:1-22.
74. Han H, Monroe N, Sundquist WI, Shen PS, & Hill CP (2017) The AAA ATPase Vps4 binds ESCRT-III substrates through a repeating array of dipeptide-binding pockets. *Elife* 6.
75. Puchades C, Rampello AJ, Shin M, Giuliano CJ, Wiseman RL, Glynn SE, & Lander GC (2017) Structure of the mitochondrial inner membrane AAA+ protease YME1 gives insight into substrate processing. *Science* 358(6363).
76. Thomsen ND & Berger JM (2009) Running in reverse: the structural basis for translocation polarity in hexameric helicases. *Cell* 139(3):523-34.
77. Zehr E, Szyk A, Piszczek G, Szczesna E, Zuo X, & Roll-Mecak A (2017) Katanin spiral and ring structures shed light on power stroke for microtubule severing. *Nat Struct Mol Biol* 24(9):717-25.
78. Rubin DM, Glickman MH, Larsen CN, Dhruvakumar S, & Finley D (1998) Active site mutants in the six regulatory particle ATPases reveal multiple roles for ATP in the proteasome. *The EMBO journal* 17(17):4909-19.

79. Hersch GL, Burton RE, Bolon DN, Baker Ta, & Sauer RT (2005) Asymmetric interactions of ATP with the AAA+ ClpX6 unfoldase: allosteric control of a protein machine. *Cell* 121(7):1017-27.
80. Yakamavich JA, Baker TA, & Sauer RT (2008) Asymmetric nucleotide transactions of the HslUV protease. *J Mol Biol* 380(5):946-57.
81. Nyquist K & Martin A (2013) Marching to the beat of the ring: polypeptide translocation by AAA+ proteases. *Trends in biochemical sciences*:1-8.
82. Horwitz AA, Navon A, Groll M, Smith DM, Reis C, & Goldberg AL (2007) ATP-induced structural transitions in PAN, the proteasome-regulatory ATPase complex in Archaea. *J Biol Chem* 282(31):22921-9.
83. Smith DM, Kafri G, Cheng Y, Ng D, Walz T, & Goldberg AL (2005) ATP binding to PAN or the 26S ATPases causes association with the 20S proteasome, gate opening, and translocation of unfolded proteins. *Molecular cell* 20(5):687-98.
84. Iosefson O, Nager AR, Baker TA, & Sauer RT (2015) Coordinated gripping of substrate by subunits of an AAA+ proteolytic machine. *Nature chemical biology* advance on.
85. Iosefson O, Olivares AO, Baker TA, & Sauer RT (2015) Dissection of Axial-Pore Loop Function during Unfolding and Translocation by a AAA+ Proteolytic Machine. *Cell Rep* 12(6):1032-41.
86. Prakash S, Tian L, Ratliff KS, Lehotzky RE, & Matouschek A (2004) An unstructured initiation site is required for efficient proteasome-mediated degradation. *Nature structural & molecular biology* 11(9):830-7.
87. Takeuchi J, Chen H, & Coffino P (2007) Proteasome substrate degradation requires association plus extended peptide. *The EMBO journal* 26(1):123-31.
88. Chau V, Tobias JW, Bachmair A, & Marriott D (1989) A multiubiquitin chain is confined to specific lysine in a targeted short-lived protein. *Science* 243(4898):1576-83.
89. Jin L, Williamson A, Banerjee S, Philipp I, & Rape M (2008) Mechanism of ubiquitin-chain formation by the human anaphase-promoting complex. *Cell* 133(4):653-65.
90. Xu P, Duong DM, Seyfried NT, Cheng D, Xie Y, Robert J, Rush J, Hochstrasser M, Finley D, & Peng J (2009) Quantitative proteomics reveals the function of unconventional ubiquitin chains in proteasomal degradation. *Cell* 137(1):133-45.
91. Johnson ES, Ma PC, Ota IM, & Varshavsky A (1995) A proteolytic pathway that recognizes ubiquitin as a degradation signal. *J Biol Chem* 270(29):17442-56.
92. Kim W, Bennett EJ, Huttlin EL, Guo A, Li J, Possemato A, Sowa ME, Rad R, Rush J, Comb MJ, Harper JW, & Gygi SP (2011) Systematic and quantitative assessment of the ubiquitin-modified proteome. *Mol Cell* 44(2):325-40.
93. Saeki Y, Kudo T, Sone T, Kikuchi Y, Yokosawa H, Toh-e A, & Tanaka K (2009) Lysine 63-linked polyubiquitin chain may serve as a targeting signal for the 26S proteasome. *EMBO J* 28(4):359-71.
94. Zhang D, Chen T, Ziv I, Rosenzweig R, Matiuhin Y, Bronner V, Glickman MH, & Fushman D (2009) Together, Rpn10 and Dsk2 can serve as a polyubiquitin chain-length sensor. *Mol Cell* 36(6):1018-33.
95. Riedinger C, Boehringer J, Trempe J-F, Lowe ED, Brown NR, Gehring K, Noble MEM, Gordon C, & Endicott JA (2010) Structure of Rpn10 and its interactions with polyubiquitin chains and the proteasome subunit Rpn12. *The Journal of biological chemistry* 285(44):33992-4003.

96. Elsasser S, Chandler-Militello D, Muller B, Hanna J, & Finley D (2004) Rad23 and Rpn10 serve as alternative ubiquitin receptors for the proteasome. *J Biol Chem* 279(26):26817-22.
97. Mayor T, Graumann J, Bryan J, MacCoss MJ, & Deshaies RJ (2007) Quantitative profiling of ubiquitylated proteins reveals proteasome substrates and the substrate repertoire influenced by the Rpn10 receptor pathway. *Mol Cell Proteomics* 6(11):1885-95.
98. Lu Y, Lee B-h, King RW, Finley D, & Kirschner MW (2015) Substrate degradation by the proteasome: A single-molecule kinetic analysis. *Science* 348(6231).
99. Shabek N, Herman-Bachinsky Y, Buchsbaum S, Lewinson O, Haj-Yahya M, Hejjaoui M, Lashuel HA, Sommer T, Brik A, & Ciechanover A (2012) The size of the proteasomal substrate determines whether its degradation will be mediated by mono- or polyubiquitylation. *Mol Cell* 48(1):87-97.
100. Zhang M, Pickart CM, & Coffino P (2003) Determinants of proteasome recognition of ornithine decarboxylase, a ubiquitin-independent substrate. *The EMBO journal* 22(7):1488-96.
101. Erales J & Coffino P (2014) Ubiquitin-independent proteasomal degradation. *Biochimica et Biophysica Acta (BBA) - Molecular Cell Research* 1843(1):216-21.
102. Janse DM, Crosas B, Finley D, & Church GM (2004) Localization to the proteasome is sufficient for degradation. *J Biol Chem* 279(20):21415-20.
103. Wilmington SR & Matouschek A (2016) An Inducible System for Rapid Degradation of Specific Cellular Proteins Using Proteasome Adaptors. *PLoS One* 11(4):e0152679.
104. Fishbain S, Prakash S, Herrig A, Elsasser S, & Matouschek A (2011) Rad23 escapes degradation because it lacks a proteasome initiation region. *Nat Commun* 2:192.
105. Yu H, Kago G, Yellman CM, & Matouschek A (2016) Ubiquitin-like domains can target to the proteasome but proteolysis requires a disordered region. *EMBO J* 35(14):1522-36.
106. Kraut DA & Matouschek A (2011) Proteasomal degradation from internal sites favors partial proteolysis via remote domain stabilization. *ACS Chem Biol* 6(10):1087-95.
107. Prakash S, Inobe T, Hatch AJ, & Matouschek A (2009) Substrate selection by the proteasome during degradation of protein complexes. *Nat Chem Biol* 5(1):29-36.
108. Ye Y, Tang WK, Zhang T, & Xia D (2017) A Mighty "Protein Extractor" of the Cell: Structure and Function of the p97/CDC48 ATPase. *Front Mol Biosci* 4:39.
109. Bodnar NO & Rapoport TA (2017) Molecular Mechanism of Substrate Processing by the Cdc48 ATPase Complex. *Cell* 169(4):722-35.e9.
110. Blythe EE, Olson KC, Chau V, & Raymond J (2017) Ubiquitin-and ATP-dependent P97/VCP•NPLOC4•UFD1L1 is enhanced by a mutation that causes multisystem proteinopathy. *bioRxiv*.
111. Peth A, Uchiki T, & Goldberg AL (2010) ATP-dependent steps in the binding of ubiquitin conjugates to the 26S proteasome that commit to degradation. *Molecular cell* 40(4):671-81.
112. Fishbain S, Inobe T, Israeli E, Chavali S, Yu H, Kago G, Babu MM, & Matouschek A (2015) Sequence composition of disordered regions fine-tunes protein half-life. *Nature Structural & Molecular Biology* 22(3):214-21.
113. Kraut Da, Israeli E, Schrader EK, Patil A, Nakai K, Nanavati D, Inobe T, & Matouschek A (2012) Sequence- and species-dependence of proteasomal processivity. *ACS chemical biology* 7(8):1444-53.

114. Yu H, Singh Gautam AK, Wilmington SR, Wylie D, Martinez-Fonts K, Kago G, Warburton M, Chavali S, Inobe T, Finkelstein IJ, Babu MM, & Matouschek A (2016) Conserved Sequence Preferences Contribute to Substrate Recognition by the Proteasome. *The Journal of biological chemistry* 291(28):14526-39.
115. Tian L, Holmgren RA, & Matouschek A (2005) A conserved processing mechanism regulates the activity of transcription factors Cubitus interruptus and NF-kappaB. *Nat Struct Mol Biol* 12(12):1045-53.
116. Piwko W & Jentsch S (2006) Proteasome-mediated protein processing by bidirectional degradation initiated from an internal site. *Nat Struct Mol Biol* 13(8):691-7.
117. Schreiner P, Chen X, Husnjak K, Randles L, Zhang N, Elsasser S, Finley D, Dikic I, Walters KJ, & Groll M (2008) Ubiquitin docking at the proteasome through a novel pleckstrin-homology domain interaction. *Nature* 453(7194):548-52.
118. Zhang N, Wang Q, Ehlinger A, Randles L, Lary JW, Kang Y, Haririnia A, Storaska AJ, Cole JL, Fushman D, & Walters KJ (2009) Structure of the s5a:k48-linked diubiquitin complex and its interactions with rpn13. *Molecular cell* 35(3):280-90.
119. Mueller TD & Feigon J (2003) Structural determinants for the binding of ubiquitin-like domains to the proteasome. *EMBO J* 22(18):4634-45.
120. Chen X, Randles L, Shi K, Tarasov Sergey G, Aihara H, & Walters Kylie J (2016) Structures of Rpn1 T1:Rad23 and hRpn13:hPLIC2 Reveal Distinct Binding Mechanisms between Substrate Receptors and Shuttle Factors of the Proteasome. *Structure* 24(8):1257-70.
121. VanderLinden RT, Hemmis CW, Yao T, Robinson H, & Hill CP (2017) Structure and energetics of pairwise interactions between proteasome subunits RPN2, RPN13, and ubiquitin clarify a substrate recruitment mechanism. *Journal of Biological Chemistry*:jbc.M117.785287-jbc.M117.
122. Sakata E, Bohn S, Mihalache O, Kiss P, Beck F, Nagy I, Nickell S, Tanaka K, Saeki Y, Förster F, & Baumeister W (2012) Localization of the proteasomal ubiquitin receptors Rpn10 and Rpn13 by electron cryomicroscopy. *Proceedings of the National Academy of Sciences of the United States of America* 109(5):1479-84.
123. Wang Q, Young P, & Walters KJ (2005) Structure of S5a bound to monoubiquitin provides a model for polyubiquitin recognition. *Journal of molecular biology* 348(3):727-39.
124. Lam YA, Lawson TG, Velayutham M, Zweier JL, & Pickart CM (2002) A proteasomal ATPase subunit recognizes the polyubiquitin degradation signal. *Nature* 416(6882):763-7.
125. Elsasser S, Gali RR, Schwickart M, Larsen CN, Leggett DS, Müller B, Feng MT, Tübing F, Dittmar GaG, & Finley D (2002) Proteasome subunit Rpn1 binds ubiquitin-like protein domains. *Nature cell biology* 4(9):725-30.
126. Funakoshi M, Sasaki T, Nishimoto T, & Kobayashi H (2002) Budding yeast Dsk2p is a polyubiquitin-binding protein that can interact with the proteasome. *Proc Natl Acad Sci U S A* 99(2):745-50.
127. Schauber C, Chen L, & Tongaonkar P (1998) Rad23 links DNA repair to the ubiquitin/proteasome pathway. *Nature* 391(February):715-8.
128. Kaplun L, Tzirkin R, Bakhrat A, Shabek N, Ivantsiv Y, & Raveh D (2005) The DNA damage-inducible UbL-UbA protein Ddi1 participates in Mec1-mediated degradation of Ho endonuclease. *Mol Cell Biol* 25(13):5355-62.

129. Hofmann K & Bucher P (1996) The UBA domain: a sequence motif present in multiple enzyme classes of the ubiquitination pathway. *Trends Biochem Sci* 21(5):172-3.
130. Gomez TA, Kolawa N, Gee M, Sweredoski MJ, & Deshaies RJ (2011) Identification of a functional docking site in the Rpn1 LRR domain for the UBA-UBL domain protein Ddi1. *BMC Biol* 9:33.
131. Walters KJ, Kleijnen MF, Goh AM, Wagner G, & Howley PM (2002) Structural studies of the interaction between ubiquitin family proteins and proteasome subunit S5a. *Biochemistry* 41(6):1767-77.
132. Chen L & Madura K (2002) Rad23 promotes the targeting of proteolytic substrates to the proteasome. *Mol Cell Biol* 22(13):4902-13.
133. Kim I, Mi K, & Rao H (2004) Multiple interactions of rad23 suggest a mechanism for ubiquitylated substrate delivery important in proteolysis. *Mol Biol Cell* 15(7):3357-65.
134. Hanzelmann P, Stingele J, Hofmann K, Schindelin H, & Raasi S (2010) The yeast E4 ubiquitin ligase Ufd2 interacts with the ubiquitin-like domains of Rad23 and Dsk2 via a novel and distinct ubiquitin-like binding domain. *J Biol Chem* 285(26):20390-8.
135. Itakura E, Zavodszky E, Shao S, Wohlever ML, Keenan RJ, & Hegde RS (2016) Ubiquilins Chaperone and Triage Mitochondrial Membrane Proteins for Degradation. *Mol Cell* 63(1):21-33.
136. Sims JJ, Haririnia A, Dickinson BC, Fushman D, & Cohen RE (2009) Avid interactions underlie the Lys63-linked polyubiquitin binding specificities observed for UBA domains. *Nat Struct Mol Biol* 16(8):883-9.
137. Raasi S & Pickart CM (2003) Rad23 ubiquitin-associated domains (UBA) inhibit 26 S proteasome-catalyzed proteolysis by sequestering lysine 48-linked polyubiquitin chains. *Journal of Biological Chemistry* 278(11):8951-9.
138. Tsuchiya H, Ohtake F, Arai N, Kaiho A, Yasuda S, Tanaka K, & Saeki Y (2017) In Vivo Ubiquitin Linkage-type Analysis Reveals that the Cdc48-Rad23/Dsk2 Axis Contributes to K48-Linked Chain Specificity of the Proteasome. *Mol Cell* 66(4):488-502 e7.
139. Saeki Y, Saitoh A, Toh-e A, & Yokosawa H (2002) Ubiquitin-like proteins and Rpn10 play cooperative roles in ubiquitin-dependent proteolysis. *Biochem Biophys Res Commun* 293(3):986-92.
140. Verma R, Oania R, Graumann J, & Deshaies RJ (2004) Multiubiquitin chain receptors define a layer of substrate selectivity in the ubiquitin-proteasome system. *Cell* 118(1):99-110.
141. Hamazaki J, Sasaki K, Kawahara H, Hisanaga S, Tanaka K, & Murata S (2007) Rpn10-mediated degradation of ubiquitinated proteins is essential for mouse development. *Mol Cell Biol* 27(19):6629-38.
142. Hamazaki J, Hirayama S, & Murata S (2015) Redundant Roles of Rpn10 and Rpn13 in Recognition of Ubiquitinated Proteins and Cellular Homeostasis. *PLoS Genet* 11(7):e1005401.
143. Al-Shami A, Jhaver KG, Vogel P, Wilkins C, Humphries J, Davis JJ, Xu N, Potter DG, Gerhardt B, Mullinax R, Shirley CR, Anderson SJ, & Oravecz T (2010) Regulators of the proteasome pathway, Uch37 and Rpn13, play distinct roles in mouse development. *PLoS One* 5(10):e13654.
144. Chojnacki M, Mansour W, Hameed DS, Singh RK, El Oualid F, Rosenzweig R, Nakasone MA, Yu Z, Glaser F, Kay LE, Fushman D, Ovaa H, & Glickman MH (2017) Polyubiquitin-Photoactivatable Crosslinking Reagents for Mapping Ubiquitin

Interactome Identify Rpn1 as a Proteasome Ubiquitin-Associating Subunit. *Cell Chem Biol* 24(4):443-57 e6.
145. Crosas B, Hanna J, Kirkpatrick DS, Zhang DP, Tone Y, Hathaway Na, Buecker C, Leggett DS, Schmidt M, King RW, Gygi SP, & Finley D (2006) Ubiquitin chains are remodeled at the proteasome by opposing ubiquitin ligase and deubiquitinating activities. *Cell* 127(7):1401-13.
146. Aguileta MA, Korac J, Durcan TM, Trempe JF, Haber M, Gehring K, Elsasser S, Waidmann O, Fon EA, & Husnjak K (2015) The E3 ubiquitin ligase parkin is recruited to the 26 S proteasome via the proteasomal ubiquitin receptor Rpn13. *J Biol Chem* 290(12):7492-505.
147. Leggett DS, Hanna J, & Borodovsky A (2002) Multiple associated proteins regulate proteasome structure and function. *Molecular cell* 10:495-507.
148. Cope GA, Suh GS, Aravind L, Schwarz SE, Zipursky SL, Koonin EV, & Deshaies RJ (2002) Role of predicted metalloprotease motif of Jab1/Csn5 in cleavage of Nedd8 from Cul1. *Science* 298(5593):608-11.
149. Maytal-Kivity V, Reis N, Hofmann K, & Glickman MH (2002) MPN+, a putative catalytic motif found in a subset of MPN domain proteins from eukaryotes and prokaryotes, is critical for Rpn11 function. *BMC biochemistry* 3:28-.
150. Guterman A & Glickman MH (2004) Complementary roles for Rpn11 and Ubp6 in deubiquitination and proteolysis by the proteasome. *The Journal of biological chemistry* 279(3):1729-38.
151. Rinaldi T, Pick E, Gambadoro A, Zilli S, Maytal-Kivity V, Frontali L, & Glickman MH (2004) Participation of the proteasomal lid subunit Rpn11 in mitochondrial morphology and function is mapped to a distinct C-terminal domain. *Biochem J* 381(Pt 1):275-85.
152. Worden EJ, Padovani C, & Martin A (2014) Structure of the Rpn11-Rpn8 dimer reveals mechanisms of substrate deubiquitination during proteasomal degradation. *Nature structural & molecular biology* 21(3):220-7.
153. Pathare GR & Nagy I (2014) Crystal structure of the proteasomal deubiquitylation module Rpn8-Rpn11. *Proceedings of the …*:6-11.
154. Dambacher CM, Worden EJ, Herzik MA, Martin A, & Lander GC (2016) Atomic structure of the 26S proteasome lid reveals the mechanism of deubiquitinase inhibition. *eLife* 5:e13027-e.
155. Sato Y, Yoshikawa A, Yamagata A, Mimura H, Yamashita M, Ookata K, Nureki O, Iwai K, Komada M, & Fukai S (2008) Structural basis for specific cleavage of Lys 63-linked polyubiquitin chains. *Nature* 455(7211):358-62.
156. Davies CW, Paul LN, Kim MI, & Das C (2011) Structural and thermodynamic comparison of the catalytic domain of AMSH and AMSH-LP: nearly identical fold but different stability. *J Mol Biol* 413(2):416-29.
157. Shrestha RK, Ronau JA, Davies CW, Guenette RG, Strieter ER, Paul LN, & Das C (2014) Insights into the mechanism of deubiquitination by JAMM deubiquitinases from cocrystal structures of the enzyme with the substrate and product. *Biochemistry* 53(19):3199-217.
158. Borodovsky a, Kessler BM, Casagrande R, Overkleeft HS, Wilkinson KD, & Ploegh HL (2001) A novel active site-directed probe specific for deubiquitylating enzymes reveals proteasome association of USP14. *The EMBO journal* 20(18):5187-96.

159. Kim HT & Goldberg AL (2017) The deubiquitinating enzyme Usp14 allosterically inhibits multiple proteasomal activities and ubiquitin-independent proteolysis. *J Biol Chem* 292(23):9830-9.
160. Mansour W, Nakasone Ma, von Delbrueck M, Yu Z, Krutauz D, Reis N, Kleifeld O, Sommer T, Fushman D, & Glickman MH (2014) Disassembly of Lys11- and mixed-linkage polyubiquitin conjugates provide insights into function of proteasomal deubiquitinases Rpn11 and Ubp6. *The Journal of biological chemistry*.
161. Bohn S, Beck F, Sakata E, Walzthoeni T, Beck M, Aebersold R, Forster F, Baumeister W, & Nickell S (2010) Structure of the 26S proteasome from Schizosaccharomyces pombe at subnanometer resolution. *Proc Natl Acad Sci U S A* 107(49):20992-7.
162. Dambacher CM & Lander GC (2015) Site-specific labeling of proteins for electron microscopy. *J Struct Biol* 192(2):151-8.
163. Nguyen DP, Lusic H, Neumann H, Kapadnis PB, Deiters A, & Chin JW (2009) Genetic encoding and labeling of aliphatic azides and alkynes in recombinant proteins via a pyrrolysyl-tRNA Synthetase/tRNA(CUA) pair and click chemistry. *Journal of the American Chemical Society* 131(25):8720-1.
164. Amiram M, Haimovich AD, Fan C, Wang YS, Aerni HR, Ntai I, Moonan DW, Ma NJ, Rovner AJ, Hong SH, Kelleher NL, Goodman AL, Jewett MC, Soll D, Rinehart J, & Isaacs FJ (2015) Evolution of translation machinery in recoded bacteria enables multi-site incorporation of nonstandard amino acids. *Nat Biotechnol* 33(12):1272-9.
165. van Geel R, Pruijn GJ, van Delft FL, & Boelens WC (2012) Preventing thiol-yne addition improves the specificity of strain-promoted azide-alkyne cycloaddition. *Bioconjug Chem* 23(3):392-8.
166. Suraweera A, Munch C, Hanssum A, & Bertolotti A (2012) Failure of amino acid homeostasis causes cell death following proteasome inhibition. *Mol Cell* 48(2):242-53.
167. Groll M, Bajorek M, & Köhler A (2000) A gated channel into the proteasome core particle. *Nature Structural & ...* 7(11):1062-7.
168. Saeki Y, Toh-E A, Kudo T, Kawamura H, & Tanaka K (2009) Multiple proteasome-interacting proteins assist the assembly of the yeast 19S regulatory particle. *Cell* 137(5):900-13.
169. Funakoshi M, Tomko RJ, Kobayashi H, & Hochstrasser M (2009) Multiple assembly chaperones govern biogenesis of the proteasome regulatory particle base. *Cell* 137(5):887-99.
170. Roelofs J, Park S, Haas W, Tian G, McAllister FE, Huo Y, Lee B-H, Zhang F, Shi Y, Gygi SP, & Finley D (2009) Chaperone-mediated pathway of proteasome regulatory particle assembly. *Nature* 459(7248):861-5.
171. Tomko RJ, Jr. & Hochstrasser M (2011) Order of the proteasomal ATPases and eukaryotic proteasome assembly. *Cell Biochem Biophys* 60(1-2):13-20.
172. Estrin E, Lopez-Blanco JR, Chacón P, & Martin A (2013) Formation of an intricate helical bundle dictates the assembly of the 26S proteasome lid. *Structure (London, England : 1993)* 21(9):1624-35.
173. Chin JW, Santoro SW, Martin AB, King DS, Wang L, & Schultz PG (2002) Addition of p-azido-L-phenylalanine to the genetic code of Escherichia coli. *Journal of the American Chemical Society* 124(31):9026-7.

174. Chen PR, Groff D, Guo J, Ou W, Cellitti S, Geierstanger BH, & Schultz PG (2009) A facile system for encoding unnatural amino acids in mammalian cells. *Angew Chem Int Ed Engl* 48(22):4052-5.
175. Chatterjee A, Sun SB, Furman JL, Xiao H, & Schultz PG (2013) A Versatile Platform for Single- and Multiple-Unnatural Amino Acid Mutagenesis in Escherichia coli. *Biochemistry* 52(10):1828-37.
176. Agard NJ, Prescher JA, & Bertozzi CR (2004) A strain-promoted [3 + 2] azide-alkyne cycloaddition for covalent modification of biomolecules in living systems. *J Am Chem Soc* 126(46):15046-7.
177. Ning X, Guo J, Wolfert MA, & Boons GJ (2008) Visualizing metabolically labeled glycoconjugates of living cells by copper-free and fast huisgen cycloadditions. *Angew Chem Int Ed Engl* 47(12):2253-5.
178. Seidman CE, Struhl K, Sheen J, & Jessen T (2001) Introduction of plasmid DNA into cells. *Curr Protoc Mol Biol* Chapter 1:Unit1 8.
179. Schinn SM, Bradley W, Groesbeck A, Wu JC, Broadbent A, & Bundy BC (2017) Rapid in vitro screening for the location-dependent effects of unnatural amino acids on protein expression and activity. *Biotechnol Bioeng* 114(10):2412-7.
180. Tian H, Sakmar TP, & Huber T (2016) A simple method for enhancing the bioorthogonality of cyclooctyne reagent. *Chem Commun (Camb)* 52(31):5451-4.
181. MacDonald JI, Munch HK, Moore T, & Francis MB (2015) One-step site-specific modification of native proteins with 2-pyridinecarboxyaldehydes. *Nat Chem Biol* 11(5):326-31.
182. Chen B, Retzlaff M, Roos T, & Frydman J (2011) Cellular strategies of protein quality control. *Cold Spring Harb Perspect Biol* 3(8):a004374.
183. Hershko A & Ciechanover A (1998) The ubiquitin system. *Annu Rev Biochem* 67:425-79.
184. Bard JAM, Goodall EA, Greene ER, Jonsson E, Dong KC, & Martin A (2018) Structure and Function of the 26S Proteasome. *Annu Rev Biochem* 87:697-724.
185. Albert S, Schaffer M, Beck F, Mosalaganti S, Asano S, Thomas HF, Plitzko JM, Beck M, Baumeister W, & Engel BD (2017) Proteasomes tether to two distinct sites at the nuclear pore complex. *Proc Natl Acad Sci U S A* 114(52):13726-31.
186. Hu M, Li P, Song L, Jeffrey PD, Chenova TA, Wilkinson KD, Cohen RE, & Shi Y (2005) Structure and mechanisms of the proteasome-associated deubiquitinating enzyme USP14. *The EMBO journal* 24(21):3747-56.
187. Saeki Y, Isono E, & Toh EA (2005) Preparation of ubiquitinated substrates by the PY motif-insertion method for monitoring 26S proteasome activity. *Methods Enzymol* 399:215-27.
188. Bhattacharyya S, Renn JP, Yu H, Marko JF, & Matouschek A (2016) An assay for 26S proteasome activity based on fluorescence anisotropy measurements of dye-labeled protein substrates. *Anal Biochem* 509:50-9.
189. Kenniston JA, Baker TA, Fernandez JM, & Sauer RT (2003) Linkage between ATP consumption and mechanical unfolding during the protein processing reactions of an AAA+ degradation machine. *Cell* 114(4):511-20.
190. Johnston JA, Johnson ES, Waller PR, & Varshavsky A (1995) Methotrexate inhibits proteolysis of dihydrofolate reductase by the N-end rule pathway. *J Biol Chem* 270(14):8172-8.

191. Michel MA, Elliott PR, Swatek KN, Simicek M, Pruneda JN, Wagstaff JL, Freund SM, & Komander D (2015) Assembly and specific recognition of k29- and k33-linked polyubiquitin. *Mol Cell* 58(1):95-109.
192. Anonymous (!!! INVALID CITATION !!! {}).
193. Kirkpatrick DS, Hathaway NA, Hanna J, Elsasser S, Rush J, Finley D, King RW, & Gygi SP (2006) Quantitative analysis of in vitro ubiquitinated cyclin B1 reveals complex chain topology. *Nat Cell Biol* 8(7):700-10.
194. Rape M, Reddy SK, & Kirschner MW (2006) The processivity of multiubiquitination by the APC determines the order of substrate degradation. *Cell* 124(1):89-103.
195. Rodnina MV & Wintermeyer W (2001) Ribosome fidelity: tRNA discrimination, proofreading and induced fit. *Trends Biochem Sci* 26(2):124-30.
196. Verma R, Chen S, Feldman R, Schieltz D, Yates J, Dohmen J, & Deshaies RJ (2000) Proteasomal proteomics: identification of nucleotide-sensitive proteasome-interacting proteins by mass spectrometric analysis of affinity-purified proteasomes. *Molecular biology of the cell* 11(10):3425-39.
197. Theile CS, Witte MD, Blom AEM, Kundrat L, Ploegh HL, & Guimaraes CP (2013) Site-specific N-terminal labeling of proteins using sortase-mediated reactions. *Nature protocols* 8(9):1800-7.
198. Mikolajczyk J, Drag M, Bekes M, Cao JT, Ronai Z, & Salvesen GS (2007) Small ubiquitin-related modifier (SUMO)-specific proteases: profiling the specificities and activities of human SENPs. *J Biol Chem* 282(36):26217-24.
199. Carvalho AF, Pinto MP, Grou CP, Vitorino R, Domingues P, Yamao F, Sa-Miranda C, & Azevedo JE (2012) High-yield expression in Escherichia coli and purification of mouse ubiquitin-activating enzyme E1. *Mol Biotechnol* 51(3):254-61.
200. Bard JAM & Martin A (2018) Recombinant expression, unnatural amino-acid incorporation, and site-specific labeling of 26S proteasomal subcomplexes. *Methods in Molecular Biology* In Press.
201. Bard JAM, Bashore C, Dong KC, & Martin A (2018) Deconvolution of substrate processing by the 26S proteasome reveals a selective kinetic gateway to degradation. *Science* Submitted.
202. Gautier A, Juillerat A, Heinis C, Correa IR, Jr., Kindermann M, Beaufils F, & Johnsson K (2008) An engineered protein tag for multiprotein labeling in living cells. *Chem Biol* 15(2):128-36.
203. Keppler A, Gendreizig S, Gronemeyer T, Pick H, Vogel H, & Johnsson K (2003) A general method for the covalent labeling of fusion proteins with small molecules in vivo. *Nat Biotechnol* 21(1):86-9.